



Novel electroenzymatic process for gluconic acid production

Dissertation

zur Erlangung des akademischen Grades

**Doktoringenieurin
(Dr.-Ing.)**

von:

Dipl. ing. Miroslava Varnicic

geb. am 20. August 1983 in Belgrad, Serbien

genehmigt durch die Fakultät für Verfahrens- und Systemtechnik
der Otto-von-Guericke-Universität Magdeburg

Promotionskommission: Prof. Dr. Dieter Schinzer (Vorsitz)
Prof. Dr.-Ing. Kai Sundmacher (Gutachter)
Prof. Dr.-Ing. Ulrich Kunz (Gutachter)
Dr. rer. nat. Klaus-Michael Mangold (Gutachter)

eingereicht am: 26.07.2017

Promotionskolloquium am: 25.09.2017

Acknowledgements

First and foremost, I would like to express my deepest gratitude to Prof. Dr.-Ing. Kai Sundmacher, for his kind guidance and support during my PhD studies. I am very grateful for the opportunity to work in his group on this novel, interesting and challenging topic. I would also like to extend my appreciation to my committee members: Prof. Dr.-Ing. Ulrich Kunz, Dr. rer. nat. Klaus-Michael Mangold and Prof. Dr. Dieter Schinzer for their acceptance and reviewing of the thesis.

My sincere gratitude goes to Dr. Tanja Vidaković–Koch, for all her support and help, for fruitful discussions, for her patience and time, and for believing in me since the first day I started. This work would not be completed without her substantial support.

I would also like to thank Jun.-Prof. Edgar Haak, for his help with NMR analysis and important discussions. I need to acknowledge the indispensable assistance from Bianka Stein and Markus Ikert for all their support in the experiments and for nice time during the everyday work. Also, thank to Dr. Dana Hermsdorf for AFM measurement and Helga Tietgens for FM measurements. Significant contribution to the thesis has Iva Zasheva, who was involved as a master student. I thank her for her dedication to work, effort, suggestions and friendship.

Special thanks go to my all colleagues and friends that I have met during my time in Magdeburg. Ivan Ivanov, thank you for your friendship, support and for always being there in tough times. Ivonne Peña Arias, el mejor amiga, thanks for sharing work and life, for all support and great moments. I am so happy to meet during this time my fratello Antonio Sorrentino, my greek family Georgios, Maria and Dionysi Papakonstantinou, thanks for being such a great friends and for making me feel as at home. Ivana Mutavdzin, Vinit Mittal, Samanta Cajic, Rene Hennig, Miljana Spasic, Milena Radojic, Nebojsa Korica, Nga Do, Ali Elsibai, Erdal, Thiane Carneiro, Terry and Marie for being with me and supporting me since the beginning, for all nice moments and fun time. Isaí González Martínez, Leo Alvarado Perea, Hector Rubiera and Lili Gallo for mexican telenovela coffee time and fun talks. Special thanks go to Pablo Nicolitz for his love and support through my PhD time. One simply could not wish for better colleagues and friends.

I am especially gratefully to amazing Cathleen Dedens-Richter for her friendship, support, fun and understanding through all these years.

I would like to enormously thank my family and friends in Serbia, for their understanding, support, encouragement, love and motivation during my studies abroad.

Abstract

In the present thesis, the development of a novel process for glucose partial oxidation into the industrially important product, gluconic acid, using an electroenzymatic approach was demonstrated. Electroenzymatic systems are characterized by the utilization of renewable resources (starches, glucose etc.) and green catalysts (enzymes) with one step transformations (avoiding protection-deprotection loops) that, together with low process emissions, fulfill all the requirements to materialize a sustainable production process.

Current limitations of electroenzymatic processes are related to low activity and stability of the enzymatic electrodes, as well as low reactor productivity. Therefore, the first part the present thesis aims at the rational design of porous enzymatic electrodes. The main tasks were to understand bottlenecks for the highest biocatalyst utilization within complex porous electrodes and to evaluate influence of different immobilization strategies on the electrode performance. Further, the optimized enzymatic electrodes were tested in a half-cell and flow-through electrochemical reactor, without any separator in-between. The influence of structural and essential operational parameters (i.e. flow rate, cell potential, operating time) and type of biocatalysts on the reactor performance, glucose conversion and selectivity was investigated.

The reactor performance was significantly improved by changing structural parameters like electrode surface area and biocatalyst loading (e.g. glucose conversion was increased from *ca.* 16% to *ca.* 50%). Furthermore, the reactor productivity was controlled by changing flow rate, time and mode of reactor operation. The optimal conversion of 80%, with product selectivity of 92% was achieved. Additionally, the system can work as a biofuel cell with the power density of approximately $100 \mu\text{W cm}^{-2}$. The two by-products, D-arabinose and D-formic acid, and possible pathways for their formation, have been reported for the first time for bioelectrochemical systems. It was demonstrated that the cathode of the reactor is responsible for a decreased process selectivity. Additionally, the yields of by-products could be controlled by the cathode electrode potential. The selectivity issue can be improved by replacing the enzyme cascade (glucose oxidase – horseradish peroxidase, GOx-HRP) with bilirubin oxidase (BOD). Thus, in the reactor based on BOD biocatalyst, a selectivity of 100% was achieved.

The feasibility of a GOx based electroenzymatic reactor for the gluconic acid synthesis was demonstrated. The electroenzymatic system proved to have high potential as a sustainable alternative for chemical production.

Zusammenfassung

Die vorliegende Arbeit beinhaltet die Entwicklung eines neuartigen Prozesses zur partiellen Oxidation von Glucose in das industriell relevante Produkt Gluconsäure unter Anwendung eines elektroenzymatischen Reaktors. Elektroenzymatische Systeme sind gekennzeichnet durch die Nutzung erneuerbarer Ressourcen (Stärken, Glukose, usw.) und die Verwendung von Biokatalysatoren (Enzyme), die in einstufigen Verfahren arbeiten und geringe Prozessemissionen zeigen, so dass wesentliche Anforderungen an einen nachhaltigen Produktionsprozess erfüllt werden.

Heutige Einschränkungen von elektroenzymatischen Prozessen liegen in der niedrigen Aktivität und Stabilität von enzymatischen Elektroden und einer niedrigen Reaktorproduktivität begründet. Deshalb beschäftigt sich der erste Teil der vorliegenden Doktorarbeit mit dem geeigneten Design poröser enzymatischer Elektroden. Dabei waren die Hauptaufgaben zum einen das Erzielen eines vertieften Verständnis der Engpässe für einen hohen Biokatalysator-Nutzgrad innerhalb poröser Elektroden und zum anderen die Evaluierung des Einflusses verschiedener Immobilisierungsstrategien auf die Leistungsfähigkeit der Elektroden. Weiterhin wurden die optimierten enzymatischen Elektroden in einem Halbzellen- und elektrochemischen Durchflussreaktor ohne jeglichen Separator getestet. Es wurde der Einfluss struktureller und operationeller Betriebsparameter (Flussrate, Zellenpotential, Betriebsdauer) sowie des Katalysator Typs auf die Reaktorperformance, die Glukoseumsetzung und die Selektivität untersucht.

Die Leistungsfähigkeit des Reaktors konnte durch Änderung der strukturellen Parameter (Elektrodenoberfläche, Biokatalysatorbeladung) signifikant verbessert werden. So konnte z. B. die Glukoseumsetzung von ca. 16% auf ca. 50% erhöht werden. Außerdem wurde die Reaktorproduktivität durch Änderung der Flussrate, der Zeit und des Modus des Reaktorbetriebs verbessert. Es wurde ein optimaler Umsatz von 80% bei einer Produktselektivität von 92% erreicht. Zusätzlich kann das System als Bio-Brennstoffzelle mit einer Leistungsdichte von etwa $100 \mu\text{W cm}^{-2}$ arbeiten. Erstmals wurden die beiden Nebenprodukte - D-Arabinose and D-Ameisensäure - und ihre möglichen Reaktionswege für bioelektrochemische Systeme dokumentiert. Es konnte gezeigt werden, dass die Kathodenseite des Reaktors ursächlich für eine sinkende Prozessselektivität ist. Allerdings konnte der Umsatz der Nebenprodukte durch das kathodenseitige Elektrodenpotential kontrolliert werden. Die Selektivität kann durch das Austauschen der Enzymkaskade (glucose oxidase – horseradish

peroxidase, GOx-HRP) durch Bilirubin Oxidase (BOD) erhöht werden. So konnte in dem Reaktor mit BOD-Biokatalysator eine Selektivität von 100% erreicht werden.

Die Machbarkeit eines GOx-basierten elektroenzymatischen Reaktors für die Synthese von Gluconsäure wurde demonstriert. Es konnte gezeigt werden, dass das elektroenzymatische System ein hohes Potential als nachhaltige Prozessalternative für die chemische Produktion besitzt.

List of Abbreviations

3-D	three-dimensional
A	D-arabinose
ABTS	2,2'-azino-bis(3-ethylbenzthiazoline-6-sulphonic acid)
AFM	atomic force microscopy
BES	bioelectrochemical systems
BOD	bilirubin oxidase
C	conversion
CA	carbon aerogel
CC	coral carbon
CHS	carbon hollow spheres
CL	cross linking
CV	cyclic voltammetry
DET	direct electron transfer
DMF	dimethylformamide
ESTM	electrochemical scanning tunneling microscopy
FA	formic acid
FAD	flavin adenine dinucleotide
FM	fluorescence microscopy
FMN	flavin mononucleotide
GA	gluconic acid
GDE	gas-diffusion electrode
GDH	glucose dehydrogenase
GOx	glucose oxidase
HOPG	highly ordered pyrolytic graphic
HRP	horseradish peroxidase

HQS	8-hydroxyquinoline-5-sulfonic
MET	mediated electron transfer
MWCNTs	multi-walled carbon nanotubes
NAD(P)	nicotinamide adenine dinucleotide(phosphate)
NHS	N-hydroxysulfosuccinimide
NMP	N-methylphenazinium
NMR	nuclear magnetic resonance
OCP	open circuit potential
OCV	open circuit voltage
PBS	phosphate buffer solution
PEM	polymer electrolyte membrane
PTFE	polytetrafluoroethylene
PVDF	poly(vinylidene fluoride)
RDE	rotating disc electrode
S	selectivity
SCE	saturated calomel electrode
SDS	sodium dodecyl sulfate
SECM	scanning electrochemical microscopy
SEM	scanning electron microscopy
SPG	spectroscopic graphite
STY	space time yield
SWCNTs	single-walled carbon nanotubes
TTF	tetrathiafulvalene
Y	yield

Table of Contents

1. Introduction	1
1.1 Motivation.....	1
1.2 Case study: Partial oxidation of glucose.....	2
1.2.1 Glucose as renewable platform chemical.....	2
1.2.2 Overview of the gluconic acid production processes.....	3
1.2.3 Electroenzymatic process for gluconic acid production.....	7
1.3 Aim and objectives of the thesis.....	9
2. Theoretical part	11
2.1 Enzymes as catalysts in electroenzymatic systems.....	11
2.2 Enzymatic electrodes development.....	14
2.3 Enzymatic electrochemical cells.....	17
3. Experimental part	24
3.1 Chemicals and materials.....	24
3.2 Enzymatic electrode preparation: monolayer electrode.....	25
(flat surfaces).....	25
3.2.1 HRP-modified graphite surface for electrochemical studies.....	25
3.2.2 Enzymatic electrodes for microscopy studies.....	25
3.3 Electrode preparation: porous enzymatic electrodes.....	26
(3-D electrodes).....	26
3.3.1 Vulcan-Gelatin procedure.....	26
3.3.2 Vulcan-PVDF procedure.....	27
3.3.3 Electrodes used in electrochemical cells.....	28
3.4 Half-Cell electrochemical investigations.....	29
3.4.1 Measurements setup.....	29
3.4.2 Rotating disk electrode (RDE) as WE.....	29
3.5 Electroenzymatic reactor setup.....	31
3.6 Measurements and characterization methods.....	34
3.6.1 Cyclic voltammetry measurements (CV).....	34
3.6.2 Steady state measurements (SSV).....	34
3.6.3 Chronoamperometry (ChA).....	34
3.6.4 Fluorescence microscopy (FM).....	35

3.6.5 Atomic-force microscopy (AFM)	35
3.6.6 Scanning electron microscopy (SEM).....	35
3.6.7 Nuclear magnetic resonance spectroscopy (NMR).....	35
3.6.8 Enzymatic assay for concentration test	35
4. Design of the enzymatic electrodes.....	36
4.1 Monolayer enzymatic electrode configuration	38
4.1.1 Bioelectrochemical cycle of hydrogen peroxide reduction at the HRP-electrode	38
4.1.2 Electrochemical characterization of HRP-graphite electrode	39
4.2 Three dimensional enzymatic electrodes.....	44
4.2.1 Influence of the supporting material (nanomaterial).....	44
4.2.2 Influence of the immobilization strategy.....	50
4.2.3 Characterization of the electrode structures	57
4.3 Characterization of the enzyme distribution at the electrode surface	59
4.3.1 Influence of the surface morphology.....	59
4.3.2 Influence of cross-linking.....	65
4.4 Summary and concluding remarks.....	68
5. GOx-modified enzymatic electrode for glucose oxidation.....	71
5.1 Biocathode: GOx–HRP enzymatic electrode	71
5.1.1 Influence of the immobilization procedure	72
5.1.2 Optimization of the operating conditions.....	75
5.2 Bioanode: GOx–TTF enzymatic electrodes	77
5.2.1 Influence of the immobilization procedure	79
5.2.2 Optimization of the operating conditions.....	80
5.3 Summary and concluding remarks.....	82
6. Electroenzymatic reactor for partial glucose oxidation to gluconic acid.....	84
6.1 Reactor Concept.....	84
6.2 Development of GOx GOx-HRP electroenzymatic reactor	85
6.2.1 Electrochemical performance as an enzymatic fuel cell.....	85
6.2.2 Comparison of enzymatic electrode performances.....	87
6.2.3 Evaluation of reactor performance toward glucose conversion.....	90
6.3 Optimization of GOx GOx-HRP reactor performance and selectivity analysis	96
6.3.1 Influence of flow rate on reactor performance	96
6.3.2 Analysis of the reactor selectivity and product yield.....	99

6.3.3 Influence of cell potential and operating time.....	106
6.3.4 Comparison of electroenzymatic to establish fermentation processes.....	108
6.4 Preliminary results regarding GOx BOD electroenzymatic reactor	109
6.5 Summary and concluding remarks.....	112
7. Conclusions and outlook	115
7.1 Conclusions.....	115
7.2 Outlook.....	117
8. Appendix	119
9. List of Tables.....	126
10. List of Figures	127
11. Literature (References).....	132

1. Introduction

1.1 Motivation

In the past few decades, raised awareness of possible negative impacts of the chemical industry to the environment has changed the focus of chemical production towards more sustainable alternatives. New manufacturing technologies must provide safe, clean, resource efficient, energy saving and environmentally friendly production routes [1-4]. These requirements introduce new research challenges in chemical transformations. By merging the unique features of biological components (e.g. high specificity, self-replication) and electrochemical technology in bioelectrochemical systems (BES), it is possible to design sustainable and efficient chemical and energy conversion processes [5, 6].

So far, a high portion of bioelectrochemical research has been focused on biosensors and biofuel cells. However, an emerging field of application of bioelectrochemical systems is chemical production. The advantages of redox enzymes as catalysts in synthetic processes are high regio- and stereo- selectivity and high activity under mild operating conditions (pH, temperature, pressure). On the other hand, the use of redox enzymes requires a smart strategy for the cofactor regeneration. In this respect, electrochemical methods offer a clean alternative, since no co-substrate is needed and no further by-products are formed during reactivation of cofactors.

Based on BES concept, the model reaction of glucose partial oxidation to obtain industrially valuable product in an electroenzymatic reactor, was studied in the present thesis. However, the major challenges that must be addressed in order to make this process competitive for industrial applications are related to enzymatic electrode performance and system integration. Thus, the focus of the thesis will be on these two aspects.

1.2 Case study: Partial oxidation of glucose

1.2.1 Glucose as renewable platform chemical

In the past few decades, there has been a growing interest for application of carbohydrates as a feedstock in the chemical industry. These organic compounds (starch, cellulose, glucose etc.) obtained from biomass, are abundant, renewable, low-cost and non-toxic. All these aspects make them a suitable alternative to the use of fossil raw materials [6].

Glucose is considered as platform chemical for many syntheses. Large spectra of organic compounds that can be produced with its transformations are presented in Fig. 1-1 [7]. Additionally, it is also a good candidate as fuel, in the so-called direct glucose fuel cell (DGFC). This replaces the need for the utilization of hydrogen and Pt as a catalyst, thus providing a sustainable concept for energy production. Depending on the system and conditions, glucose can serve as C-source for chemical synthesis, where energy can be also obtained (co-generation systems) [8].

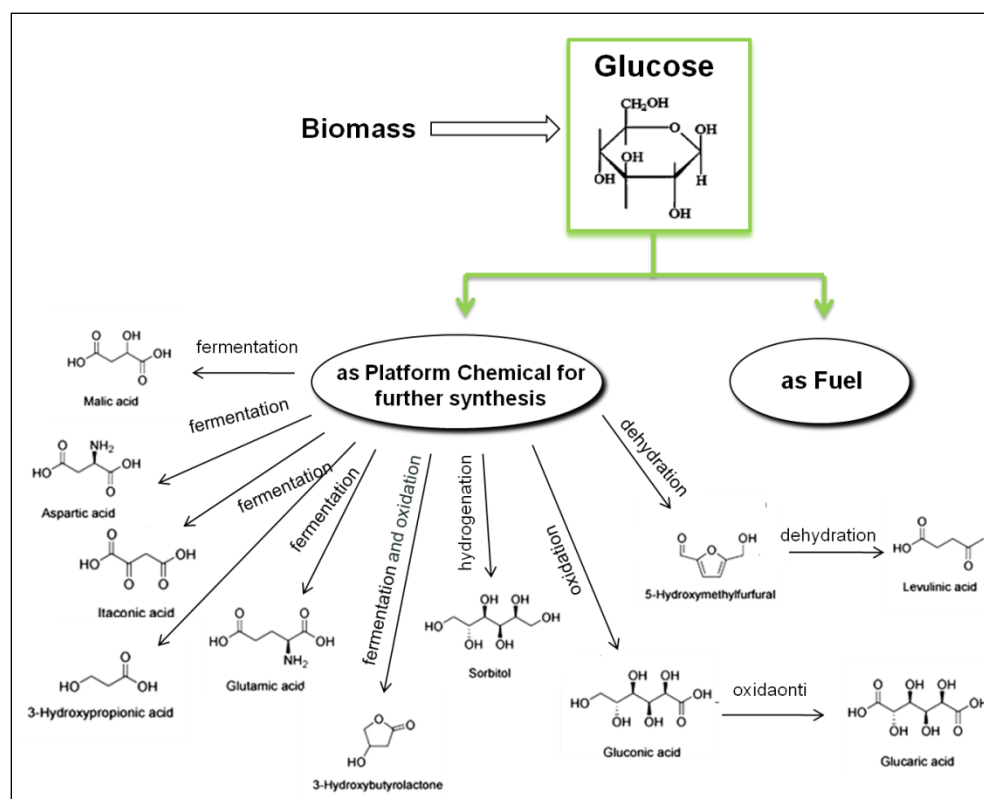


Fig. 1-1 Glucose as platform chemical for synthesis and renewable energy source

Gluconic acid can be obtained by selective partial glucose oxidation. It is a valuable product, which has an annual production of 100 000 tones. It is a mild organic acid belonging to the third largest category in the global market of high-volume bulk chemicals derived by biotechnology, after antibiotics and amino acids [9]. Due to its chemical and physiological characteristics (*i.e.* highly reactive hydroxyl and carboxyl groups and excellent sequestering power), gluconic acid has found applications in different industrial branches. Additionally, derivatives of gluconic acid (metal based salts, *i.e.* gluconates) have been used in food, pharmaceutical (*e.g.* iron and calcium deficiency) and cosmetic industries [10]. A short overview of industry fields and applications of gluconic acid and its derivatives has been presented in Fig. 1-2.

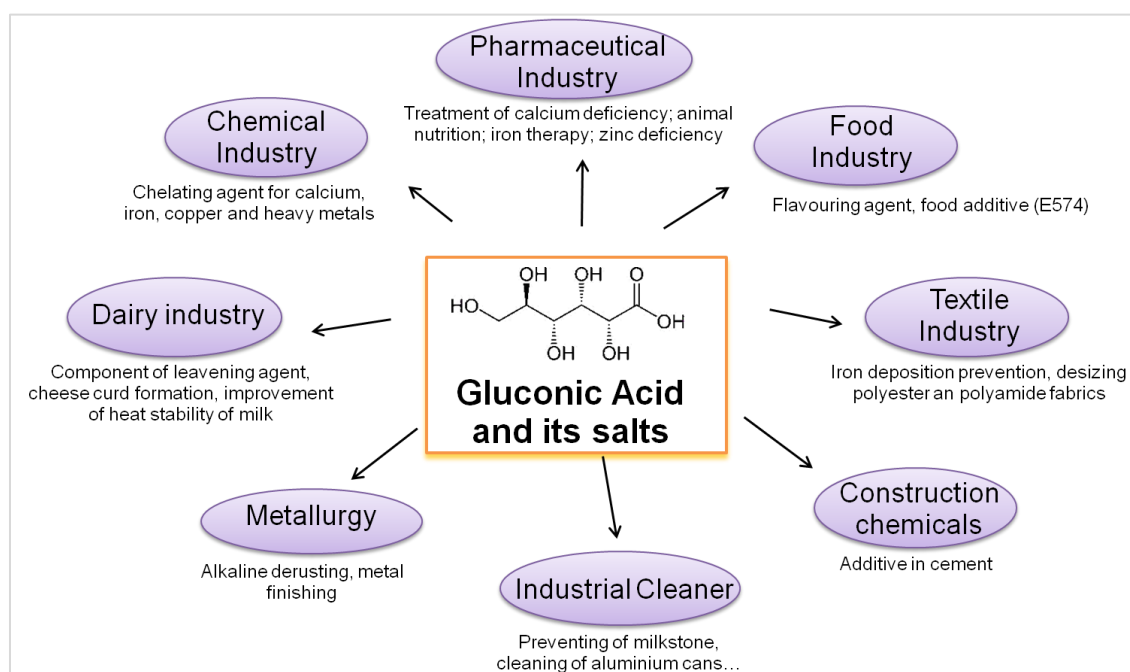


Fig. 1-2 Examples for the use of gluconic acid and its derivatives

1.2.2 Overview of the gluconic acid production processes

As described before, gluconic acid can be obtained by oxidation of glucose (Fig. 1-3). The aldehyde group at the C 1 atom of β -D-glucose ($C_6H_{12}O_6$) oxidizes to the carboxyl group resulting in D-glucono- δ -lactone ($C_6H_{10}O_6$). This compound further spontaneously hydrolyzes to D-gluconic acid (pentahydroxycaproic or 2,3,4,5,6-pentahydroxyhexanoic acid, $C_6H_{12}O_7$).

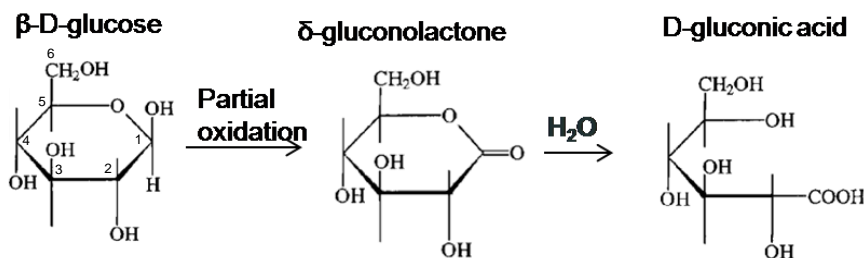


Fig. 1-3 Partial glucose oxidation at the C1 carbon atom

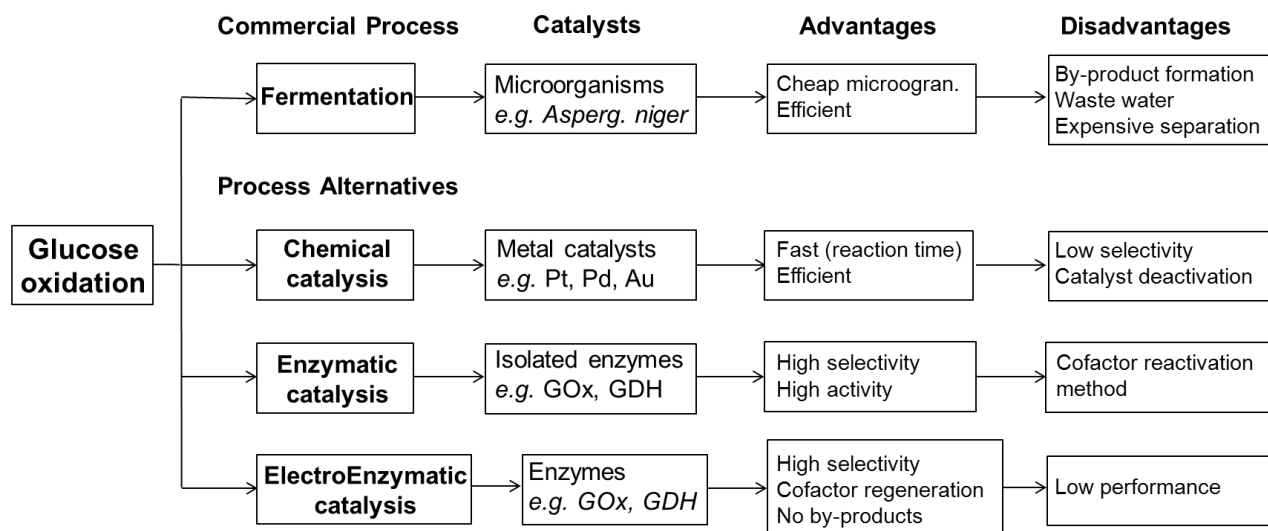


Fig. 1-4 Different production routes for glucose oxidation to gluconic acid

In the past few decades, numerous manufacturing processes including chemical, microbial, enzymatic and bioelectrochemical have been employed for glucose oxidation (Fig. 1-4) [6, 11]. The commercial route for the production of gluconic acid is fermentation [9]. Large efforts have been put into the investigation and development of different fermentation processes, including discontinuous and continuous fermentation using free-growing or immobilized cells. Various species like *Gluconobacter suboxidans* [12], *Aspergillus niger* [13, 14], *Aureobasidium pullulans* [15] etc. were analyzed. The first reported patent for production of gluconic acid using mixed cultures of *Penicillium luteum* and *Aspergillus niger* dates back to 1931 by Currie *et al.* [16]. Later on, the process developed by Blom *et al.* in 1952 using *A. niger*, became the basis for the current commercial production of sodium gluconate [13]. Typical fermentation process for the production of gluconic acid with the separation unit has been

presented in Fig. 1-5 [17]. The selected fermentations, along with their performances have been summarized in Table 1-1. The productivity of fermentation processes for GA production varies from very low values of 0.13 until 21 g h⁻¹ dm⁻³. Although the fermentation is well developed and economically affordable, major drawbacks to this technology are related to downstream processing, control of by-product formation, large amount of waste production and environmental friendliness [18]. This creates the need to develop and focus on other routes.

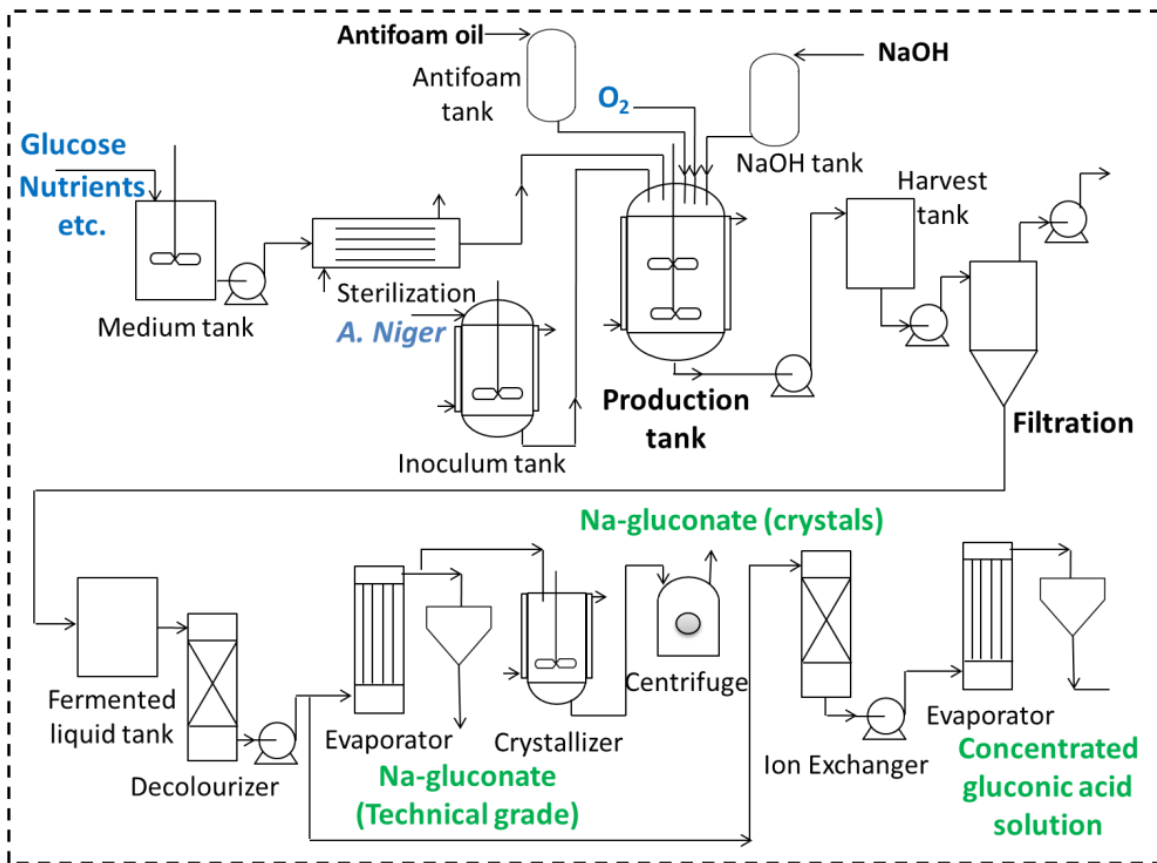


Fig. 1-5 Flow sheet of a conventional fermentation process for the gluconic acid production

Table 1-1 Overview of fermentation processes for the production of gluconic acid

Species	Substrate	pH	Productivity / g h ⁻¹ dm ⁻³	Ref.
<i>Aspergillus niger</i> AN151	Glucose	7.0	21	[19]
<i>Aureobasidium pullulans</i>	Glucose	6.5	15	[15]
<i>Pseudomonas fluorescens</i>	Corn starch	6.5	7.1	[20]
<i>Aspergillus niger</i>	Glucose	5.5	4.6	[21]
<i>Aspergillus niger</i> CCM 8004	Glucose	5.5	4	[22]
<i>P. fluorescens</i> AR4	Glucose	6.5	3.05	[23]
<i>Penicillium variabile</i> P16	Glucose	5.0	2.02	[24]
<i>Aspergillus niger</i> IAM 2029	Waste paper	5-6	1.13	[25]
<i>Aspergillus niger</i> ORS-4410	Banana, grape must	6.5	0.132	[26]

The chemical process for the gluconic acid production consists of glucose oxidation with molecular oxygen under alkaline conditions, in the presence of noble metal catalysts like gold, palladium or platinum [27, 28]. Although chemical catalysis of glucose attracts a lot of attention as a fast and efficient method, it suffers from low selectivity towards gluconic acid, resulting in further gluconic acid oxidation to glucaric acid [29]. Additionally, it is hindered by high energy cost and catalyst deactivation [9].

Enzymatic catalysis is a broadly investigated alternative, which should provide numerous advantages over classical fermentation processes. Due to decreased side reactions, the absence of biomass and zero by-products, separation and purification steps might be largely simplified. Glucose oxidation can be performed either by utilization of bacterial enzyme glucose dehydrogenase (GDH) or fungal glucose oxidase (GOx). GDH catalyzes the oxidation reaction of glucose and the coenzyme nicotinamide adenine dinucleotide (NAD⁺) as an electron

acceptor. Due to requirements, such as the addition of an expensive cofactor and a continuous enzyme-coupled regenerating system, this process is not favorable.

On the other hand, GOx from *Aspergillus niger* is the most widely investigated enzyme for glucose oxidation. Practical application of GOx based reaction for GA production is limited by hydrogen peroxide formation, which strongly inhibits the enzyme performance during time. Two different routes were investigated in order to avoid production or decomposition of H₂O₂, ensuring high process stability. One approach of hydrogen peroxide removal is based on the use of the additional enzyme, catalase, whose role is to decompose H₂O₂ to water and oxygen. Nevertheless, the main drawback is related to the fast catalase inactivation in excess of H₂O₂ [30]. Another practical alternative to avoid H₂O₂ formation is through an electrochemical approach used for co-factor recycling. In this approach, the glucose oxidation is done at the GOx enzymatic electrode, where the co-factor regeneration is simultaneously done by the electrode, providing higher process stability. Therefore, the electroenzymatic process for GA production has high potential as an efficient alternative to the processes investigated to date.

1.2.3 Electroenzymatic processes for gluconic acid production

The reported electroenzymatic processes for glucose oxidation, have been summarized in Table 1-2. One of the first works for GA production based on this approach has been described by Bourdillon *et al.* [31]. In this process, glucose oxidase is immobilized on the carbon felt electrode, serving as the working electrode in a three-electrode configuration, and employed for glucose oxidation, while benzoquinone serves as a mediator. Later, two types of membrane reactors are preferably used. The first type is based on a dialysis membrane [32], while the second one implements an ion-exchange membrane [33, 34]. The essential differences in these reactors are the type of enzyme and the mechanism for its regeneration. A dialysis membrane reactor utilizes enzyme regeneration with O₂ as an electron acceptor, where the role of electrochemistry is the removal of H₂O₂ formed as the by-product. It has been shown that such an electroenzymatic process is 50% more efficient in comparison to a non-electrochemical enzymatic process, based on the same quantity of enzymes [35]. On the contrary, a reactor with Nafion as ion exchange membrane, usually employs glucose-dehydrogenase rather than glucose oxidase for glucose oxidation. The role of the electrochemical step is in co-factor regeneration (NAD), with the help of different mediators (e.g. 3, 4-dihydroxybenzaldehyde or phenazine methosulfate) [30, 34, 36, 37].

For all described processes, operating conditions are adjusted to the conditions under which enzymes show the highest activity. Thus, pH 7 and a temperature of $T = 30\text{ }^{\circ}\text{C}$ or room temperature was used. Glucose concentrations were in the range from 10 to 248 mM. Most systems were operated in a semi-batch mode with total volumes in the range between 10 and 200 ml and electrode surface areas between 3 and 30 cm^2 .

So far, the highest reported STY of $4.86\text{ g h}^{-1}\text{ dm}^{-3}$ was achieved in a dialysis membrane electrochemical reactor with GOx [32]. It is clear that the improvement of the reactor productivity is the main obstacle to the implementation of BES systems in the chemical production. In order to develop economically efficient process, the enzymes must be immobilized at the electrode surface in an active and stable way. However, in presented publications (Table 1-2), the electrodes employ either a monolayer of enzymes or enzymes in the solution, which leads to less utilization. The systematic approach for development of highly active and stable three-dimensional (3-D) porous enzymatic electrodes, optimization of reactor performance toward high productivity and product selectivity analysis are still absent in order to make an electroenzymatic process competitive, compared to the current commercial process (*i.e.* fermentation).

Table 1-2 Overview of electroenzymatic processes for the production of gluconic acid

System	Enzyme	Enzyme Immobilization	Electron transfer	Glucose concentration / mM	STY / $\text{g h}^{-1}\text{ dm}^{-3}$	Ref.
Membrane (Nafion)	GDH	In solution	Direct	10	0.14	[33]
Membrane (Nafion)	GDH	Covalent attachment	Mediated (3,4 – DHB)	100	2.94	[34]
Membrane (Dialysis)	GOx	Entrapment in dialysis membrane	Mediated (O_2)	248	4.86	[32]
Batch	GOx	In polypyrrole film	Mediated (O_2)	20	0.30	[35]
RDE system	G6PDH	Covalent attachment	Mediated (PMS)	9.3	0.13	[36]

Abbreviations: GDH - glucose dehydrogenase, G6PDH - glucose-6-phosphat-dehydrogenase, GOx – glucose oxidase, NAD - nicotinamide adenine dinucleotide, NADP - nicotinamide adenine dinucleotide phosphate, TTF – Tetrathiafulvalene, 3,4 – DHB- 3,4-dihydroxybenzaldehyde, PMS- phenazine methosulfate

1.3 Aim and objectives of the thesis

The core of the present thesis entitled “Novel electroenzymatic process for gluconic acid production” is the development of a novel process based on an electroenzymatic approach. The partial oxidation of the renewable platform chemical, D-glucose, to the valuable product D-gluconic acid (GA), was chosen as an exemplary reaction. Gluconic acid and its salts are widely used in the food, pharmaceutical and chemical industries. The glucose oxidation was performed in the membrane-less, flow-through electrochemical reactor, comprising the enzymatic catalyst: glucose oxidase (GOx). The uniqueness of the proposed process is the utilization of the immobilized GOx on both sides of the electrochemical reactor. Thus, glucose oxidation occurs simultaneously at the anode and the cathode. This provides increased STY of the gluconic acid and enables a membrane-less reactor design, decreasing the costs related to the expensive membranes. Additionally, the process operates in co-generation mode, which gives the possibility of chemical and energy conversions.

The major challenges that must be addressed in order to make electroenzymatic systems competitive for industrial applications are related to the electrode performance and the system integration. Therefore, the objectives of this work are divided into three main parts: A) the rational design of 3-D porous enzymatic electrodes, B) the development and optimization of an electroenzymatic reactor and C) product selectivity.

To date, available enzyme immobilization procedures are quite useful for analytical studies, sensors and biofuel cells applications. However, in most cases they are not suitable for synthetic applications. Therefore, part A (chapters 4 and 5), aimed at the design of the porous enzymatic electrodes. One strategy for overcoming the main limitation related to a low electrode activity is to increase the electrochemically active surface area for catalytic reaction using nanomaterials. In addition, a good contact between enzymes and the electrode surface is necessary, since it ensures the efficient electron transfer and enzyme regeneration. This communication can be improved by choosing the suitable method for the enzyme immobilization at the electrode surface. However, due to an overlap of many phenomena that influence the enzyme activity inside the electrode structure, the optimization of the electrode activity is a challenging task. In this part, porous enzymatic electrodes employing HRP as a model enzyme were developed and tested in respect to different procedures and types of nanomaterials. Their influence on the electrode structural parameters, e.g. porosity and the electrode thickness and

the enzyme organization at the conductive surfaces, were investigated as well. The next step was the transferring of the gained knowledge for the development of the electrodes based on GOx, BOD and GOx-HRP. All criteria such as a good electrode-biocatalysts communication, the preservation of enzyme activity and stability, as well as a high surface area for bioelectrocatalytic reactions have to be satisfied.

Parts B and C that are presented in chapter 6, include the coupling of the optimized enzymatic electrodes in the membrane-less electrochemical reactor, operated in both co-generation (fuel cell and ion-pump) and ion-pump mode. The reactor performances (electrochemical, STY, glucose conversion, selectivity and yield of GA) were investigated by a variation of the essential electrode structural features (electrode surface area and catalyst loading), the operational parameters (flow rate, cell potential and operating time) and different cathode catalysts (GOx-HRP and BOD). Additionally, having in mind the high importance of the selectivity for technical applications, this issue was studied in detail.

In chapter 7, the conclusions and the outlook for the future work are discussed. The experimental methods and equipment are summarized in chapter 3.

The present thesis addresses important questions related to crucial requirements for the design of enzymatic electrodes, the system integration, the optimization of the electroenzymatic reactor, the adjustment of optimal conditions toward high conversion and product selectivity issues. The aim is to develop an electroenzymatic reactor for glucose oxidation, and to show all the important steps in the electroenzymatic process development; starting from the understanding of the heterogeneous mechanism of biocatalysts at the electrode surface, all the way to the overall process evaluation.

2. Theoretical part

2.1 Enzymes as catalysts in electroenzymatic systems

Enzymes are proteins that catalyze almost all biochemical processes in living organisms. They accelerate the rate of a chemical reaction by a factor of 10^8 - 10^{20} in comparison to an uncatalyzed reaction, without themselves undergoing any permanent chemical change or being consumed. Most of the enzymes are macromolecule globular proteins with a molecular mass between 10–100 kDa. Their native structure and function is determined by their number and sequence of amino acids (primary structure). They are subsequently connected by hydrogen bonds and folded to a β -sheet and an α -helical structure (secondary structure). Further stabilizing interaction (e.g. disulfide bonds) makes an ordered tertiary three-dimensional structure, which is a prerequisite for the catalytic function of enzymes. However, this structure is only stable under specific conditions: at a temperature under 50° C and at a medium pH (exceptions are some enzymes that are isolated from microorganisms adapted to harsh conditions e.g. temperature above 90° C). A local cavity in the tertiary structure, with a characteristic construction and stereo-configuration, forms a catalytically active center, where substrates are converted to products [38]. The mechanism of catalysis follows the lock-and-key model proposed by E. Fischer in 1894, due to the precise fit between the enzyme active site and its substrate, which accounts for the high selectivity of enzyme catalysis (Fig. 2-1). Based on the type of the reaction they catalyze, enzymes are roughly classified into six main groups.

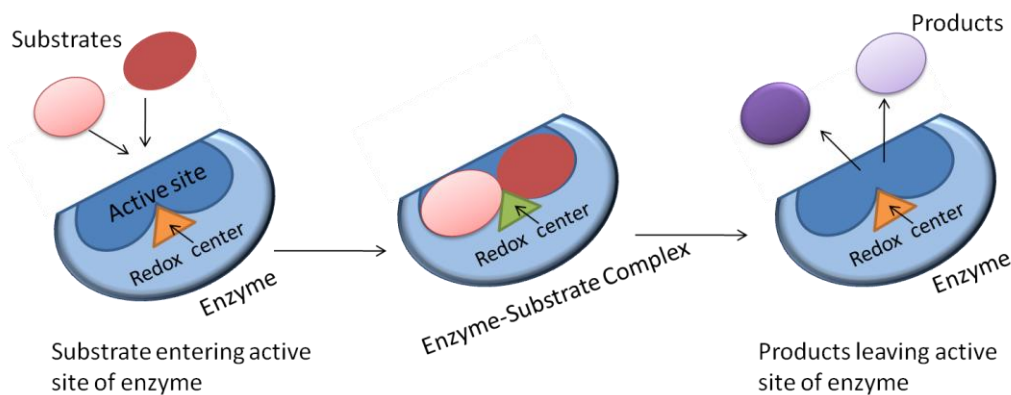


Fig. 2-1 Simplistic presentation of the enzyme and the “lock-and-key” mechanism for the group of oxidoreductases

Oxidoreductases represent a large group of enzymes relevant for bioelectrochemical systems, due to their ability to catalyze oxidation and reduction reactions by transferring hydrogen or electrons. They feature the presence of a redox cofactor, an essential, non-protein component, which can be tightly or loosely bound to the enzyme to assist the catalysis (Fig 2-2).

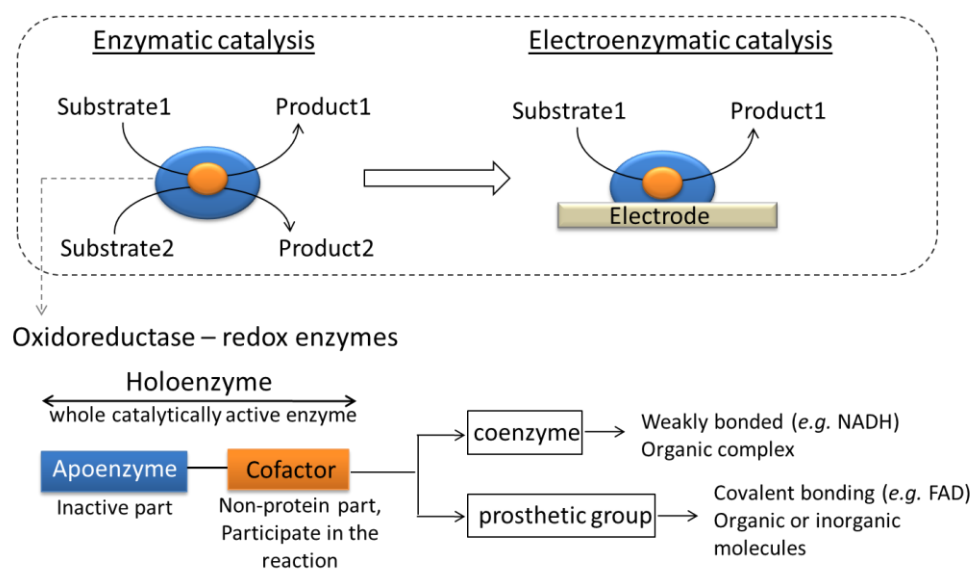
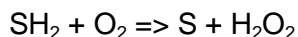


Fig. 2-2 Enzymatic vs. electroenzymatic catalysis and basic enzyme components (cofactor is further subdivided)

In the contexts of bioelectrochemical systems, the enzymes are catalyzing redox reactions at the electrode surface, thus the communication between the active site and conductive surface is crucial for the system to work efficiently. Based on the location of the active center, two different electron transfer mechanisms can be distinguished. If the active center is located at the periphery of the enzyme molecule (e.g. peroxidase), direct electron transfer (DET) can be achieved. This means that the electrons are exchanged directly between the electrode surface and the active site of enzyme. For efficient DET, the distance between the two must not be greater than 1.4 nm. However, most of the enzymes are not capable of exhibiting DET. Their cofactors are most often bounded to the internal sites in the secondary structure that make communication with the electrode difficult, resulting in a slow electron exchange rate. In such cases, the presence of a suitable redox-active molecule (mediator) is required (mediated electron transfer, MET).

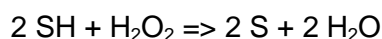
The following groups of redox enzymes are of the most importance for bioelectrochemical systems and are discussed in the present thesis.

Oxidases catalyze hydrogen transfer from the substrate to the molecular oxygen.



Glucose oxidase (GOx, EC 1.1.3.4), employed in this thesis as catalyst for glucose oxidation, is one of the most studied representatives of this group. It is a dimer, composed of two identical subunits with a mean molecular mass of 160 kDa and an average size of 8 nm [39]. The cofactor responsible for catalytic action is a tightly bonded flavin adenine dinucleotide (FAD) group. GOx catalyzes the oxidation reaction of D-glucose to glucono- δ -lactone, where hydrogen from the -CHOH group is transferred to FAD resulting in FADH₂. Formed glucono- δ -lactone spontaneously hydrolyzes to gluconic acid. Oxygen, as a natural electron acceptor in this cycle, receives hydrogen forming H₂O₂, while the reduced form of enzyme (FADH₂) is regenerated back to FAD. However, merging FAD enzymes with the electrode surface shows slow electron transfer rate due to the location of the active site, thus this enzyme is considered incapable of exchanging electrons with the electrode directly. The use of mediators as electron shuttles is necessary for the fast and efficient process of glucose oxidation at GOx-modified electrodes [40, 41].

Peroxidases catalyze oxidation of a substrate by hydrogen peroxide. An example of this group is horseradish peroxidase (HRP, EC 1.11.1.7).



HRP with a molecular weight of 42 kDa is one of the most studied members of the large class of heme peroxidase. It consists of four disulfide bridges, two calcium ions with ferriprotoporphyrin IX as the prosthetic group [42]. HRP catalyzes the reduction of hydrogen peroxide to water with the oxidation reactions of many organic and inorganic compounds [43]. The advantage of HRP utilization in bioelectrochemistry is in its capability to perform direct electron transfer when immobilized at the electrode surface. It is extensively employed for biosensors, enzymatic fuel cells and as a model enzyme in BES research [44]. In combination with GOx, in the enzymatic cascade at the electrode surface, glucose oxidation can be performed while H₂O₂ is simultaneously consumed by HRP, which is further directly regenerated at the electrode.

2.2 Enzymatic electrodes development

Enzymatic electrodes, comprising of immobilized redox enzymes at the conductive surface, are basic components of any bioelectrochemical system. Depending on the application, there are many devices employing enzymatic electrode structures e.g. biosensors for detection and quantification of an analyte of interest from a sample matrix, biofuel cells for energy conversion or electroenzymatic reactors for the purpose of the chemical synthesis. The overview of the general steps and key parameters relevant in enzymatic electrode development is presented in Fig. 2-3.

The first step in the design of bioelectrochemical process is the identification of a suitable biocatalyst for the reaction of interest. The electrode configuration will largely depend on the enzyme properties like shape, size, isoelectric point and position of active site, which determines the type of mechanism that the chosen enzyme is able to establish with the electrode surface. In the case of MET, the mediator must be able to transfer the electrons rapidly. Additionally, the reduction potential of the mediator is important, because it dictates the potential at which the electrode will be operated.

Generally, the enzyme features for biocatalysis can be manipulated and improved by enzyme engineering [45, 46]. However, as Cao *et al* [47] emphasized, the proper enzyme immobilization can overcome many problems related to their instability and activity under certain conditions, which could replace the need for extensive protein engineering.

The next step in the design pathway is the choice of the appropriate electrode support for the biocatalytic reaction. Biocompatibility, high conductivity and high surface area for the catalytic reaction are the crucial characteristics in the selection of the host material for enzyme immobilization. Carbon-based materials and stainless steel are typically employed electrode materials for bioelectrochemical systems, while the utilization of noble metals due to economic reasons is not desirable. In the early stages of bioelectrochemical research, monolayer electrode configurations *i.e.* enzymes immobilized in the monolayer at the electrode surface (flat electrodes) were developed [48, 49]. This electrode design was useful as a model system for fundamental research related to electro-enzymatic interactions.

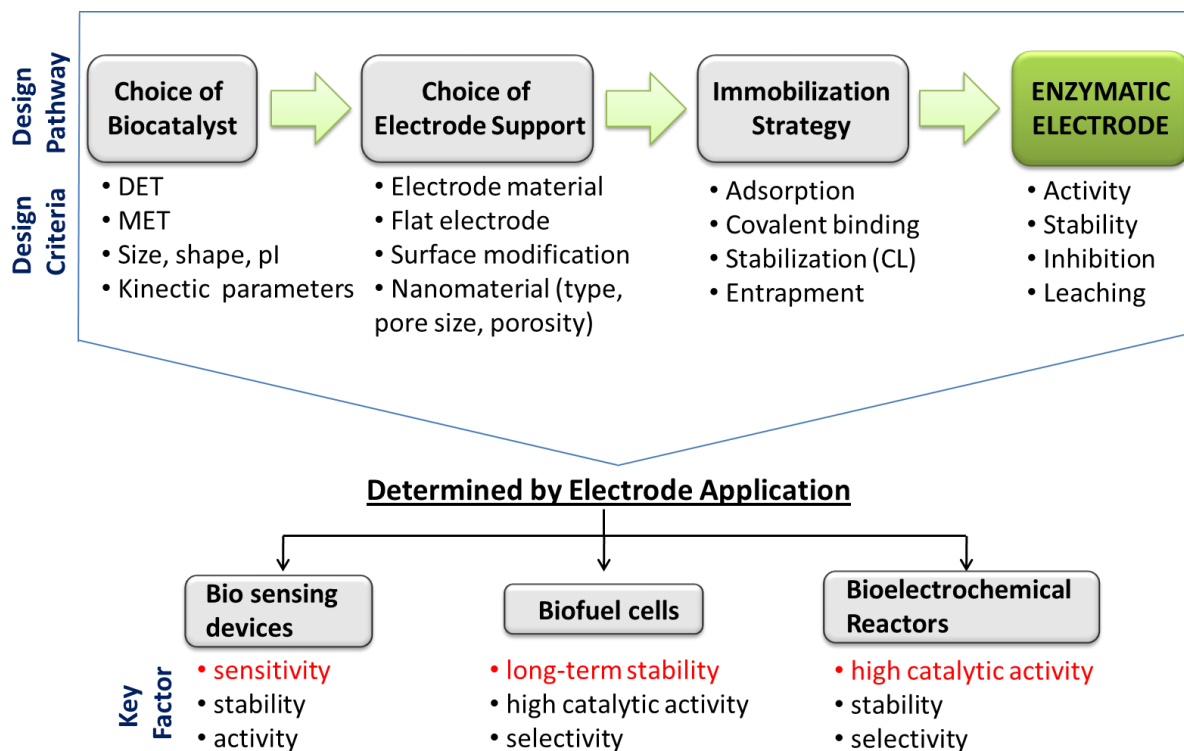


Fig. 2-3 Flow scheme of the design pathway and major characteristics for the enzymatic electrodes development

However, for improvement of electrode performance in terms of current densities, a significant increase in electrode active surface area is required. This can be manifested by utilization of nanostructured materials, resulting in so-called three-dimensional (3-D) electrode architecture. In the last decade, many publications have presented the applicability of different types of carbon based nanomaterials in biocatalysis [50-53]. Significant improvement in the electrode performance for biofuel cell application using materials like carbon nanotubes, carbon aerogel or mesoporous materials was demonstrated [54]. Additionally, the particular advantage of porous materials is the possibility to tailor pore size and pore geometry to correspond to the dimensions of the specific enzyme, preventing leaching and providing additional stabilization [47].

In addition to geometrical material characteristics, functionalization of nanomaterials has been applied in order to covalently attach higher enzyme loadings and promote DET [53]. Despite the mentioned benefits using this approach, lower activity due to the reduction in enzyme flexibility was reported [41].

The maximum electrocatalytic current depends on the density of the catalytic active sites (electroactive coverage) and the rate of catalysis per active site (turnover number of the enzyme). The current can be improved by choosing an appropriate immobilization method to ensure that all enzymes are electronically coupled to the electrode and that mass transport of substrates and products are not impeded [55]. Additionally, the accessible electrode surface area (material agglomeration degree) and the number of active enzymes (enzyme agglomeration, leaching, and denaturation) are directly dependent on the immobilization procedure. The structural electrode parameters like porosity and thickness are also determined by this choice. Thus, the enzyme immobilization procedure is the most important step in the electrode design.

Depending on the nature of enzyme–electrode interactions, the experimental methods for preparation of enzymatic electrodes can be classified into two main groups [56]. The first group is based on the enzyme physical immobilizations. The simplest approach is physical enzyme adsorption, where only weak interactions between the support and the enzyme are involved. This approach has been intensively studied at different electron conductive materials like gold or carbon surfaces and also with different types of nanomaterials [54, 57-59]. It has been shown that by using this method, enzymatic electrodes with high performance can be prepared, even without any surface modification in order to promote DET [59]. Another possibility for physical immobilization is the entrapment of enzymes into gel matrixes such as gelatin, collagen and polysaccharides. It has been demonstrated that this approach usually stabilizes enzymes more than through only physical adsorption [48, 50, 60]. The second group of methods is based on the covalent enzyme immobilization at the electrode surface, which requires functionalization of supports to create surface chemical groups for enzyme binding. Various surface modifications have been described in literature providing carboxyl, epoxy, acetyl or amino groups. These surface groups can either be further directly linked to enzymes or by using additional linkers like glutaraldehyde [61].

It is essential to produce stable electrodes with high performance in this stage of the research, since the reactor productivity is directly affected by the performance of single electrodes. Therefore, the systematic evaluation of all steps and the deep understanding of the relationship between immobilization strategy and electrode performance is highly relevant for further progress in the field of enzymatic electrodes for electroenzymatic reactor or biofuel cell applications.

2.3 Enzymatic electrochemical cells

In general, electrochemistry relates chemical energy and electrical energy transformations. In the electrolytic cell, the electrical energy is used to drive a chemical reaction ($\Delta G > 0$). On the contrary, in the galvanic cell the chemical energy released during a spontaneous chemical reaction, is transformed into electrical energy ($\Delta G < 0$). In BES, the catalyst of the chemical reaction is replaced with a biocatalyst, which can be a microorganism or an isolated enzyme [2]. In a similar manner as in conventional electrochemistry, both operation modes, electrolysis and galvanic cell, can be realized (Fig. 2-4).

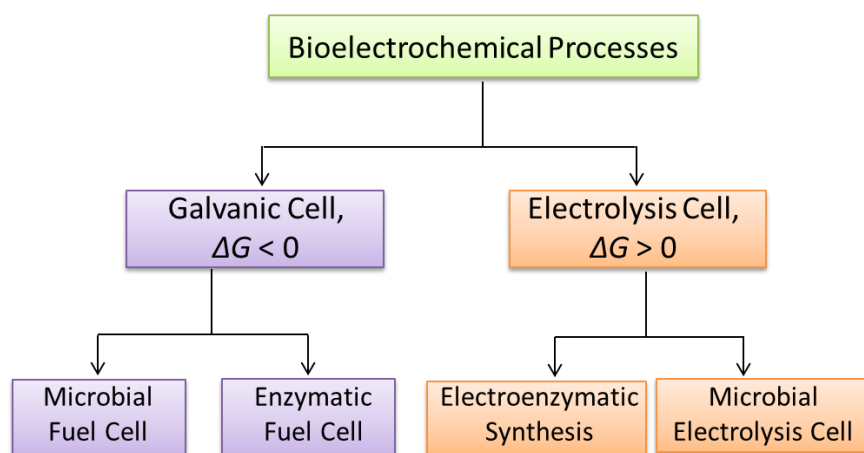


Fig. 2-4 Types of bioelectrochemical systems

Intensive research, during the past 20 years, in the field of bioelectrochemistry was mostly related to biosensors and biofuel cell applications. At the beginning of 1960s, the first report related to electric output in presence of *E. coli* and glucose oxidase was published [62]. Subsequently, a first evaluation of a biofuel cell was performed by Yahiro *et al.* in 1964 [63]. From then on, numerous publications evaluating the performances and applicability of enzymatic electrodes and enzymatic fuel cells have been reported [40, 41, 50, 64-66]. Furthermore, an emerging field application of bioelectrochemical systems is chemical production. From the electrochemical point of view, enzymes, used as catalysts, provide high process selectivity, which is a limitation in the classical electrolytic process. On the other hand, from the perspective of enzyme technology, electrochemistry offers a mass-free regenerating co-factor mechanism.

Reactor concepts used for bioelectrochemical systems are presented in Fig. 2-5. They have been classified in three main groups: a) separated, b) non-separated and c) packed or fluidized bed reactors [1]. In general, biocatalysts can be either immobilized at the working electrode or dispersed in the electrolyte. Based on system demands, the different operating modes (*i.e.* continuous, semi-batch and batch mode) and different reactors geometries (*i.e.* flat plate or tubular setups) can be chosen. The advantages and disadvantages between different reactor types are difficult to determine due to the large variety in setups, dimensions, conditions, electrochemical active surface areas and biological components. However, it has been shown that *e.g.* the membrane-less system using an air-cathode results in improved performance in comparison to the case when a PEM membrane was used [67]. Another study shows that the productivity of hydrogen peroxide is higher for a system based on a gas diffusion electrode compared to the fixed bed reactor system [68, 69].

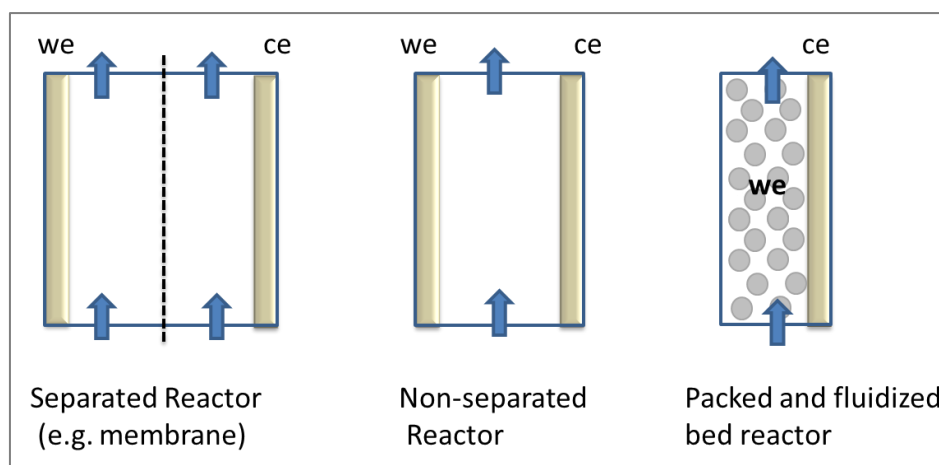


Fig. 2-5 Reactor concepts for bioelectrochemical processes [1]

Recent advances in reactor design used in BES for synthetic processes have been reviewed by Krieg *et al.* in 2014 [1]. Simple, compact and scalable designs are preferable in order to maximize the electroenzymatic reactor productivity and minimize the costs. Since bioelectrochemical reactors are conceptually equivalent to electrochemical reactors, the same criteria can be used for process evaluation and design optimization. From the cell potential analysis, valuable information on how to improve reactor performance can be gained [65, 70]. The cell potential of the electroenzymatic reactor can be defined by the equation presented in

Fig. 2-6. The actual cell potential (E_{cell}) is governed by the reversible cell potential ($E_{cell,0}$) and the potential losses (also referred to as overpotentials). There are three major contributions to potential losses: activation overpotential, concentration overpotential and ohmic losses. For a given current density, the values of these losses should be maintained as low as possible. As indicated in Fig. 2-6, there are different cell design parameters that can be changed in order to decrease the contributions of certain potential losses.

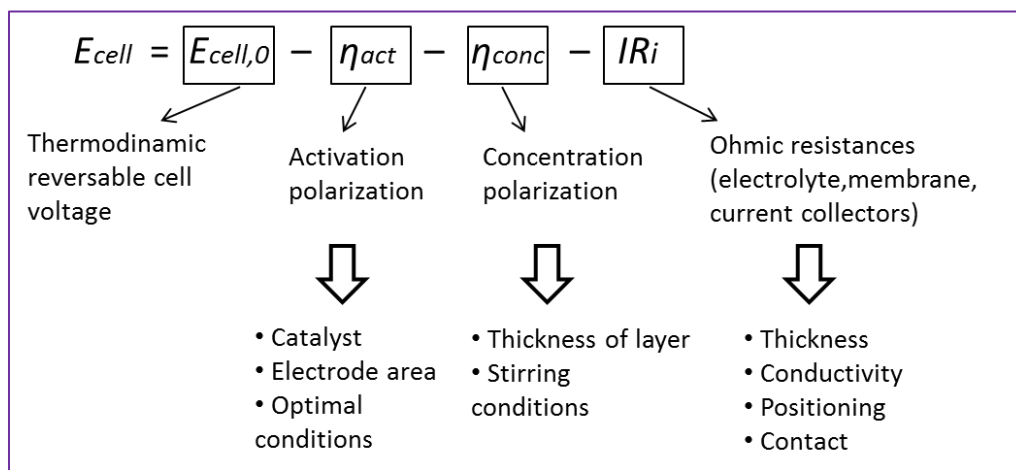


Fig. 2-6 Cell potential decomposition to main resistances and depended parameters [70]

At low currents, the activation overpotentials, caused by energy barrier to charge transfer from enzyme/mediator to the electrode, are dominant. These losses can be reduced by improving the amount of catalyst, increasing the electrode surface area or optimizing the operating conditions (pH, temperature). Ohmic losses occur due to resistance to charge transport in various components in the cell (e.g. electrolyte, membrane, electrode material, connections, current collectors). In order to minimize these losses, it is suggested to have small inter-electrode spacing, high electrolyte conductivity, and good contact between all components. Ultimately, concentration losses are caused by mass transfer resistance, which leads to a large concentration gradient resulted by the change in concentration of the reactant close to the electrode surface as the reaction proceeds. These losses are usually dominant at higher current densities. For example, they can be minimized by providing well-mixed solutions (stirring and recirculation conditions).

It is clear that for the development of an efficient electroenzymatic reactor, the utilization of a 3-D electrode with high activity and stability is required. The use of expensive separators (e.g. membranes), should be avoided if possible. The distance between electrodes should be kept minimal with high electrolyte and electrode conductivity.

In addition to desired reaction at the working electrode, the reaction at the counter electrode should be fast enough as well. It has been reported, especially in biofuel cell research, that due to the poor mass transfer or high activation overpotentials at the cathode, the electrochemical performance is drastically low [71]. Therefore, gas diffusion electrodes were suggested as counter electrodes to reduce mass transfer limitations. The use of platinum was replaced with suitable alternatives; such as metal-based carbon material or stainless steel to lower activation overpotentials [72-75].

Electrochemical cells can be used for energy and/or material conversions, thus different modes of operation are possible (Fig. 2-7) [70]. At zero current, the difference in the electrode potentials at both electrodes is defined as open circuit potential or OCP. The value of OCP is correlated with the reversible cell potential $E_{cell,0}$ (typical convention: $E_{cell,0} = E_{cathode,0} - E_{anode,0}$, can be calculated based on Nernst equation). However, the actual open circuit potential can deviate from the value of $E_{cell,0}$, as a result of internal currents and reactant crossover [76].

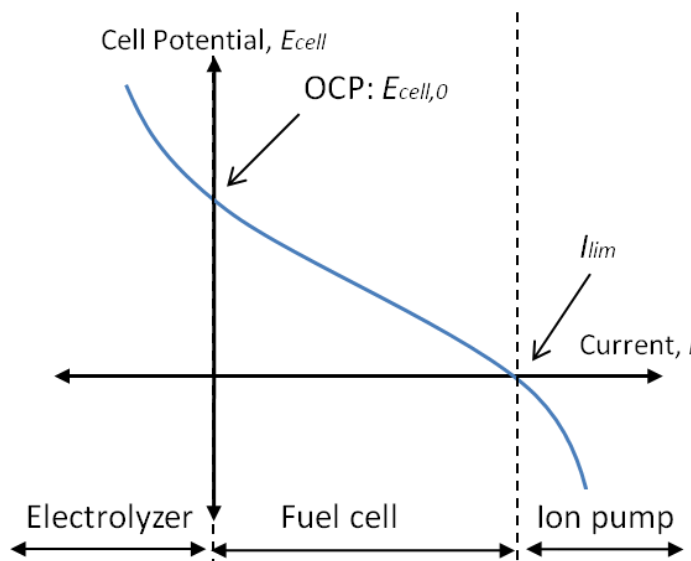


Fig. 2-7 Possible modes of electrochemical reactor operations [70]

In the fuel cell mode of operation, the cell current is positive, while the cell potential is below OCP due to internal resistances (in this mode power is positive, $P > 0$). If the current density is forced to extend under certain limiting value ($I > I_{lim}$), cell potential becomes negative, which presents a special type of electrolysis, called ion pump mode. The direction of current is the same as in the fuel cell mode, but the transport of the charged species is supported by the external electric energy input. If the negative currents are applied, cell potential exceeds the value of OCP ($E_{cell} > E_{cell,0}$) and this represents the classical electrolysis mode ($P < 0$). In the case of partial oxidation reactions of hydrocarbons, the simultaneous generation of valuable products and energy in the fuel cell mode is possible [8]. The electroenzymatic reactor investigated in this study will be operated in this co-generation mode or in the ion pump mode.

Additionally, the focus of the output performance is determined by the applications (fuel cell or production system). For example, for energy conversion, the power (P) that is calculated from the current (I) and cell potential (E_{cell}), allows the characterization and comparisons of the biofuel cell performances (eq. 2-1). Since the cell potential is determined by the enzymatic electrode potentials, it is desired that the oxidation potential is kept as negative as possible and the reduction as positive as possible. The power output is usually normalized to the active surface for calculation of power density.

$$P = E_{cell} \times I \quad \text{eq. 2-1}$$

On the other hand, production processes are related to the amount of reactant converted to products. By Faraday's law, the total number of moles (n) produced or consumed during an interval of time (t), can be calculated from the charge passed through (*i.e.* flow of current (I)), (eq. 2-2). In the equation, z is the number of electrons and F is Faraday's constant (96485 C mol⁻¹).

$$n = \frac{Q}{zF} = \frac{I t}{zF} \quad \text{eq. 2-2}$$

The reactor performance can be evaluated by a number of parameters. In order to measure the degree of which a reaction in the electrochemical reactor has preceded, the conversion (C) is introduced. It can be defined as the amount of reactant converted per number of reactant at the beginning (eq. 2-3).

$$C = \frac{\text{Moles of Reactant consumed}}{\text{Moles of Reactant total}} \quad \text{eq. 2-3}$$

However, due to parallel reactions and/or consecutive reactions with intermediate steps that take place, an ideal situation of the reactant conversion only to a desired product is rarely achieved. Therefore, a variety of products can be obtained in addition to the product of interest. Generally, the undesired products can considerably reduce the market value of the product and they have to be separated. Therefore, the relative production can be also discussed in terms of two additional parameters, selectivity (S) and yield (Y). Different definitions regarding selectivity and yield can be found in literature. In this study, selectivity is defined as the amount of product divided by the amount of converted reactant (eq. 2-4). It is the indication of the amount of the specific product formed in the reaction. On the other hand, the yield is expressed by the ratio of the amount of the product and the total amount of reactant at the beginning, and is a product of conversion and selectivity (eq. 2-5). It expresses the amount of the desired product in the total reaction mixture and indicates to the complexity of the downstream process.

$$S = \frac{\text{Moles of Product}}{\text{Moles of Reactant consumed}} \quad \text{eq. 2-4}$$

$$Y = \frac{\text{Moles of Product}}{\text{Moles of Reactant total}} \quad \text{eq. 2-5}$$

The most common way to evaluate the reactor production capacity is the rate of the species production per unit volume of reactor or electrode surface (*i.e.* space time yield). Space time yield (STY) represents the mass of the product formed per time and volume of the reactor (eq. 2-6) or the electrode surface (eq. 2-7) [1]. For comparison of different heterogeneous processes, one can also compare productivity in terms of unit mass of catalyst, unit surface of catalyst or even specific surface (per unit volume).

$$STY = \frac{\text{MASS}_{\text{Product}}}{\text{Time Volume}_{\text{Reactor}}} \quad \text{eq. 2-6}$$

$$STY = \frac{\text{MASS}_{\text{Product}}}{\text{Time Area}_{\text{Electrode}}} \quad \text{eq. 2-7}$$

In general, STY is proportional to the applied current density and specific electrode surface area. The current density is determined by a number of complex phenomena associated by enzyme-electro kinetics and mass transport conditions, while the specific surface depends on the cell and type of electrode structure used. Clearly, high specific surfaces are required to achieve high space time yields, especially for systems with low current densities. Thus, there has been growing interest for the development and use of 3-D enzymatic electrodes for synthetic redox reactions, instead of conventional two-dimensional monolayer enzymatic electrode in parallel plates or other configurations [1].

3. Experimental part

3.1 Chemicals and materials

Biocatalysts, glucose oxidase (EC 1.1.3.4, GOx) from *Aspergillus niger*, bilirubin oxidase from *Myrothecium verrucaria* (EC 1.3.3.5, BOD) and catalase (EC 1.11.1.6) from bovine liver, were purchased by Sigma-Aldrich. Horseradish peroxidase (EC 1.11.1.7, HRP) from *America rusticana* was provided by Serva Electrophoresis GmbH.

Hydrogen peroxide (H₂O₂, 30%) and gelatin for microbiology were supplied from Merck. The hydrogen peroxide solution, with concentration of 3%, was prepared daily by dilution of 30% hydrogen peroxide. Potassium dihydrogenphosphate was provided by Carl Roth GmbH&Co.KG. All other reagents, D-glucose, D-glucose-1-¹³C, tetrathiafulvalene (TTF), poly(vinylidene fluoride) (PVDF), glutaraldehyde, 1-methyl-2-pyrrolidone (MP), and sodium phosphate dibasic were purchased from Sigma-Aldrich. All solutions were prepared using ultrapure water from Millipore and all chemicals were of analytical reagent grade.

Vulcan XC72R nanomaterial (Vulcan) that was used for preparation of porous enzymatic electrodes, was provided by Cabot Corporation. Coral Carbon (CC), Carbon Hollow Sphere (CHS) and Carbon Aerogel (CA) were supplied by a group of Prof. Dr. Markus Antonietti (Max Planck Institute of Colloids and Interfaces, Potsdam, Germany). Spectroscopically pure carbon rods with impurities equal to or less than 2 ppm were supplied by Ted Pella, 330 INC, USA. Non-treated (in text names as hydrophilic) Toray paper, type TGP-H-060, was purchased from Toray Deutschland GmbH. To obtain hydrophobic Toray paper, non-treated Toray paper was immersed in 25.1% of polytetrafluoroethylene (PTFE) emulsion for 60 min and after that dried in the oven at 90 °C. Highly oriented pyrolytic graphite (HOPG), also supplied from Ted Pella, 330 INC, USA was used for AFM experiments.

DyLight 350 NHS ester dye, with an excitation wavelength of 353 nm and an emission wavelength of 432 nm, used for protein labeling in the fluorescence measurements, was provided by Thermo scientific.

3.2 Enzymatic electrode preparation: monolayer electrode (flat surfaces)

3.2.1 HRP-modified graphite surface for electrochemical studies

Spectroscopically pure carbon (SPG) rods were cut in 11 mm diameter discs and were used as supports for enzyme adsorption. Before modification with enzymes, they were polished by fine emery paper (P500 and P1000), rinsed with ultrapure water and then further polished with ordinary white paper to smoothen the surface [77, 78]. As shown in Fig. 3-1, SPG discs were mounted in the sample holder used in half-cell experiments.

HRP modified electrodes were obtained by placing 50 μl of HRP solution in phosphate buffer (6 mg ml^{-1} , pH 6.00) on the top of the SPG disc and left for 2 h under ambient conditions. After that, they were washed with a phosphate buffer solution (PBS) and used for electrochemical measurements. The surface area of the electrode that was used for HRP adsorption and for electrochemical measurements was 0.28 cm^2 .

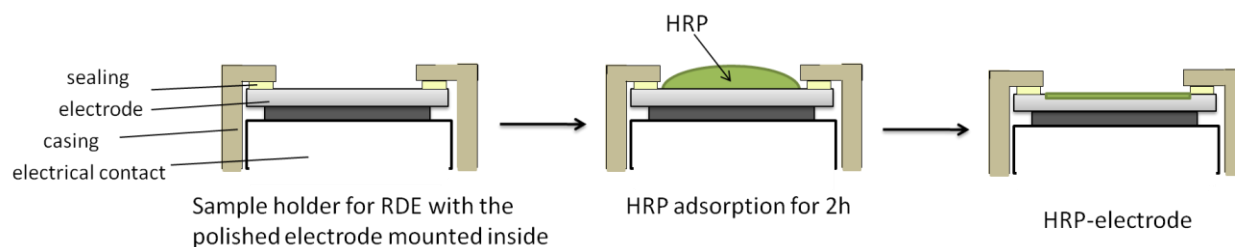


Fig. 3-1 Preparation of HRP modified electrodes at spectroscopically pure carbon (SPG) used in the electrochemical experiments

For obtaining cross-linked electrodes, HRP modified SPG discs were dipped in glutaraldehyde solution (1, 2, 3, 4 or 5% in ultrapure water) and left for 1 minute. Subsequently, electrodes were washed with phosphate buffer solution and were ready for use.

3.2.2 Enzymatic electrodes for microscopy studies

For atomic force microscopy (AFM), HOPG, previously polished and cut in the size of 5 mm x 4 mm, was used. For preparation of HRP electrodes, a droplet of diluted HRP solution in phosphate

buffer (6 mg ml⁻¹, pH 6.00 and pH 7.00) was placed on the top of the HOPG and left to dry. The dilution was made in order to obtain a monolayer on the HOPG surface.

For fluorescence microscopy tests, both SPG and HOPG supports were employed. Before surface modification, the enzyme was labeled in the following way: HRP solution (pH 7.00, 2 mg ml⁻¹) was mixed with fluorescence dye dissolved in dimethylformamide (DMF) and left for 1 h at room temperature. Afterwards, the excess of non-reacted dye was removed by dialysis for 4 h using three dialysis buffer changes. The labeled enzymes were stored at 4 °C. For modification of SPG and HOPG surfaces, a droplet of diluted HRP solution was applied on an appropriate surface and left to dry.

For obtaining fluorescence microscopy images with carbon nanomaterial, 1 mg of carbon material (Vulcan or Coral Carbon) was added to the HRP-labeled solution (2 mg ml⁻¹, pH 7.00). The mixture was stirred and cast on the glass plate to be used for microscopy investigation.

3.3 Electrode preparation: porous enzymatic electrodes (3-D electrodes)

3.3.1 Vulcan-Gelatin procedure

Porous enzymatic electrodes were prepared following two different procedures. The first one, referred in text as “Vulcan-Gelatin” was based on gelatin as binder and cross-linking procedure. For the preparation of these enzymatic electrodes, stainless steel discs (11 mm diameter) were used as mechanical and electrical support. The disks were made in-house, with the dent of 6 mm that served for enzymatic electrode preparation (Fig. 3-4).

The procedure for preparation of Vulcan-Gelatin porous enzymatic electrode involves several steps (Fig. 3-2). At first, gelatin solution (2% in ultrapure water) was prepared by heating the solution up to 37 °C. In the next step, 20 mg of respected nanomaterial (Vulcan or nanomaterials obtained from MPI Potsdam) and 10 mg of biocatalyst (HRP, GOx or BOD) were suspended in 1 ml gelatin at 37 °C. Next, the stainless steel discs were degreased with acetone and 50 µl of described ink was cast on the disk. At the end, after drying at room temperature, electrodes were cross linked. The cross-linking procedure consisted of the following: the Vulcan-Gelatin electrodes were dipped in 5% glutaraldehyde solution in ultrapure water and left for 1

minute. Then, electrodes were washed with deionized water and were stored in the refrigerator at temperature $-18\text{ }^{\circ}\text{C}$.

For preparation of the GOx-TTF/Vulcan-Gelatin electrode, 10 mg of TTF, which served as the mediator, was additionally added in the described Vulcan and biocatalyst suspension. When GOx-HRP/Vulcan-Gelatin electrodes were prepared, the mixture of GOx and HRP with optimized ratio of 1:3 ($3:9\text{ mg ml}^{-1}$) was applied.

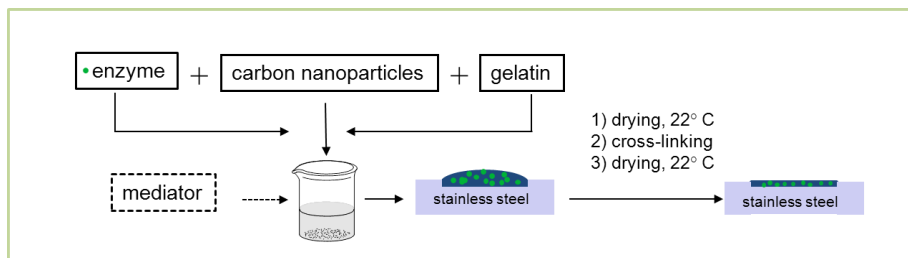


Fig. 3-2 Schematic presentation of the Vulcan-Gelatin preparation procedure

3.3.2 Vulcan-PVDF procedure

For the second procedure, denoted as “Vulcan-PVDF”, the binder of choice was poly(vinylidene fluoride) (PVDF). Following this procedure (Fig. 3-3), 20 mg of carbon nanomaterial was first dissolved in 1 ml of 0.25% PVDF in MP and left in the ultrasonic bath (Bandelin Sanorex, Germany) for 3 minutes. Next, the ink was cast on the SPG discs or Toray paper (for further details, see next section 3.3.3). The prepared electrodes were left to dry at $60\text{ }^{\circ}\text{C}$ for 5 h. After the drying step, the electrodes were ready for modification with enzymes. For preparation of Vulcan-PVDF with TTF, 10 mg of TTF was added to the suspension.

For preparation of the HRP/Vulcan-PVDF electrodes, $50\text{ }\mu\text{l}$ of HRP solution (6 mg ml^{-1} in 0.1 M PBS) was placed on the top of already prepared Vulcan-PVDF electrode, which was mounted in the sample holder (as shown in Fig. 3-1) and left for 2 h at room temperature to complete adsorption. If the adsorption time was different (18 h), it was specified in the result section. Afterwards, electrodes were washed with 0.1 M PBS and were ready for use.

Next, for preparation of the GOx-HRP/Vulcan-PVDF electrodes, enzyme cascade solutions with different ratios (1:1 ($6:6\text{ mg ml}^{-1}$), 1:2, 1:4, 3:1, 4:1 of HRP:GOx) were prepared in 0.1 M PBS. Afterwards, $50\text{ }\mu\text{l}$ of GOx-HRP mixtures were cast on Vulcan-PVDF electrodes, mounted in sample holders, and left to adsorbed for 2 h. The optimal ratio was estimated to be 3:1, and if not denoted differently, this enzyme ratio was used. After enzyme adsorption, the

prepared electrodes were rinsed with PBS solution and were ready for electrochemical experiments.

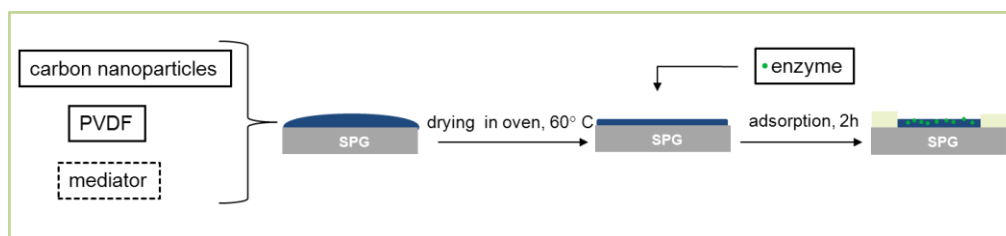


Fig. 3-3 Schematic presentation of the Vulcan-PVDF preparation procedure

3.3.3 Electrodes used in electrochemical cells

The difference between the electrodes used in half-cell and the electrodes tested in the electrochemical cell (reactor/fuel cell), is in the geometrical surface area. The electrodes are presented in Fig. 3-4.

The ones tested in the 3-set up, were prepared using the disks (SPG or stainless steel) with a diameter of 11 mm and they were mounted in sample holder for RDE (6 mm opening) thus, the electrochemical surface area (geometrical) used in experiment was 0.28 cm². The electrode surface area for the electrochemical reactor was 1 cm². As an anode, the GOx-TTF/Vulcan-Gelatin electrode, prepared as described in section 3.3.1, was used. GOx-HRP (150 μl, HRP:GOx - 3:1) or BOD (150 μl, 10 mg ml⁻¹), was adsorbed on the Vulcan-PVDF (Vulcan-PVDF electrode prepared as described in previous section) and was employed as cathode side. For the adsorption of the enzymes, the surface area was fixed to 1 cm² by the stainless steel frame, as shown in Fig. 3-4.

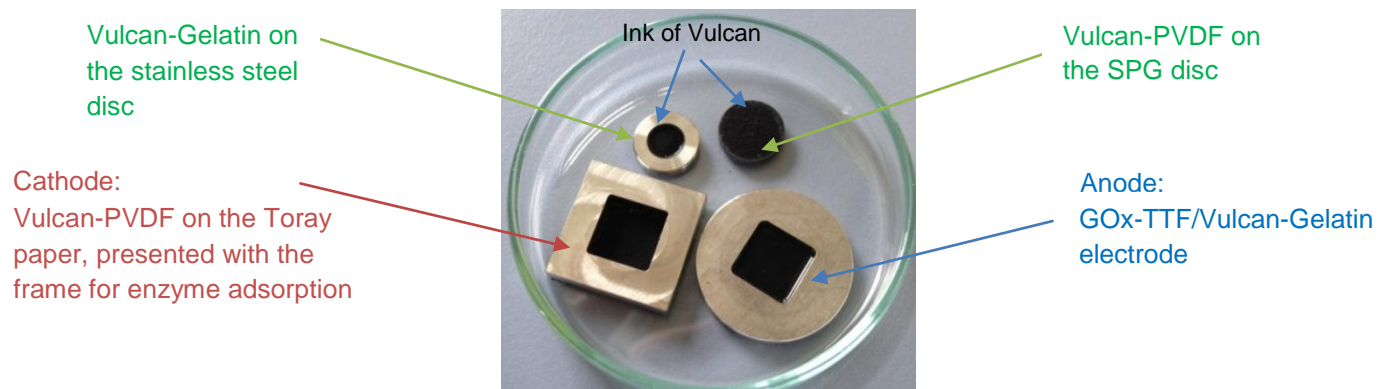


Fig. 3-4 Electrodes used for the electrochemical measurements

3.4 Half-cell electrochemical investigations

3.4.1 Measurements setup

The three-electrode setup, presented in the Fig. 3-5, is one of the most common electrochemical setup used for investigations of half-cell reactions. In this case, the reaction of interest takes place at the working electrode (WE). The reference electrode (RE) is typically the electrode with a well-known and relatively stable redox potential, while the counter electrode (CE) is used to close the current circuit. In this kind of electrochemical set up, the current flows between WE and CE, while the potential of WE is controlled with respect to RE.

The electrochemical cell used for the half-cell analysis, is a double-jacketed Pyrex glass cell provided by Rettberg, with the PTFE cover (Fig. 3-5). The rotating disk electrode (RDE, Radiometer Analytical, model ED101) was used as a working electrode. Saturated calomel electrode (SCE, REF421, Radiometer Analytical) was employed as a reference and Pt (M231P, Radiometer Analytical) was implemented as a counted electrode. The electrolyte was a 0.1 M phosphate buffer, prepared at different pH values and supplied with nitrogen or oxygen.

Glucose oxidation at the GOx-electrode, hydrogen peroxide reduction at HRP-modified electrode and the oxygen reduction reaction by BOD-electrode were characterized separately in the half-cell measurements using the three-electrode configuration. Subsequently, the enzymatic electrodes were integrated and tested in the electrochemical cell (2-electrode setup).

3.4.2 Rotating disk electrode (RDE) as WE

In order to have defined mass transport conditions, the rotating disk electrode was used. The working principle of RDE is shown in Fig. 3-6. As can be seen, the disk rotates with the angular velocity (ω) in the electrolyte solution, bringing up liquid along the rotation axis and flinging it out radially.

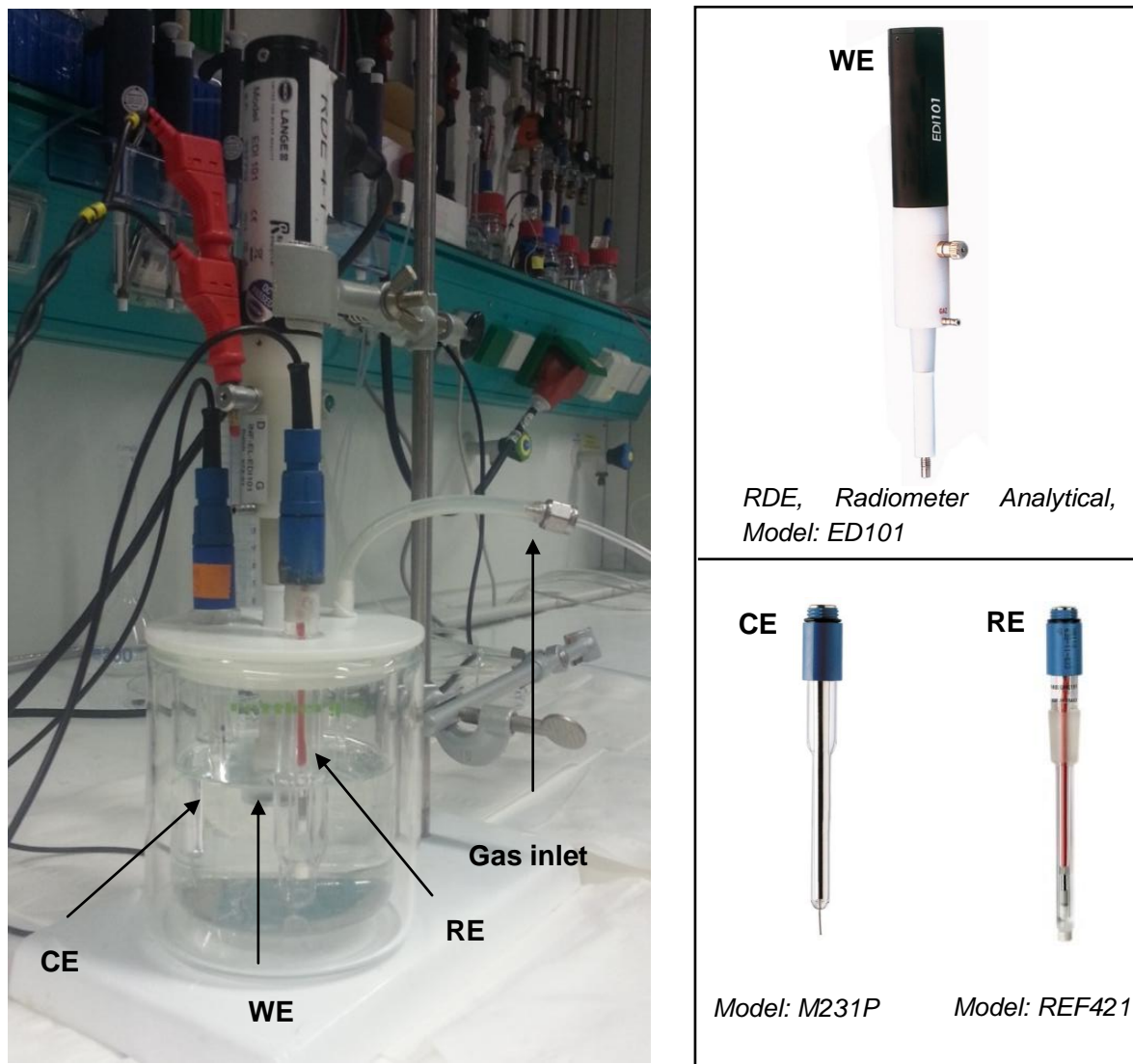


Fig. 3-5 Schematic presentation of the 3-electrode set up (left), working, counter and reference electrode (right)

In the close vicinity of the electrode surface, a Nernst diffusion layer is formed. It is assumed that in this layer, the transport of reacting species is determined by diffusion. The thickness of this layer is dependent on the chosen rotation rate. Increasing the rotation rate will decrease the layer thickness and improve mass transport. Thus, in the present thesis, different rotation rates were investigated. However, the effect of enzymatic electrode stability also has to be taken into account, when choosing a working rotation rate. Namely, depending on the immobilization procedure and method for enzyme stabilization, the leaching effect could be

prompted at higher rotation rates. Thus, after mass transport and electrode stability investigations, a rotation rate of 400 rpm was chosen for all experiments in order that all criteria are satisfied.

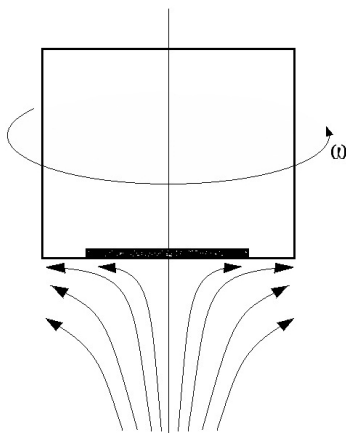


Fig. 3-6 Qualitative flow field at the rotating disk electrode

3.5 Electroenzymatic reactor setup

The schematic drawing of the electroenzymatic reactor with its components is shown in Fig. 3-7. It is a membrane-less, flow-through reactor with a similarity to developed fuel cell device in Ivanov *et al.* [79]. Enzymatic anode and cathode were placed facing each other in the transparent cell body (component 4), separated by a single channel of 3 mm width. At the cathode side, a double layer of Toray paper was implemented. One layer was hydrophilic and it was employed as a support for the catalyst layer (component 5a), while the second layer was hydrophobic (component 5b). It served as a gas diffusion layer and was directly contacted with the graphite flow-field (component 6) and used for gas distribution. A gold-plated copper plate (component 7) and stainless steel cover (component 1) were used as current collectors at the cathode and anode side, respectively.

The scheme of the experimental facility is presented in Fig. 3-8. The reactor was mounted vertically in an appropriate holder and a glucose solution, prepared at least one day before, was recirculated from well-mixed reservoir ($V_r = 70$ ml) with different flow rate ranges from 0 till 14 ml min^{-1} . Oxygen was supplied to the cathode from the gas phase (flow rate ca. 500 ml min^{-1}). The concentration of the glucose solution was 20 mM. All reactor experiments were performed at pH

6.0 in a 0.1 M phosphate buffer at room temperature. The reactor experiments were performed as a two-electrode set up, which was achieved by connecting the reference to the counter electrode (Cable connection: Anode: WE-S; Cathode: CE-RE). Additionally, during the reactor operation, the anode and cathode electrode potentials were measured with the help of the reference electrode (RE2, component 10) that was installed in the reactor design. Measurements of the anode potential (between RE2 and WE-S) and cathode potential (between RE2 and CE-RE) were achieved with two external voltmeters.

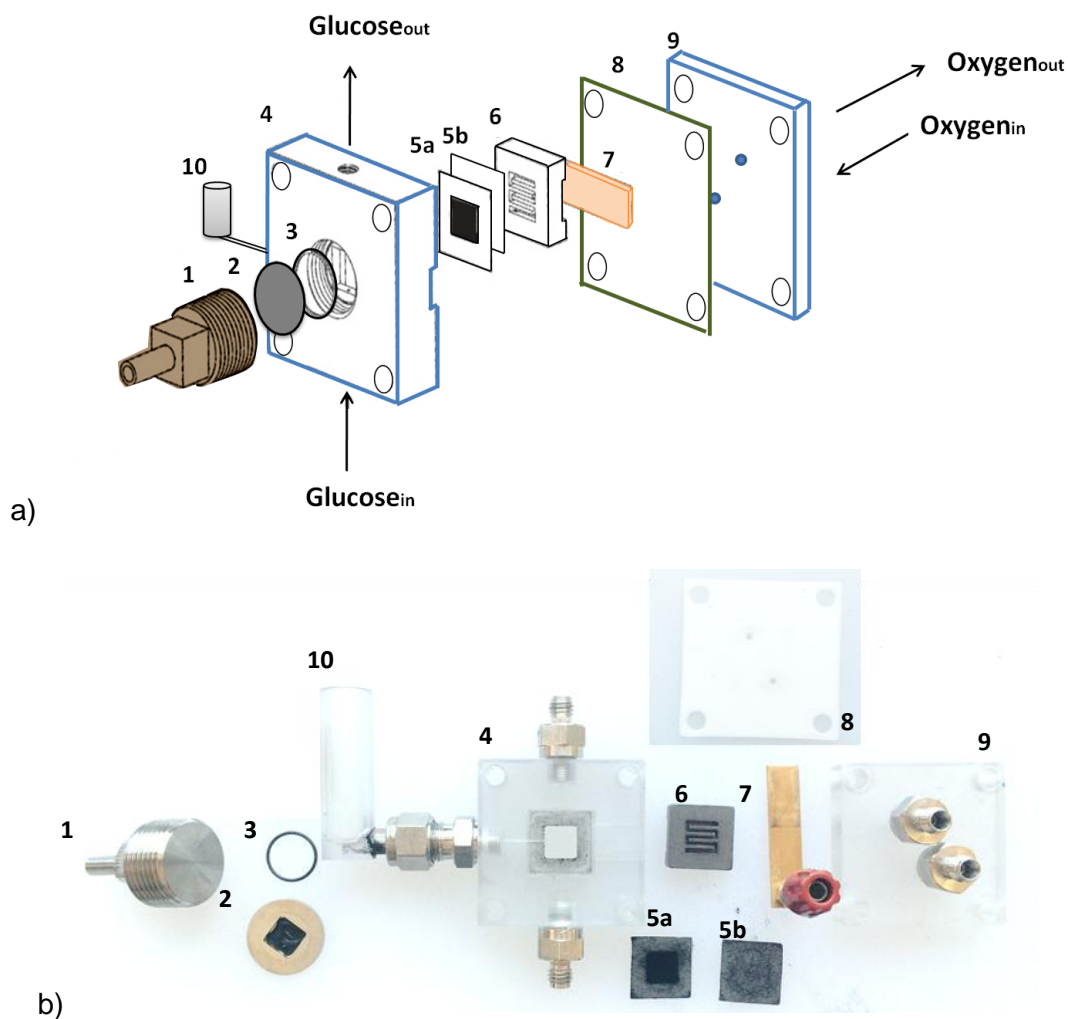


Fig. 3-7 a) Schematic representation and **b)** laboratory parts, of a BFC device with components as follows: 1-anode current collector, 2-stainless steel disc with enzymatic catalyst, 3-O-ring, 4-cell body, 5a-toray paper with enzymatic catalyst, 5b-toray paper with PTFE, 6-graphite flow field, 7- cathode current collector, 8-PTFE gasket, 9-end plate 10- Reference electrode

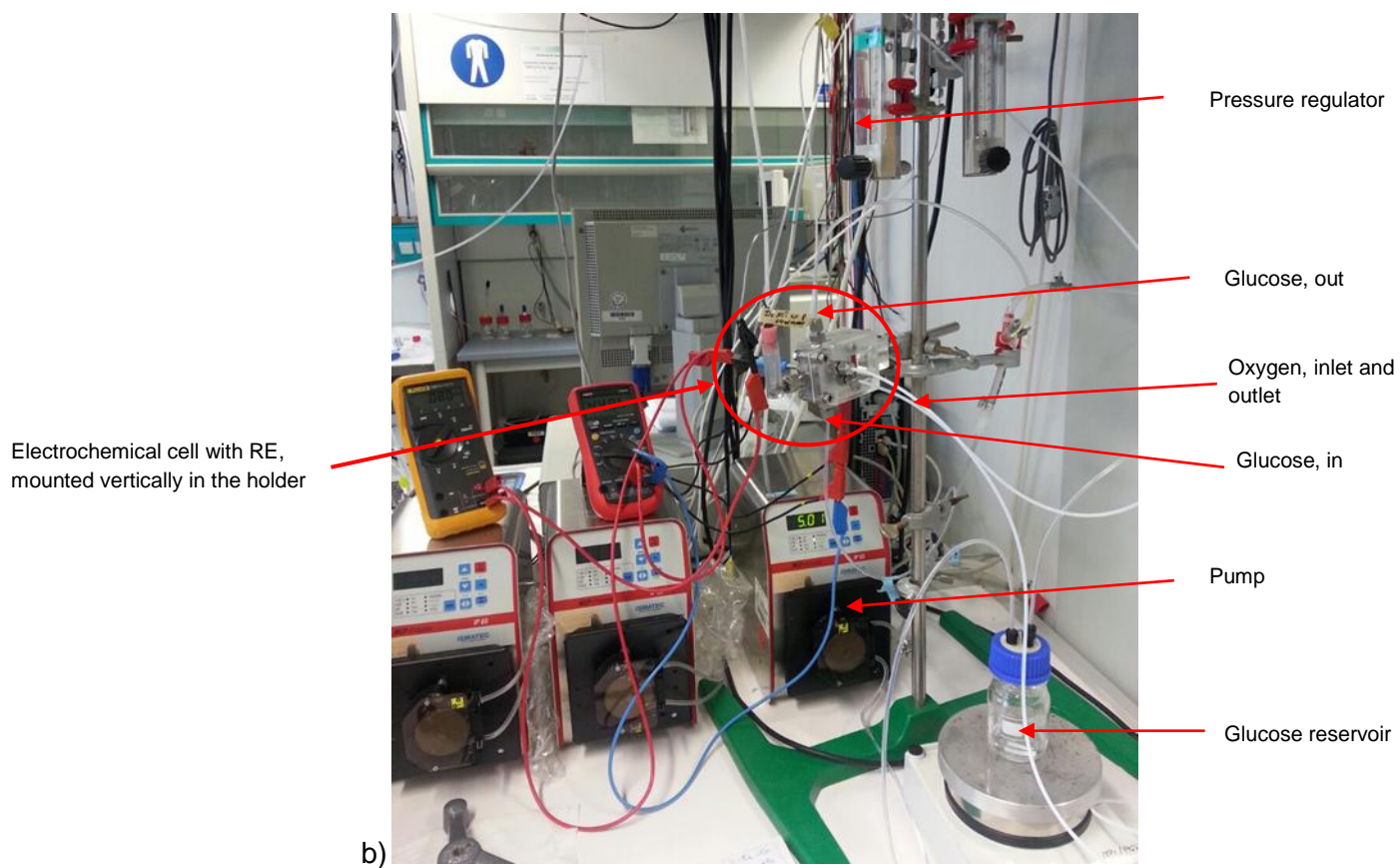
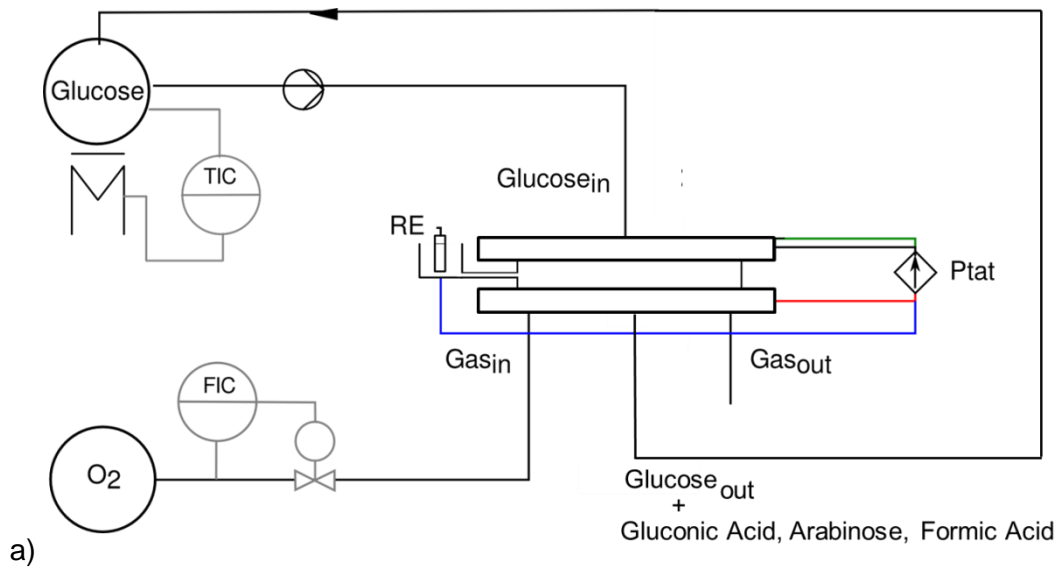


Fig. 3-8 Electrochemical reactor: **a)** schematic presentation **b)** laboratory setup

3.6 Measurements and characterization methods

All electrochemical experiments were carried out using Autolab potentiostat (PGSTAT302, Eco Chemie). The potentials presented in the thesis were cited versus SCE (0.24 V vs. Standard Hydrogen Electrode (SHE)). All of the results were presented in respect to current density (obtained current was divided by geometrical electrode surface area). As already described, the reactor was operated as a 2-electrode system, while for all half-cell investigations, a 3-set up with RDE was implemented.

3.6.1 Cyclic voltammetry measurements (CV)

Cyclic voltammetry was employed for characterization and comparison of electrochemical active surface area of the electrodes prepared with different nanomaterials and immobilization procedures. Measurements were done in 0.1 M PBS as electrolyte under nitrogen atmosphere. The potential range for HRP-based electrodes (HRP and GOx-HRP) was between 0.0 V and 0.6 V vs. SCE. For the electrodes employing GOx and TTF as the mediator, the potential range was between -0.2 and 0.2 V vs. SCE.

3.6.2 Steady state measurements (SSV)

Polarization curves were obtained as steady state data extracted from chronoamperometry measurements after 60 or 120 s at constant potential, with potential step of 0.05 V. The potentials used, were the same as described for CV measurements.

3.6.3 Chronoamperometry (ChA)

ChA was used to obtain stability measurements for the enzymatic electrodes. In these experiments, electrodes were kept for 7 h at constant potential, while the change of current was measured. It is important to note that the concentration of the reactant during this period of time was kept constant. This was achieved in the 3-set up, by using a small ratio between electrode surface area (0.28 cm²) and the total reaction volume (250 ml). Additionally, based on the current obtained in this analysis, the change in reactant concentration during the time was calculated according to the Faraday's law (presented in result section). It was proved that, due to low conversion of the reacting species, concentration change in the electrochemical cell can be considered negligible. These results make this kind of experiment suitable for enzymatic electrode stability analysis.

3.6.4 Fluorescence microscopy (FM)

Fluorescence microscopy was employed for visualization of enzyme distribution at the electrode surfaces. The images were obtained with the Imager M1 Microscope, Carl Zeiss. The objective, EC Plan Neofluar and filter set with excitation 365, beamer splitter 395 and emission 445/50 were used. In order to obtain high-contrast images and at the same time to avoid saturation, different exposure times were used for different images (for further information please see the respective figure captions in the results section). The FM measurements were done with help of Helga Tietgens (Max Planck Institute (MPI), Magdeburg).

3.6.5 Atomic-force microscopy (AFM)

AFM measurements were performed in air using 5500 SPM (Agilent Technologies), with the tapping mode (Acoustic AC Mode). A rectangular silicon cantilever (PPP-NCSTAuD, Nanosensors) with a nominal force constant of 7.4 N m^{-1} was used for the measurements. All AFM microscopy images were obtained with the help of Dr. Dana Hermsdorf (MPI, Magdeburg).

3.6.6 Scanning electron microscopy (SEM)

Cross-sectional scanning electron microscopy (SEM) analysis of the enzymatic electrodes was performed using XL30 FEG (FEI Company, Vulcan electrode, Fig. 4-18) and CURRENTA (Figures with CC, CA, CHS, Fig. 4-7, 4-11). For the SPG surface (Fig. 4-22), microscopy images were obtained by Surfaceprofiler TENCOR P_10, Firma Tencor Instruments. The SEM was obtained with the help of Markus Ikert and Bianka Stein (Max Planck Institute, Magdeburg).

3.6.7 Nuclear magnetic resonance spectroscopy (NMR)

Nuclear magnetic resonance spectroscopy (NMR, Bruker DPX 400 MHz and Bruker AV 600 MHz, AVANCE III, Bruker) was used for obtaining information of system conversion, selectivity and products yields. The analysis and discussions related to NMR results were supported by Prof. Edgar Haak (Institute for Chemistry, Otto von Guericke University, Magdeburg)

3.6.8 Enzymatic assay for concentration test

The glucose concentrations were measured spectrophotometrically (UV/Vis spectrophotometer, SPECORD S600, Analytikjena, Jena, Germany) using glucose assay kits (UV-test, R-Biopharm, Darmstadt, Germany).

4. Design of the enzymatic electrodes

A bioelectrocatalytic process requires the development of highly active and stable enzymatic electrodes *i.e.* immobilization of redox enzymes with conservation of their activity in the heterogeneous state at the electrode surfaces. Basic criteria for enzymatic electrode development are 1) good electrical contact between enzymes and electrode surface for efficient electron transfer, which can be improved by the right choice of an immobilization procedure and 2) high biocatalyst loading per electrode volume in order to provide high electrode performance. The strategy to increase current densities per geometrical surface area is a development of multilayer enzymatic electrodes: the so-called 3-D electrodes [40, 65, 80, 81]. 3-D electrode design is based on utilization of various materials: 1) enzymes as catalysts, 2) nanomaterials for increase of the active surface area and 3) additives like hydrogels or cross-linkers to enhance the electrode stability [56]. Despite broad research in this direction, the state-of-the-art enzymatic electrodes have a very low performance (in the range of a couple of $\mu\text{A cm}^{-2}$), [40]. This implies that despite high surface area materials and possibility of high catalyst loading, the enzyme utilization *i.e.* biocatalyst in the active state within the electrode structure is low (Fig. 4-1).

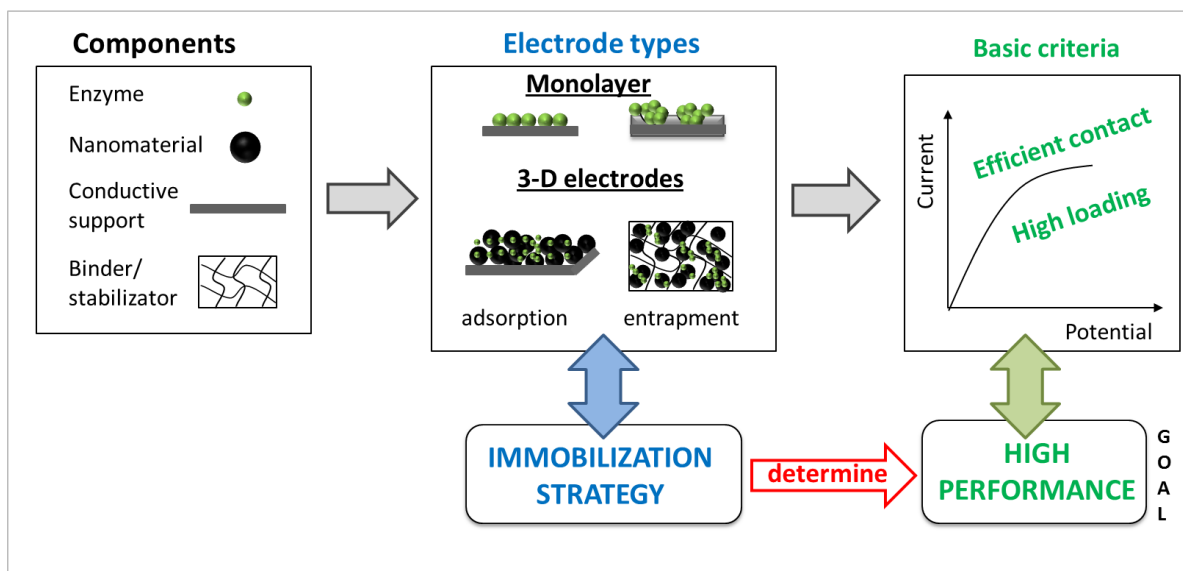


Fig. 4-1 Schematic representation of optimal electrode designing, including different electrode types and criteria for electrode performance with targeted goal

Development of 3-D enzymatic electrodes with high enzyme utilization is still challenging. The influence of the immobilization procedure on the electrode structure and the organization of the mentioned components within (nanomaterials, catalysts, stabilization additives and binders), is crucial, since it determines the electrode performance (Fig. 4-2). For instance, in the case of electrodes based on the DET mechanism, different electrode structures can occur and this leads to low catalyst utilization, as shown in Fig. 4-2. In order for the electroenzymatic reaction to take place, the biocatalyst should be in contact with an electron-conductive and ion-conductive phase, as well as with the substrate. In addition, for the optimal electrode design, all immobilized biocatalysts should be active and utilized through the catalyst layer. However, the formation of enzyme agglomerates within the electrode structure and/or nanomaterial agglomeration can drastically reduce enzyme utilization, leading to a decrease in electrode activity. Usually, the agglomeration process occurs due to unsuitable choices of enzyme immobilization. Similarly, different structural components (binders) during the preparation procedure can break the electron conductive network leaving a part of the catalyst layer inactive thus, reducing the overall electrode efficiency. Therefore, the understanding of the relationship between immobilization strategies and electrode performances is crucial for the optimal electrode design.

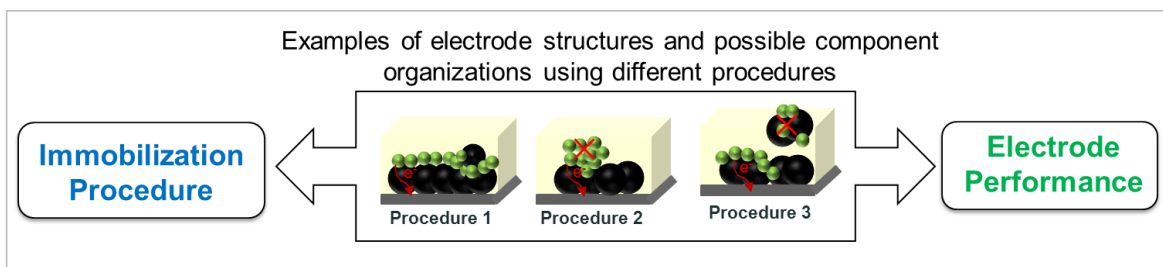


Fig. 4-2 Importance of the immobilization procedure choice

Various experimental methods for preparation of enzymatic electrodes have been mentioned in theoretical part 2.2. In this study, the focus is on the physical immobilization methods. Questions raised are the influence of nanomaterial type (particle, porous), electrode morphology, thickness and porosity on the electrode performance. The next question is how the enzyme distribution at the conductive supports is dependent on the immobilization procedures. To answer these questions, we have studied model reactions of a hydrogen peroxide bioelectrochemical reduction with HRP as the biocatalyst in different electrode types.

Due to the fact that the individual influence of some parameters cannot be separated by studying only complex structures, the monolayer enzymatic electrodes were used for investigation to determine how electrode morphology and the stabilization procedure influences the enzyme distribution. Additionally, an electrode with enzyme monolayer was developed to gain information about the bioelectroreduction process occurring at the electrode surface. Different parameters like influence of pH, substrate concentration and inhibition effect were analyzed on these model electrodes. Next, different types of nanomaterials were tested in order to obtain suitable support and to provide high surface area for the biocatalytic reaction. At the end, porous electrodes were prepared using different immobilization techniques and its influence on the electrode activity was evaluated. The main objectives were to find bottlenecks for optimal 3-D electrode design, conditions for highest biocatalyst utilization within electrode structure and to improve electrode performance for practical application.

4.1 Monolayer enzymatic electrode configuration

4.1.1 Bioelectrochemical cycle of hydrogen peroxide reduction at the

HRP-electrode

HRP-modified carbon electrodes for the reduction of hydrogen peroxide have been investigated from 1978 [82]. Since then, various electrode materials have been analyzed as suitable support for establishing direct electron transfer with HRP e.g. carbon and graphite [82-87], gold [82, 88], viologen-modified gold [89, 90], silver, mercury [44] and platinum [91, 92]. It has been shown that biocatalytic reduction of peroxide is more efficient on carbon electrodes compared to metal surfaces [83, 85, 86]. In order to achieve a monolayer of enzyme at the electrode, an adsorption approach for enzyme immobilization was used. Using this approach, enzymes are connected to the support via weak interactions such as Van der Waal's, electrostatic and/or hydrophobic. The advantage of this technique is in the preservation of enzyme catalytic activity at the support, *i.e.* enzymes maintained their flexibility due to weak interactions [93].

The bioelectrocatalytic cycle of HRP at the electrode surface starts with the oxidation of the ferriheme group of HRP by hydrogen peroxide, resulting in an intermediate form called Compound-I (eq. 4-2). The oxidized form of HRP, Compound-I, consists of oxyferryl iron ($\text{Fe}^{4+}=\text{O}$)

and a porphyrin π cation radical (oxidation state +5). Furthermore, Compound-I loses one oxidizing equivalent in the reduction reaction at the electrode and subsequently forms Compound-II (oxidizing state +4), which in the next step returns to the native form of HRP (Fe^{3+}), (eq.4-3 and 4-4) [43, 44, 77]. This direct electroreduction of Compound-I/II at the electrode surface is considered as DET and characterized by a heterogeneous ET rate constant denoted by $k_{e,i}$ ($i= 1, 2$) (Fig. 4-3).

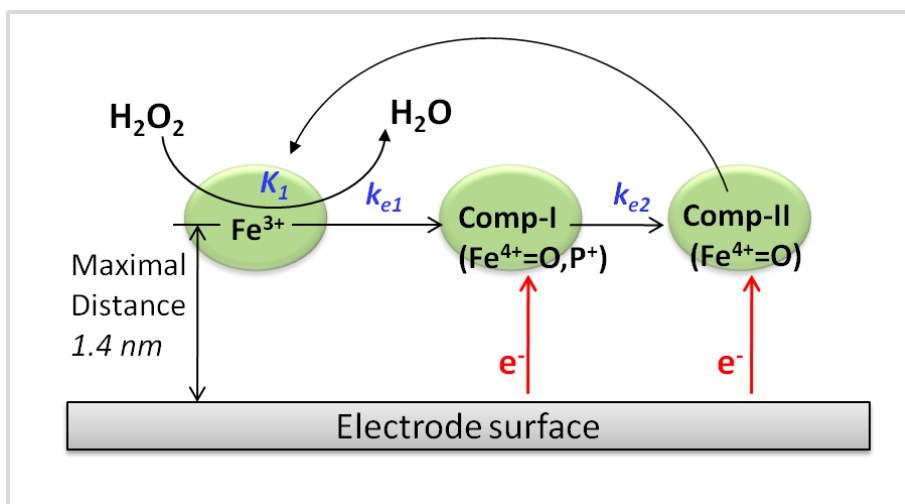
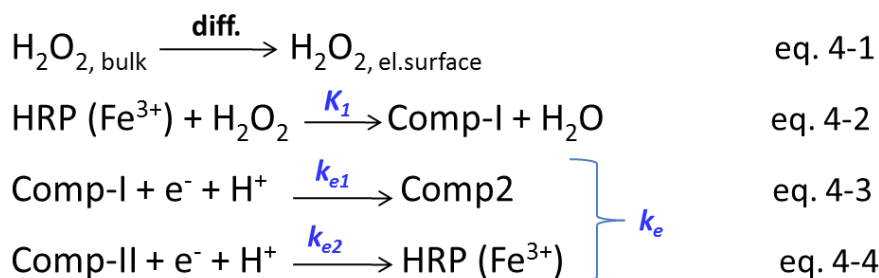


Fig. 4-3 Schematic representation of HRP reaction mechanism at the electrode surface

4.1.2 Electrochemical characterization of HRP-graphite electrode

The cyclic voltammogram of graphite electrode in phosphate buffer (black line), has a rectangle-like shape, showing no redox process that can be ascribed to DET of the heme group at the graphite (Fig. 4-4). This is in accordance to the literature results for other graphite electrodes [94].

However, direct electrochemistry of the HRP active site at the modified carbon (HRP-Fe³⁺ / HRP-Fe²⁺), at the formal potential of -0.363 V vs. SCE, has been reported [95]. The observed direct ET of HRP and electrode surface is ascribed to be promoted by active carbon, since in the control experiment at the glassy carbon, no voltammetry response was reported.

Upon hydrogen peroxide addition, the reduction process can be observed (Fig. 4-4). This is in accordance to the literature results, showing that hydrogen peroxide reduction at the HRP-modified electrodes starts when the electrode is poised at a potential more negative than 0.6 V vs. SCE. The reduction potential is close to the formal potential of Compound-I/II and Compound-II/HRP (Fe³⁺) determined in [96, 97] thus, confirming peroxide reduction at the HRP-electrode.

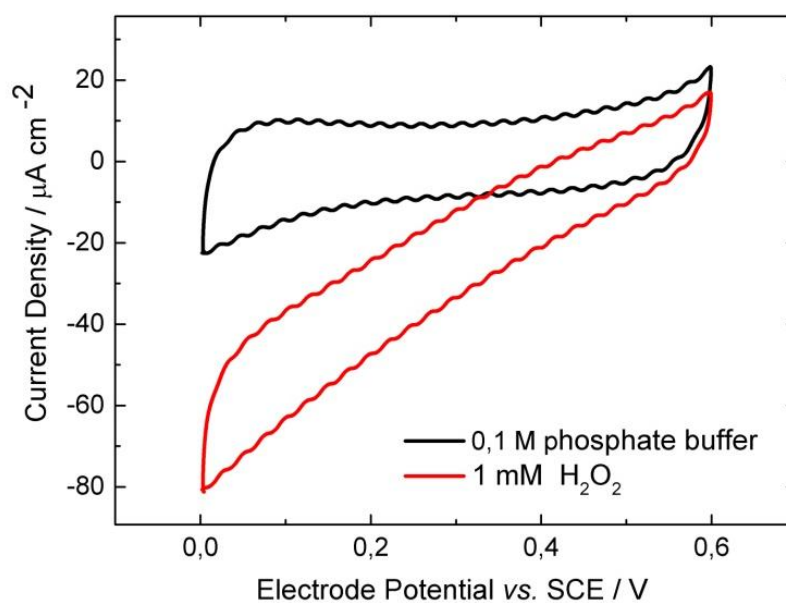


Fig. 4-4 Cyclic voltammetry of HRP adsorbed on the graphite electrode, in presence of 0.1 M phosphate buffer and 1 mM hydrogen peroxide, 400 rpm, N₂ atmosphere, 5 mV s⁻¹

One of the disadvantages of the physical adsorption method is a possible enzyme desorption process (also referred in literature as leaching effect). Thus, in order to make stable and reproducible measurements, after adsorption of HRP at the graphite surface, the electrode performance was evaluated in RDE experiment during time. A HRP-modified electrode was used as the working electrode and it was checked for possible leaching effects. As can be seen in Fig. 4-5, the current density decreases during first 2 h at a constant rotation rate of 400 rpm. It gets stabilized after 2 h at approximately 30% lower current value compared to the current density at

the beginning (0 h). Therefore, all further experiments have been done under the same conditions following the pathway that after enzyme adsorption, the electrode was rotated for 2 h at constant rotation rate (400 rpm).

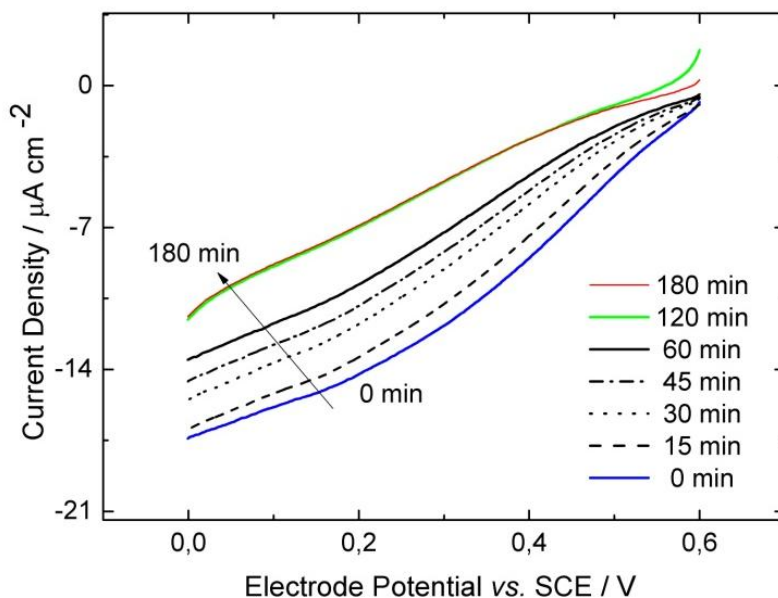


Fig. 4-5 Enzyme leaching effect evaluated in RDE experiment, under constant rotation rate, WE: HRP-graphite electrode, 40 μM hydrogen peroxide, 400 rpm, N_2 atmosphere

Reduction current is also correlated to the concentration of H_2O_2 and pH of the solution, as presented in Fig. 4-6. It can be noted that catalytic current is increasing with hydrogen peroxide concentration increase and/or with more negative values of applied potential. Additionally, the investigated bioelectrocatalytic process is pH dependent, where current response is increasing in the more acidic solution (Fig. 4-6c). According to the literature, the reaction of HRP with peroxide (eq. 4-2, Fig. 4-3), is pH independent in the range from 4.5 until 7.5 [43]. However, the electrochemical steps are pH dependent (eq. 4-3 and 4-4, Fig. 4-3), showing higher reaction rate with pH decrease [43, 44]. This means, when the current density of the HRP electrode is mass transport limited, the electrode response should be pH independent, which can be noticed at low H_2O_2 concentrations e.g. 10 μM . In the case when the electrode signal is limited by electrochemical steps (eq. 4-3 and 4-4), the pH dependence is more pronounced. This corresponds to the electrode performance at higher H_2O_2 concentrations (Fig. 4-6).

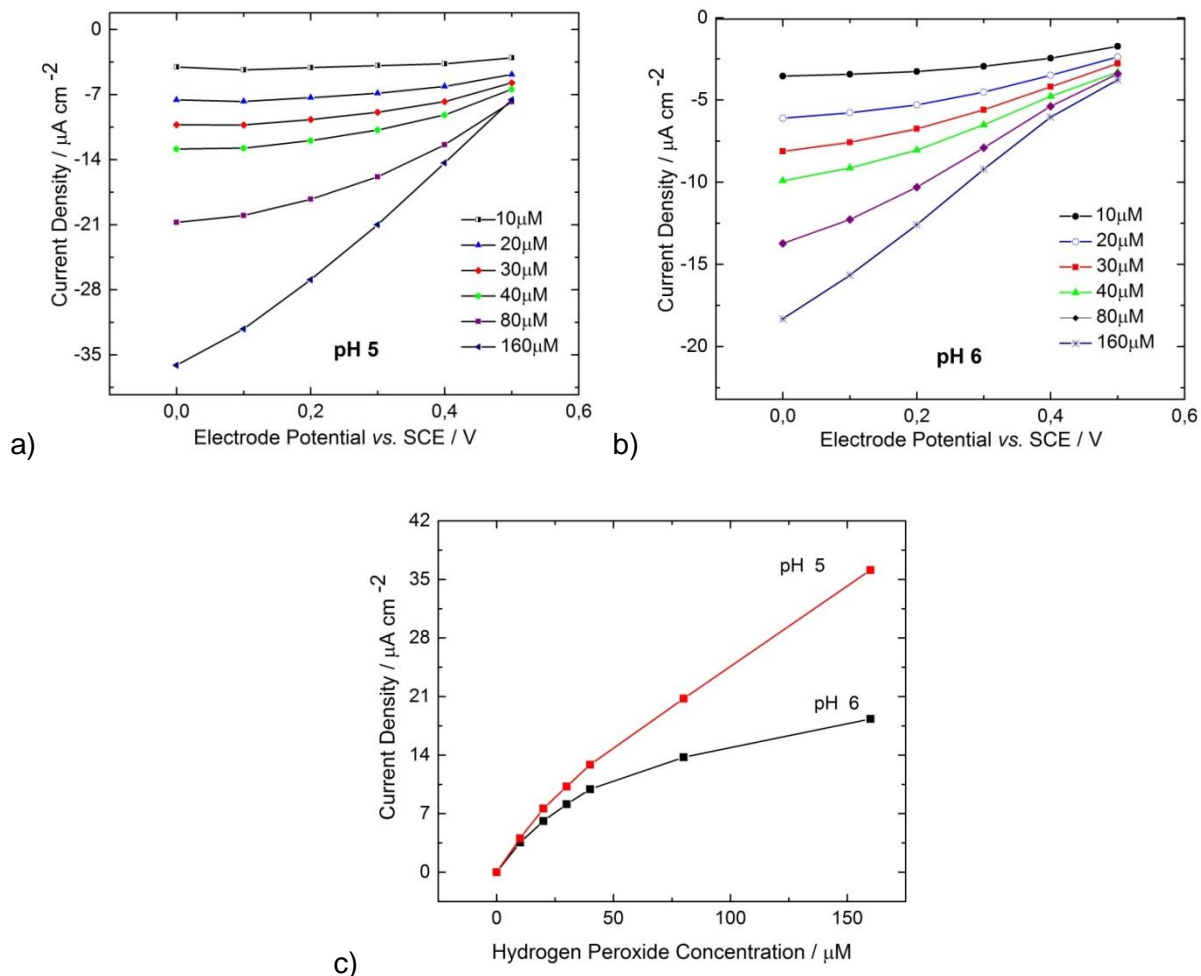


Fig. 4-6 Steady state experiments of HRP electrode at **a)** pH 5.00, **b)** pH 6.00 and **c)** different hydrogen peroxide concentrations at the $E = 0.0$ vs. SCE, 400 rpm, N_2 atmosphere

Additionally, these experimental results were used for the evaluation of the HRP kinetics at the electrode surface reported in a publication by Vidakovic *et al.*, using a modeling approach for studying redox enzyme kinetics [78]. The values obtained for K_1 (eq. 4-2) are $7 \times 10^6 \text{ M}^{-1} \text{ s}^{-1}$ at pH 5.00 and $6.78 \times 10^6 \text{ M}^{-1} \text{ s}^{-1}$ at pH 6.00, and they are close to values reported for the enzyme in the solution ($15 \times 10^6 \text{ M}^{-1} \text{ s}^{-1}$) [98]. On the other hand, they differ significantly in comparison to other values of K_1 for HRP electrodes, where enzyme is adsorbed on different kind of electrodes ($0.031 \times 10^6 \text{ M}^{-1} \text{ s}^{-1}$ on graphite coating [99], $0.13 \times 10^6 \text{ M}^{-1} \text{ s}^{-1}$ on graphite electrode [87] and $0.13 \times 10^6 \text{ M}^{-1} \text{ s}^{-1}$ on gold [100]). The reasons observed for this different behavior are usually due to different assumptions in enzyme surface coverage and low activity of immobilized enzymes. Furthermore, in the steady state experiment, only one apparent rate constant for electrochemical

reactions, usually referred to as k_e , can be determined. In the present case, apparent electrochemical rate constant is pH dependent and ranges from 27.74 s^{-1} at pH 5 to 17.17 s^{-1} at pH 6 [78]. These obtained values are significantly higher than the rate constant for similar HRP-graphite electrodes reported by Ruzgas *et al.* ($0.66 \pm 0.28 \text{ s}^{-1}$) [98]. As for the enzymatic constant, this electrochemical constant depends also on the total enzyme concentration that is assumed to be different in different literatures. The reported values of the enzymatic kinetic constants for the developed HRP electrode are in the range of those reported for the enzyme in the solution, indicating successful enzyme adsorption and activity at the conductive surface.

In addition to the basic catalytic HRP cycle that proceeds through Compound-I/II formation, the possibility of native ferric peroxidase conversion to Compound-III, in the presence of a large excess of hydrogen peroxide, is also demonstrated [44, 101]. However, suggested pathways are not all possible redox transformations of peroxidase, but the ones that are relevant for interpretation of the HRP cycle at the electrode surface [42]. The inhibition effect with a large excess of H_2O_2 can be observed in Fig. 4-7, where the investigated HRP electrode is exposed to concentrations higher than *approx.* $600 \mu\text{M}$ H_2O_2 . However, the range of peroxide concentration leading to inhibition strongly depends on the enzyme loading at the electrode surface. This means that the determined H_2O_2 concentration of $600 \mu\text{M}$ corresponds to this particular case of a flat electrode design.

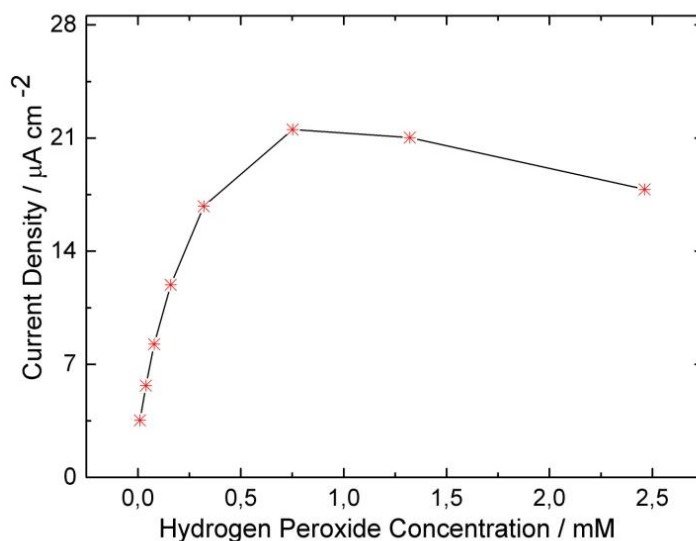


Fig. 4-7 Influence of the H_2O_2 concentration on the performance of the HRP-modified electrode, 400 rpm, pH 6.00, N_2 atmosphere, $E = 0.0$ vs. SCE

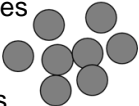
Adsorption method, as a mild way to preserve enzyme activity was chosen for HRP deposition at the electrode surface. Electrochemical performance of HRP-electrode implies successful direct ET between HRP and a graphite support. However, due to the desorption process occurring as a consequence of weak interactions between enzymes and the surface, the optimization of preparation steps is necessary. For example, the electrode lost 30% of activity in first two hours at constant rotation, where after this time electrode performance gets stabilized. An increase of the peroxide concentration leads to increase in the electrode activity, but due to the inhibition effect that occurs at higher substrate concentrations, the optimization of optimal operating H_2O_2 concentration is important. For the monolayer electrode configuration, 600 μM is estimated as the maximum.

4.2 Three dimensional enzymatic electrodes

4.2.1 Influence of the supporting material (nanomaterial)

Carbon based nanomaterials are attractive for biocatalysis due to high conductivity, high surface to volume ratios, tailoring possibility, the ability to facilitate reaction kinetics for DET and to decrease overpotential for electrochemical enzyme regeneration [102]. Various nanomaterials including nanoparticles, nanofibres and nanoporous materials have been examined as hosts for enzyme catalysis [50-52, 60]. For instance, Vulcan nanoparticles have been employed as support for oxygen reduction reaction with BOD [103] or glucose oxidation with GOx [104]. It has been shown that carbon monolith materials like Carbon Aerogel is excellent support for BOD and laccase electrode based on DET [54]. Also, Wang *et al.* [105] has proven that Carbon Hollow Sphere decreases overpotential for NADH regeneration and promotes the electroreduction reaction of laccase. In the case of HRP based electrodes, the research has been mostly focused on the utilization of different types of carbon nanotubes e.g. single [106], double [107], multi [108, 109], while other types of nanomaterials have been rarely tested. Additionally, due to diversity in preparation procedures and different experimental conditions, a systematic comparison is not possible. Therefore, the adequate nanomaterial support for peroxide electroreduction using HRP was investigated under the same conditions.

Table 4-1 Investigated types of nanomaterials and their characteristics

Type or material	Name	BET / m ² g ⁻¹	Particle /pore size / nm
Particles 	Carbon Aerogel (CA)	201	14 / -
	Vulcan XC72	250	80 / -
Porous 	Carbon Hollow Sphere (CHS)	377	168 / -
	Coral Carbon (CC)	528	- / 14

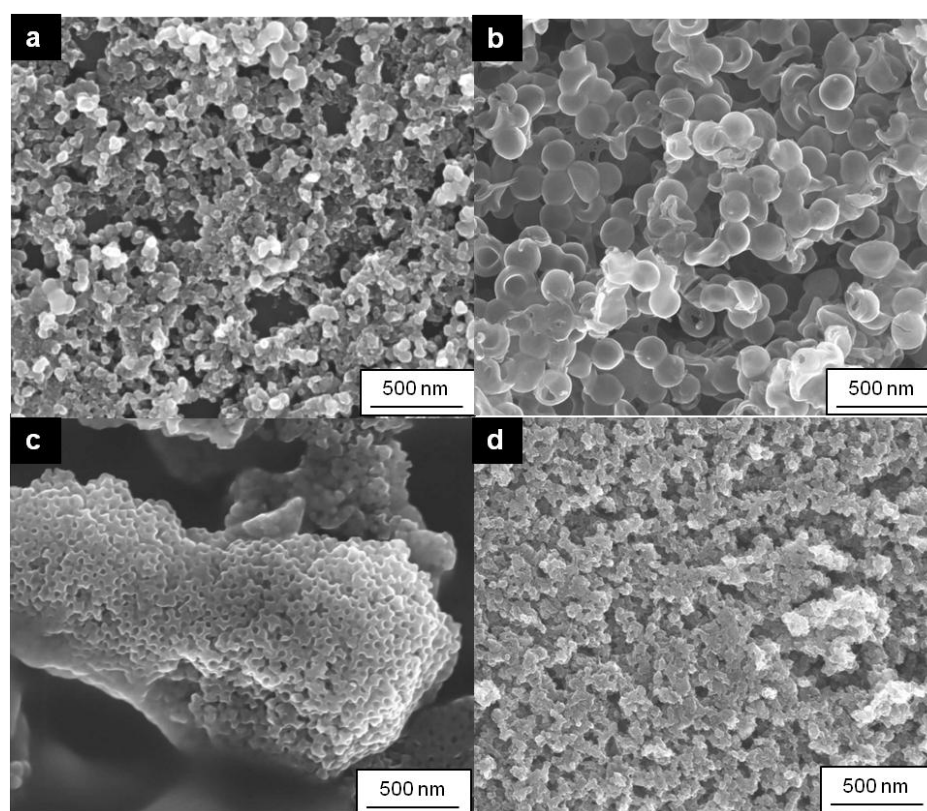


Fig. 4-8 SEM images of **a)** Vulcan nanomaterial, **b)** Carbon Hollow Sphere, **c)** Coral Carbon and **d)** Carbon Aerogel

The influences of two major nanomaterial types 1) nanoparticles and 2) nonporous material, on the electrode activity were evaluated. In Table 4-1, four different types of materials are presented. Clearly, the main difference of used nanomaterials is in their structure (SEM image, Fig. 4-8). Carbon Aerogel (CA), Vulcan XC72 and Carbon Hollow Spheres (CHS) are

spherical particles with different sizes of *approx.* 14, 80 and 168 nm and high surface areas of 201, 250 and 377 m² g⁻¹ respectively. On the other hand, the advantage of mesoporous materials like Coral Carbon (CC) is in its porous structure, providing well-order pores with the possibility to adapt to particular enzyme and substrate sizes during material synthesis. CC has high specific surface areas of 528 m² g⁻¹. The immobilization method chosen is based on enzyme entrapment (gelatin procedure, experimental section 3.3.1), where the role of gelatin is to provide a suitable microenvironment for the proteins. Additionally, taking into account the previously demonstrated leaching effect that can be a consequence of physical enzyme adsorption, a cross-linking method was used for enzyme stabilization.

The cyclic voltammograms (CVs) of the enzymatic electrodes, based on different nanomaterials obtained in the presence of a 0.1 M phosphate buffer at 5 mV s⁻¹ are presented in Fig. 4-9. In this kind of experiment, information about surface groups at the carbon materials, as well as information about enzyme redox processes can be obtained. The CVs in Fig. 4-9 do not show any redox processes which can be ascribed either to DET of enzyme or redox groups at the carbon. The absence of DET of HRP at the carbon material in phosphate buffer is in accordance to the literature [106]. In the tested potential window, voltammetry curves exhibit similar performances as the other reported electrodes based on carbon aerogel [110, 111] or CHS [105]. The observed electrical double layer currents are related to the pore size in electrode material and the movement of the ions in the pores [110]. They should be proportional to the electrochemically active surface area. However, it can be noticed that the capacitive currents cannot be correlated to estimated BET surface areas of the same materials. For instance, the capacitive current for Carbon Hollow Sphere (377 m² g⁻¹) shows the lowest response, although the BET surface area is higher in comparison to the other materials e.g. Carbon Aerogel (201 m² g⁻¹) and Vulcan nanomaterial (250 m² g⁻¹). This might be an indication of the high particle agglomeration (possibly due to high hydrophobicity and large particle size, 168 nm), when CHS material is used. Additionally, due to different working principles of these two techniques, the comparison between them might not be realistic, because small pores in the nanomaterial could be available for N₂ used for BET measurements, but might not be accessible by electrolyte. The electrode prepared with Coral Carbon nanoporous material has the highest electrochemically active surface, which may be an indication to the highest surface utilization and consequently electrode activity.

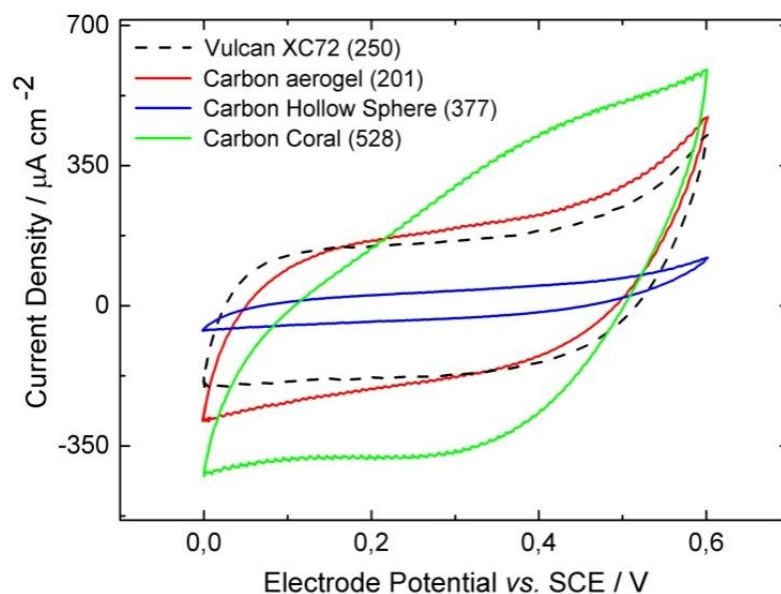


Fig. 4-9 Comparison of CVs obtained for HRP electrodes prepared with different nanomaterials, 0.1 M phosphate buffer, 5 mV s^{-1}

The polarization curves were obtained as steady state data extracted after 60 s from the chronoamperometric measurements, where the potential step was 0.1 V. Detailed experiments and extracted data in the absence and presence of H_2O_2 are presented in Fig. 4-10. All electrodes were analyzed under the same conditions. The performances of the electrodes compared with Vulcan nanomaterial are presented in Fig. 4-10b, c and d. As can be noticed, Vulcan and CHS materials show very low capacitive current, which means that the time frame of 60 s was enough to reach steady state current response (Fig. 4-10b). However, with a high contribution of the micro-/meso- pores in the electrode structure based on CA and CC, the time of 60 s was not enough to reach steady state (Fig. 4-10 c and d). For comparative results, the catalytic current of CA and CC based electrodes was calculated by subtracting the capacitive current in PBS from the total current obtained in presence of hydrogen peroxide.

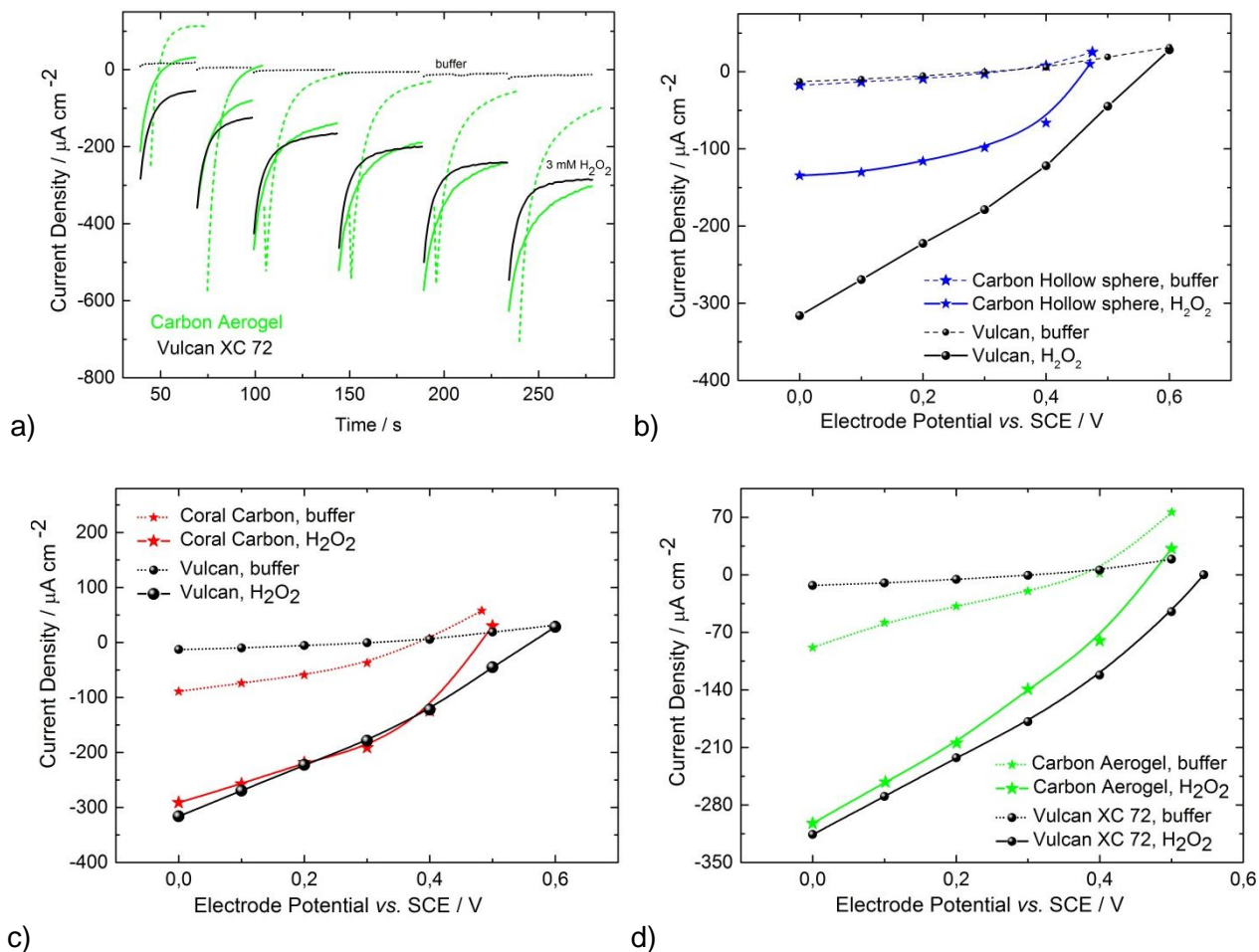


Fig. 4-10 a) Chronoamperometry response and b), c) and d) steady state curves based on current extracted from (a) experiment, in presence of 0.1 M PBS and 3 mM H₂O₂

Finally, the activities of nano-based enzymatic electrodes were compared in the presence of 3 mM hydrogen peroxide. The high surface area of materials allows immobilization of higher number of biocatalysts in comparison to the flat electrode thus, a higher concentration of peroxide could be used (mM range). As can be observed in Fig. 4-11, the Vulcan based electrode outperformed all other materials, reaching the current value of around $300 \mu\text{A cm}^{-2}$ at 0.0 V vs. SCE. For instance, Vulcan and Carbon Aerogel have the same electrochemically active surface area but different activity, which hints to different surface utilization and the number of active catalysts with proper orientation in the catalyst layer. Even though the Coral Carbon electrode has the largest electrochemically active surface area in comparison to the other tested materials, its activity (ca. $200 \mu\text{A cm}^{-2}$) is lower than electrode activity based on Vulcan (ca. $300 \mu\text{A cm}^{-2}$) and CA (ca. $240 \mu\text{A cm}^{-2}$). In addition, the onset potential of 0.57 V vs. SCE for the Vulcan

electrode is 0.12 V more positive than the value for the other nanomaterials (ca. 0.45 V), indicating promoted DET at Vulcan. The value of 0.57 V vs. SCE can be compared to the onset observed for the HRP reaction for the graphite electrode [44]. However, different values for the onset potentials at different nanosupports have been reported in the literature e.g. at graphene-modified electrode ca. 0.362 V vs. SCE at pH 7.00 [112]; at double-walled nanotubes 0.38 V vs. SCE at pH 7.00 [107].

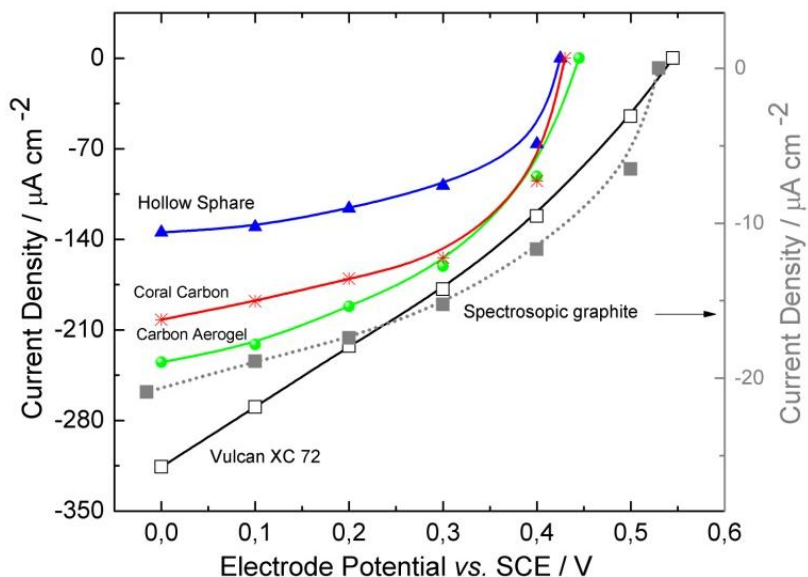


Fig. 4-11 Comparison of HRP electrode activity based on different nanomaterial types, in presence of 3 mM H₂O₂, N₂ atmosphere, 400 rpm, pH 5.00

The SEM characterizations of electrode cross sections are presented in Fig. 4-12. Strong particle agglomeration can be noticed for the electrode prepared with Coral Carbon, where agglomerates are in the range from 3 µm to 10 µm (Fig. 4-12c). Some parts of the CC particles are completely covered with gelatin (white parts), which indicates strong mass transport limitations for substrate to electrode surface. On the other hand, Vulcan nanomaterial distribution in gelatin is the most uniform, resulting in more available surface for enzyme catalysis (Fig. 4-12a). Different electrode inner morphologies emphasize the importance of the nanomaterial distribution and particle agglomeration within electrode structure. Ultimately, Vulcan material was chosen as the best candidate for the HRP bioelectrocatalytic process, not only due to a high surface utilization (high electrode activity) but also a high OCP value.

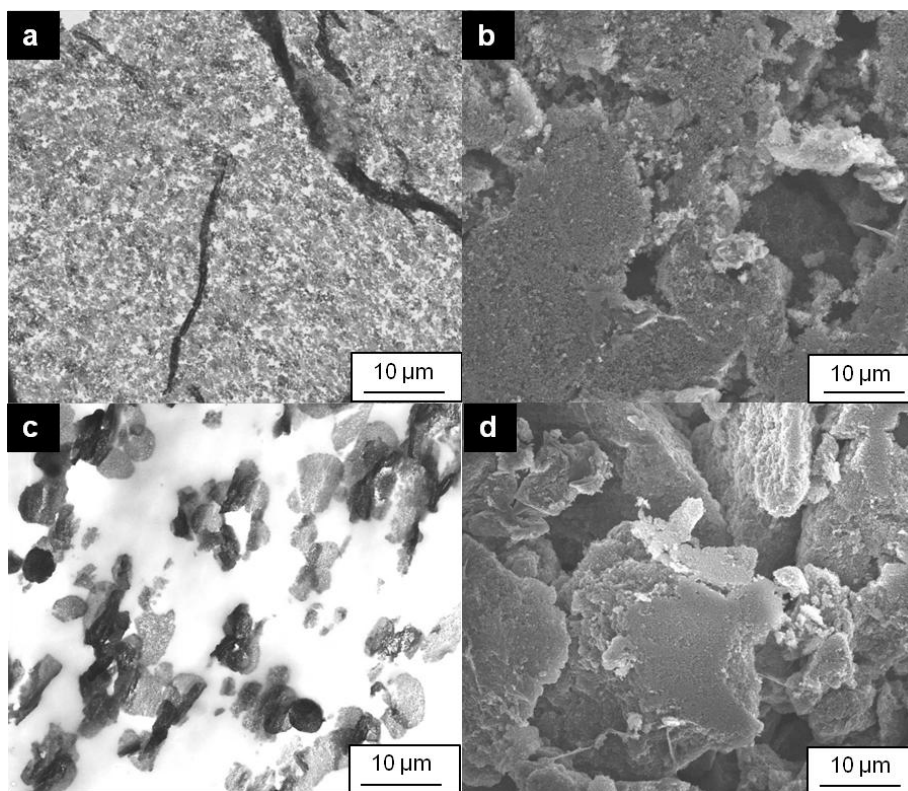


Fig. 4-12 SEM images of electrode cross sections **a)** Vulcan nanomaterial **b)** Carbon Hollow Spheres **c)** Coral Carbon and **d)** Carbon Aerogel

4.2.2 Influence of the immobilization strategy

As discussed, the electrode activity is not only influenced by nanomaterial type, but also by the choice of an immobilization procedure. Therefore, the further goal was to evaluate how electrode preparation procedures influence electrode structural parameters like porosity and electrode thickness, as well as enzyme utilization and overall electrode performance. Two main routes for HRP immobilization, using Vulcan nanomaterial were investigated. The first procedure, which was already employed in the previous section, includes enzyme entrapment in a gelatin matrix, where cross-linking was applied for stabilization of the enzyme/nanomaterial composite (in text further denoted as Vulcan-Gelatin). The second procedure is based on the enzyme physical adsorption into the porous electrode, stabilized by PVDF as a binder (Vulcan-PVDF). Both procedures were described in detail in the experimental section 3.3.

The performances of the enzymatic electrodes in the absence and presence of hydrogen peroxide were evaluated by means of cyclic voltammetry (Fig. 4-13). Furthermore, influence of rotation rate (0 and 400 rpm) on the electrode activity has been shown. Upon addition of substrate, an increase of the reduction current for both electrodes can be observed. As expected, the enzymatic activity in quiescent solution (0 rpm) is lower compared to that at 400 rpm rotation. This difference is more pronounced for Vulcan-PVDF electrode reaching ca. 0.66 mA cm⁻² with and 0.13 mA cm⁻² without stirring (values of current density after subtraction of background current). On the other hand, the rotation rate has a lower influence on the performance of the Vulcan-Gelatin electrode, achieving ca. 0.13 mA cm⁻² in quiescent solution and 0.22 mA cm⁻² at 400 rpm. These results indicated stronger mass transport limitations in the Vulcan-PVDF compared to Vulcan-Gelatin. This corresponds to higher amounts of active enzyme within the Vulcan-PVDF electrode structure.

Additionally, for quantitative description of electrode processes, the importance of the mass transfer control in the diffusion layer over time, using forced convection conditions (400 rpm) is shown. This is especially true for the processes strongly controlled by mass transfer (e.g. the case of Vulcan-PVDF). As shown in Fig. 4-13, the electrode activity of the Vulcan-PVDF electrode is underestimated in comparison to the Vulcan-Gelatin electrode, under the conditions without rotation.

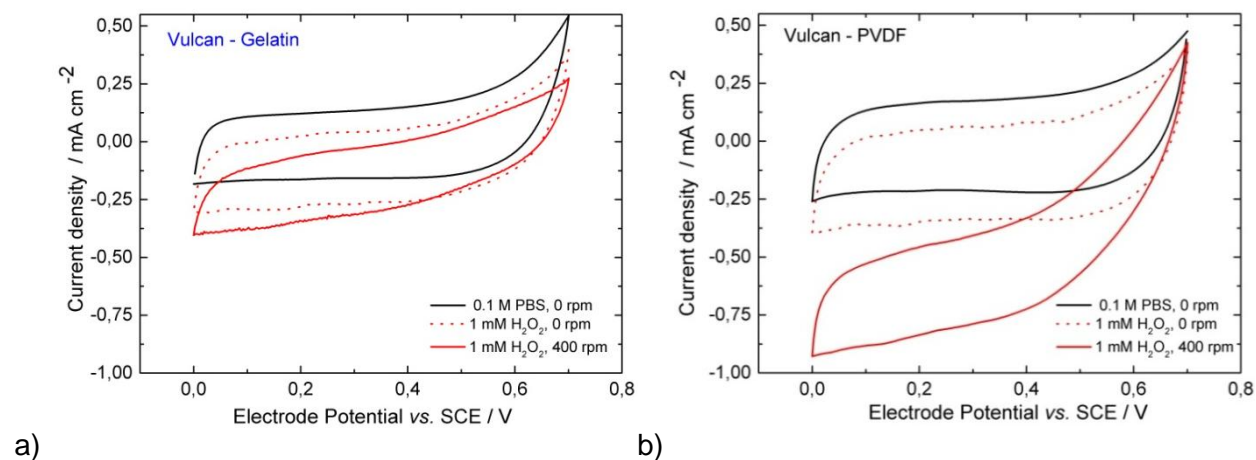


Fig. 4-13 Cyclic voltammograms of porous enzymatic electrodes in PBS and in 1 mM hydrogen peroxide, without rotation and at 400 rpm **a)** Vulcan-Gelatin and **b)** Vulcan-PVDF. Conditions: 5 mV s⁻¹, pH 6.00, room temperature, N₂ atmosphere, enzyme loadings (1 mg cm⁻² for Vulcan-PVDF and 1.75 mg cm⁻² for Vulcan-Gelatin electrodes)

The importance of choosing a sampling method is demonstrated in Fig. 4-14. Steady state electrode measurements at two different sampling times, 60 and 120 s, are compared with background subtracted cyclic voltammogram at 5 mV s^{-1} . As can be noticed, the catalytic current using cyclic voltammetry is significantly overestimated. In addition, the sampling time of 60 and 120 s provides almost identical results for which reason 60 s was chosen in all experiments.

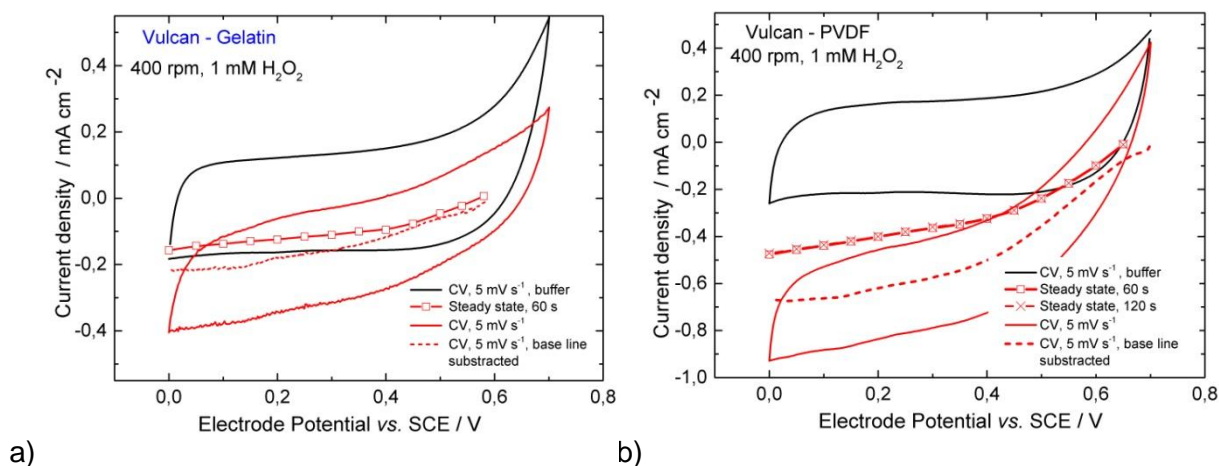


Fig. 4-14 Comparison of the electrode performance obtained using cyclic voltammetry and steady state methods **a)** Vulcan-Gelatin and **b)** Vulcan- PVDF electrodes. Conditions: scan rate 5 mV s^{-1} , pH 6.00, N_2 atmosphere, enzyme loading: Vulcan-PVDF - 1 mg cm^{-2} and Vulcan-Gelatin - 1.75 mg cm^{-2}

HRP electrodes based on Vulcan nanoparticles show high onset potentials, *approx.* 0.57 V and 0.62 V vs. SCE for Vulcan-Gelatin and Vulcan-PVDF, respectively. Those values are comparable to the onset values reported in the literature using high surface area materials *e.g.* onset potential was reported 0.63 V vs. SCE at pH 7.00 [108, 113], 0.57 V vs. SCE at pH 6.00 [114] and 0.55 V vs. SCE at pH 7.00 [115]. As can be seen, the onset potential of the Vulcan-Gelatin electrode is *ca.* 50 mV lower than the obtained value for Vulcan-PVDF. The Vulcan electrodes were prepared using different immobilization procedures, which influence the enzyme orientation at the support and the number of active enzymes. Both parameters can contribute to the observed difference in the onset potential. In the case of PVDF procedure, enzymes were physically adsorbed on the nanoparticles, while in the Gelatin procedure enzymes were additionally cross-linked. Therefore, it can be anticipated that cross-linking of enzymes leads to less favorable biocatalyst orientations than in the case of simple adsorption, which at the end results in a more negative onset potential.

The redox process which corresponds to the heme group, was reported at the potentials - 0.15 V vs. SCE at pH 7.00 in PBS [116]. This implies that there is a possibility that the heme group from denatured HRP might also participate in the electrode current response. Therefore, in order to check if the electrochemical signal is only due to the catalytic activity of the native enzyme, additional experiments were performed using denatured HRP for hydrogen peroxide reduction.

HRP was deliberately denatured using 2% SDS (sodium dodecyl sulphate) followed by further thermal treatment at 95 °C for 10 min. Denatured HRP was then used for the preparation of the enzymatic electrodes. The results of electrochemical characterization in absence and presence of hydrogen peroxide have been shown in Fig. 4-15. The same cyclic voltammetry of denatured HRP at Vulcan-PVDF electrodes in absence and presence of hydrogen peroxide proves no activity of denatured HRP toward hydrogen peroxide reduction. For comparison purposes, in the same graph, CV of native HRP-Vulcan-PVDF in the presence of hydrogen peroxide is presented, clearly showing catalytic activity. The same information can be obtained from the steady state measurements (Fig. 4-15b). Based on these results, one can conclude that the electrochemical signal or part of the electrochemical signal cannot be due to heme released from HRP or the denatured enzyme but only due to activity of the native enzyme at the electrode surface.

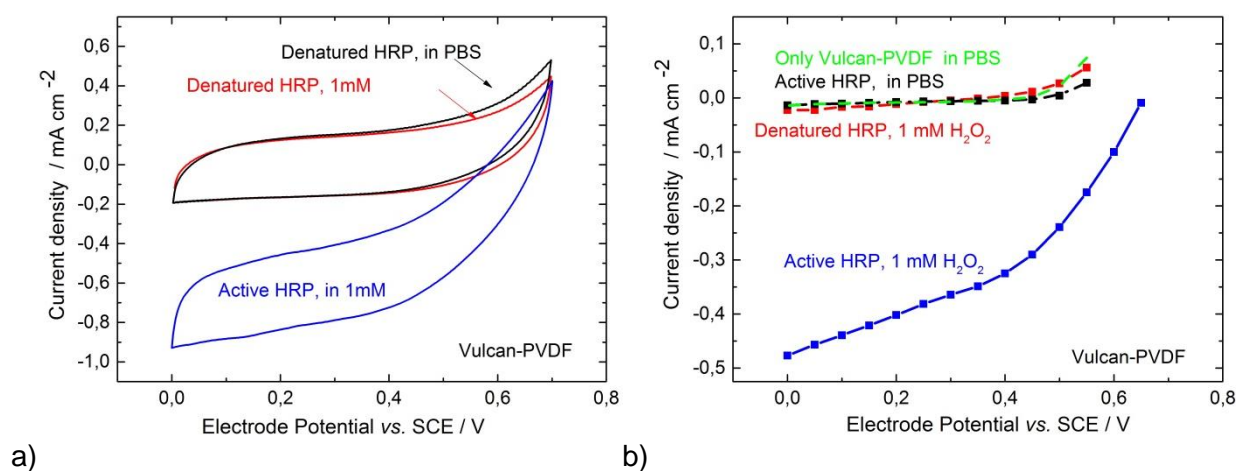


Fig. 4-15 Comparison of the performances between denatured and native HRP **a)** cyclic voltammograms **b)** steady state currents. Conditions: 400 rpm, pH 6.00, 5 mV s⁻¹, N₂ atmosphere

Next, the optimal enzyme loading at constant peroxide concentration was studied for both immobilization procedures. The influence of the enzyme loading on the electrode performance, at a potential value of 0.0 V vs. SCE and constant peroxide concentration, is presented in Fig. 4-16. The dependencies of the current densities on the enzyme loading result in a bell-shaped curve for both electrodes. Increase of electrode activity with the enzyme loading at the constant substrate concentration corresponds to the increase in the amount of active enzyme. On the other hand, the decrease of electrode activity at higher values of enzyme loading can be correlated to the increase of mass transport resistance in the catalyst layer. This leads to dead portions in the electrodes structure that are under supplied with H_2O_2 . Additionally, unfavored enzyme orientations and/or enzyme inhibition contribute to the decreased electrode activity under higher enzyme loadings [113, 117]. As can be seen, the optimal loadings are different for two different procedures, namely ca. 1.75 mg cm^{-2} for Vulcan-Gelatin and 1 mg cm^{-2} for Vulcan-PVDF. The Vulcan-Gelatin electrode requires a higher amount of catalyst to reach optimal value, while its total electrode activity is lower in comparison to Vulcan-PVDF, in the whole range of study potentials (Fig. 4-16b). This confirms lower enzyme utilization in the Vulcan-Gelatin electrode structure.

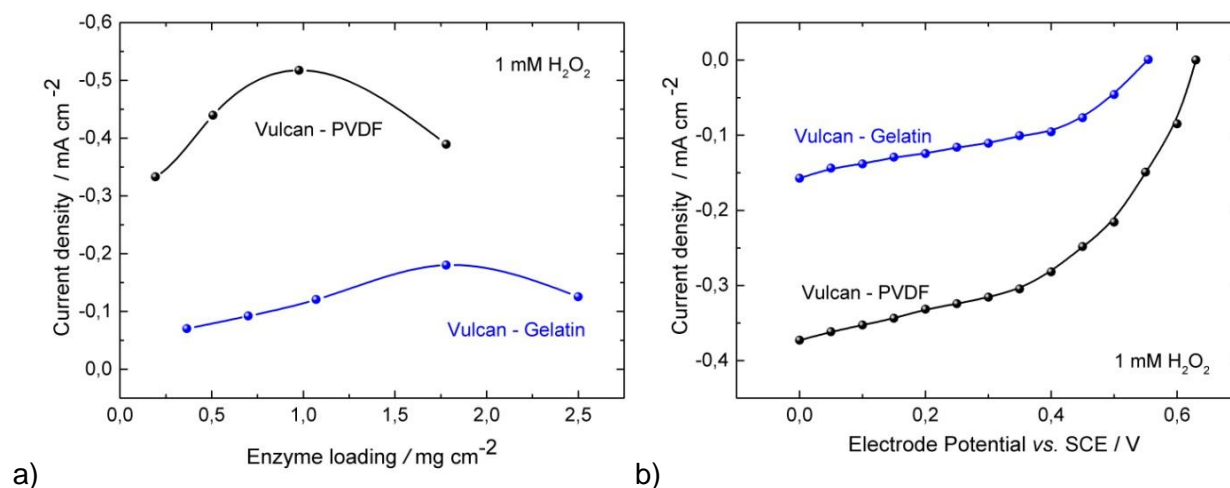


Fig. 4-16 a) Influence of enzyme loading on the activity of Vulcan HRP – electrodes **b)** Comparison of the electrode activities at the same enzyme loading of 1.75 mg cm^{-2} . Conditions: 1 mM hydrogen peroxide, 400 rpm, N_2 atmosphere, pH 6.00

The dependence of current density on the substrate concentration for both Vulcan electrodes at optimal enzyme loadings was checked (Fig. 4-17). The results show an increase in the reduction catalytic current with an increase of the peroxide concentration, reaching saturation conditions at ca. 4 mM H_2O_2 for Vulcan-Gelatin and 5 mM H_2O_2 for Vulcan-PVDF. This indicates that the immobilized HRP remains catalytically active for peroxide reduction until the saturated concentrations without inhibition effect. As can be noticed, the limit of saturated conditions for the porous electrode due to the increased number of active enzymes is significantly higher (4 and 5 mM) in comparison to the 600 μM H_2O_2 obtained for the HRP-adsorbed at the graphite surface (monolayer electrodes, Fig. 4-7).

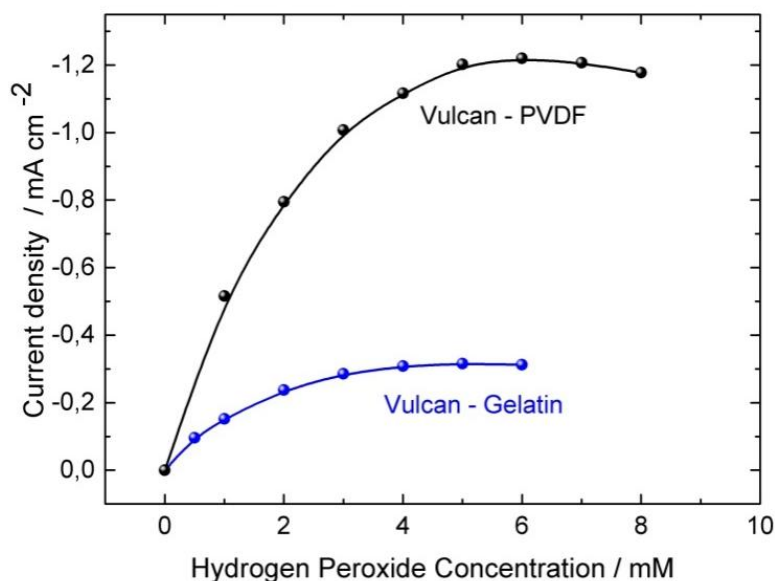


Fig. 4-17 Influence of the hydrogen peroxide concentration on the activity of Vulcan HRP – electrodes at optimized enzyme loadings; electrode potential: 0.0 V vs. SCE

As already discussed, HRP electrodes adsorbed on flat surfaces have better performance in more acidic solutions; therefore a pH of 5.00 was chosen for all experiments with enzyme monolayer. As can be seen in Fig. 4-18, HRP electrodes based on high surface area materials show similar results at both, pH 5.00 and 6.00. Therefore, 3-D enzymatic electrodes were tested at a higher pH value (6.00), which is more compatible to the conditions of the GOx biocatalyst, discussed in the next chapter.

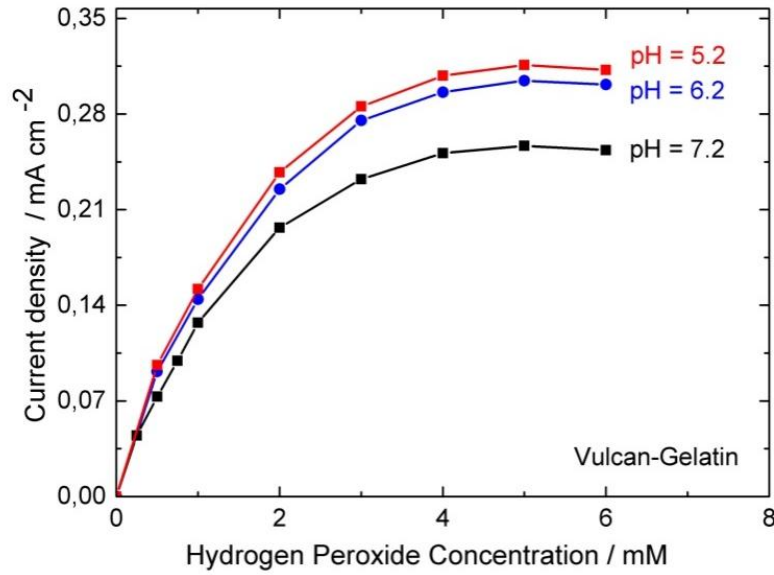


Fig. 4-18 Influence of pH on the enzymatic electrode performance, conditions as in Fig. 4-15

The comparison of the enzymatic electrode performances employing HRP for peroxide reduction with DET mechanism is presented in Table 4-2. As can be seen from the values of the maximum current densities reached under saturated conditions of H_2O_2 concentration, the electrode activity of Vulcan-Gelatin is similar to the reported values. However, the performance of the Vulcan-PVDF electrode outperforms all reported literature values. For example, electrodes based on HRP immobilization at carbon nanotubes reach a value of ca. 0.1 mA cm^{-2} at $1 \text{ mM H}_2\text{O}_2$ [115]. HRP immobilized at the double-walled carbon nanotubes reaches 0.12 mA cm^{-2} at 1 mM peroxide or at single-walled carbon nanotubes 0.03 mA cm^{-2} at 0.3 mM [107, 114]. Although concentrations of peroxide are not the same, those are values under saturated conditions thus, maximum values used for particular electrodes, and in that respect, currents, are comparable. Further increase in H_2O_2 concentration will lead to enzyme inhibition and decrease of activity.

Table 4-2 Performance comparison of the HRP porous electrodes for peroxide reduction with DET

Conditions	Concentrations /mM	OCP / V	I _{max} / mA cm ⁻²	Ref.
0.1 M PBS, pH 7.4	0.8	0.43	0.196	[109]
0.1 M PBS, pH 7.4	1	0.38	0.12	[107]
20 mM PBS, pH 6	0.3	0.57	0.03	[114]
0.1 M PBS, pH 7.0	10	0.63	0.9	[108]
67 mM PBS, pH 7.0	1	0.58	0.1	[115]
0.1 M PBS, pH 6.0	4	0.57	0.3	This work: Vulcan-Gelatin
0.1 M PBS, pH 6.0	5	0.62	1.2	This work: Vulcan-PVDF

4.2.3 Characterization of the electrode structures

To understand the origin of the difference in the electrode activities of the Vulcan-PVDF and the Vulcan-Gelatin electrodes, they were further characterized with SEM. Cross-sections, magnification views and surfaces of the Vulcan-electrodes are presented in Fig. 4-19. It can be seen that regardless of the immobilization procedure and nanomaterial organization in the different binders, the thicknesses of enzymatic electrodes were similar, ca. 47 μm and 53 μm for Vulcan-Gelatin and Vulcan-PVDF, respectively. Magnification of the electrode cross sections provides better insight into the electrode morphology (Fig. 4-19c and d). It can be noticed that nanomaterial in Vulcan-Gelatin electrodes is organized in knot-shaped agglomerates with a size of around 250 nm. In the case of Vulcan-PVDF, the nanomaterial organization is more uniform and 100 nm spherical units can be observed. It can be assumed that due to the hydrophilic nature of gelatin, used as binder in the Vulcan-Gelatin procedure, a higher agglomeration degree of hydrophobic nanoparticles is achieved. A similar structure of Vulcan porous electrodes prepared by a surfactant-stabilized colloidal method for application in direct methanol fuel cell has been reported by Bang *et al.* [118]. A higher degree of nanoparticle agglomeration in the Vulcan-Gelatin structure indicates a decrease of available surface area for enzyme immobilization that is also in accordance to the electrochemical characterization (Fig. 4-13).

The top views of Vulcan electrode surfaces are also affected by immobilization procedures (Fig. 4-19e and f). The gelatin layer formed on the top of the Vulcan-Gelatin electrode stabilizes the electrode structure preventing/decreasing the enzyme leaching, but on the other

hand, it introduces additional mass transfer resistance for substrate transfer in the catalyst layer. The electrode surface of the Vulcan-PVDF electrode appears similar to the electrode cross-section morphology (Fig. 4-19d). Furthermore, the porosities of both electrodes were estimated based on the electrode thickness measured by SEM and theoretical compact electrode thickness. Gode *et al.* [119] have reported the equation for calculation of theoretical compact thickness of the electrodes, based on loadings of all electrode components and their densities. It should be taken into account that in the calculation for the Vulcan-Gelatin electrode, the density of dry gelatin was used. The electrode porosity for the Vulcan-Gelatin electrode was estimated to be 0.27 that of Vulcan-PVDF was 0.45. This indicates lower mass transport limitation through Vulcan-PVDF electrode layer in comparison to Vulcan-Gelatin electrode.

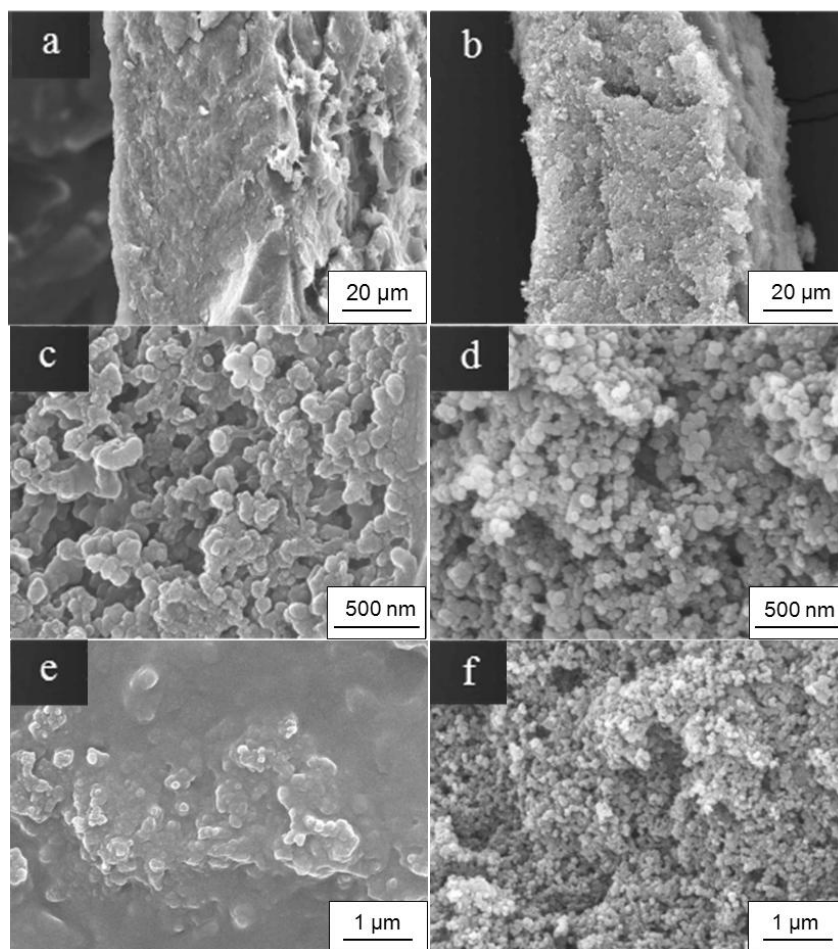


Fig. 4-19 SEM images of Vulcan HRP electrodes: cross sections of **a)** Vulcan-Gelatin and **b)** Vulcan-PVDF; magnified view of the cross-sections of **c)** Vulcan-Gelatin and **d)** Vulcan-PVDF and top views of **e)** Vulcan-Gelatin and **f)** Vulcan-PVDF

4.3 Characterization of the enzyme distribution at the electrode surface

4.3.1 Influence of the surface morphology

The enzyme distribution and potential agglomerations within the electrode structure are crucial for the electrode performance, since they determine the number of active catalysts. Typical microscopic methods used for visualization of enzymes at the electrode supports are: atomic force microscopy (AFM) [120-124], fluorescence microscopy (FM) [125], scanning electrochemical microscopy (SECM) and electrochemical scanning tunneling microscopy (ESTM) [126]. For instance, these methods have been so far successfully applied to investigate self-assembly layer formation [127, 128] or interactions of proteins entrapped in different polymers [125, 129-131]. In the present work, AFM and FM were employed to study the enzyme organization at the conductive supports. FM provides optical images of enzymes on surfaces, utilizing either their native fluorescence (e.g. flavin enzymes are fluorescent) or more common foreign fluorescence, obtained by labeling of enzymes with fluorescent markers. Due to the fact that HRP is not a naturally fluorescent compound, it was modified with amine-reactive dye, containing a NHS group (N-hydroxysuccinimide); one of the most commonly used groups for protein labeling. The modification occurs through formation of covalent bonds between surface-oriented primary amines of the protein and NHS ester (Fig. 4-20) [132].

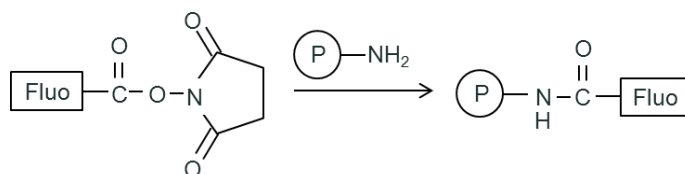


Fig. 4-20 Modification scheme of labeling procedure: Reaction between amino-reactive dye and protein (P)

In order to check if the labeling procedure was efficiently accomplished, the electrophoresis with native and labeled HRP was done (Fig. 4-21). The prepared gel contains two lanes, the first with labeled HRP and the second lane with unlabeled HRP. After protein separation and before standard staining procedure, the gel was observed under UV lamp in order to visualize fluorescent species separated at the gel (Fig. 4-21a). Furthermore, staining procedure was applied to visualize all separated proteins (Fig. 4-21b). As can be seen, in both

lanes HRP with the molecular weight of 44 kDa was observed at the expected position. The results obtained under a UV lamp show efficient labeling of HRP with NHS dye (modified HRP in the first lane, Fig. 4-21 a). Additionally, in order to check if the labeling procedure has any influence on the enzyme catalytic behavior, the electrochemical performance of modified and unmodified HRP adsorbed at the SPG electrode has been compared (Fig. 4-22). The electrode activity was almost identical, indicating that the applied modification does not affect enzyme catalytic activity.

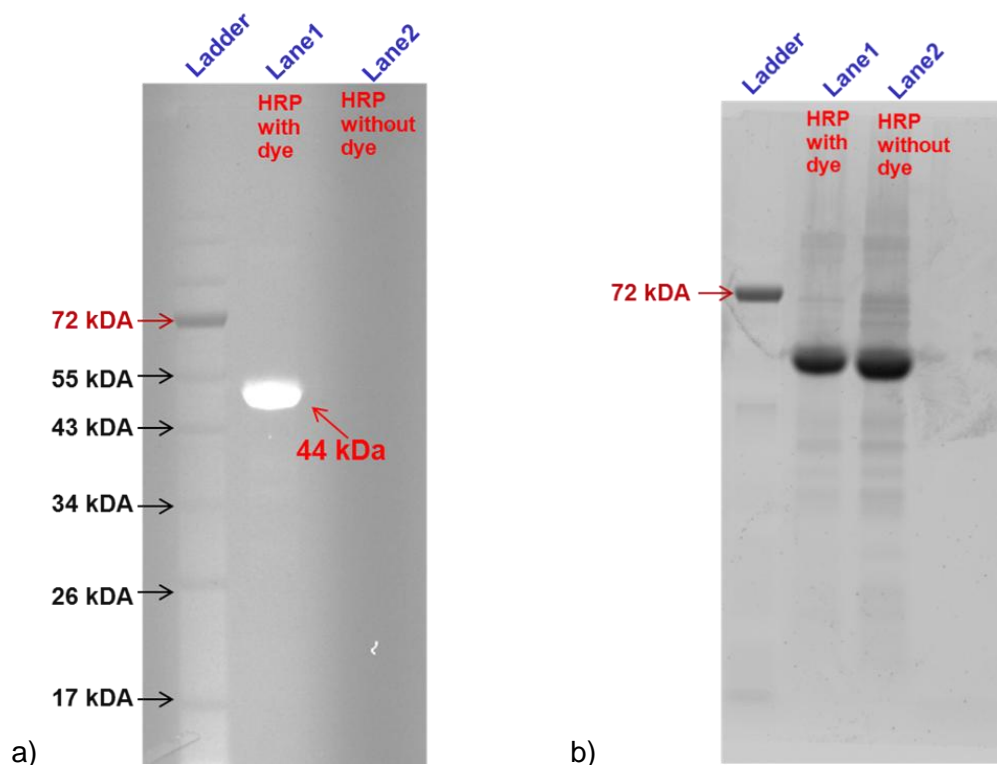


Fig. 4-21 Electrophoresis test: **a)** gel observed under UV lamp after separation and before standard staining procedure, **b)** gel with all separated proteins after staining procedure

The influences of electrode surface morphology and cross linking on the enzyme distribution were analyzed at the model surfaces. However, it can be assumed that the obtained information provides good indications of the protein organization inside the porous enzymatic structures. To test the effect of the surface roughness, labeled HRP was adsorbed at the HOPG (ideally flat surface) and SPG (roughness factor 5.00 [98]). In both cases, the quantity of the

adsorbed enzyme corresponded to the calculated monolayer coverage at the electrode surface. The surfaces of the electrodes were analyzed before enzyme modification (Fig. 4-23). HOPG electrode has very low surface roughness with a maximum profile height of 0.4 nm. On the other hand, SPG has a rough surface with some flat areas and areas with high depressions. The SPG was used as support for the investigation of the HRP catalytic activity for hydrogen peroxide reduction (section 4.1.2).

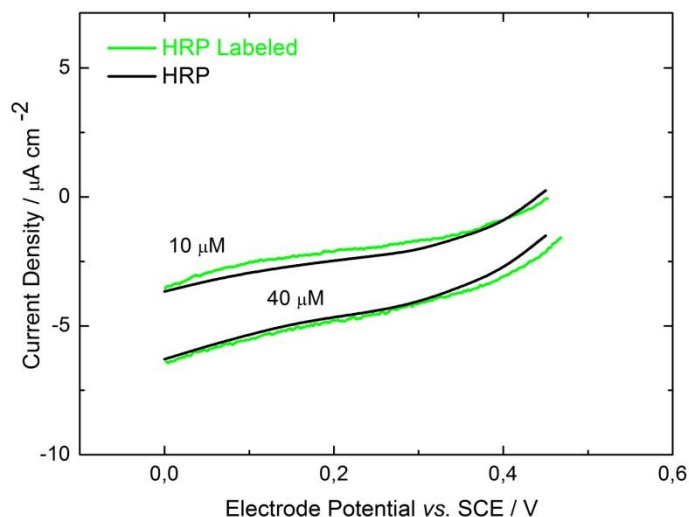


Fig. 4-22 Polarization curves obtained for native HRP and labeled HRP adsorbed at the graphite support, 400 rpm, pH 7.2, N_2 atmosphere

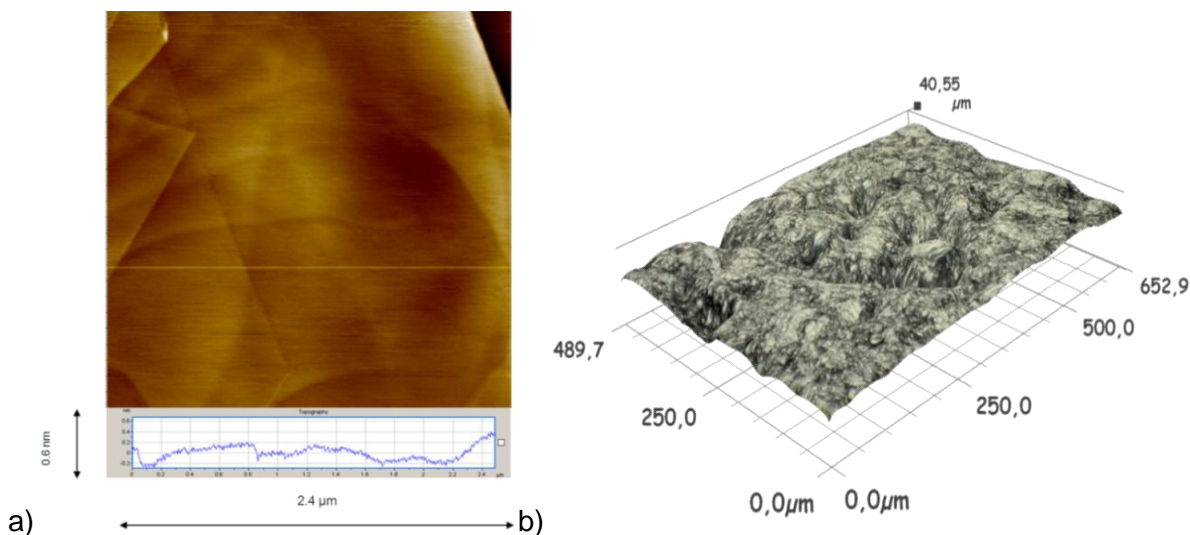


Fig. 4-23 Microscopy images of electrode surfaces before modification with enzyme **a)** Highly Ordered Pyrolytic Graphite - HOPG **b)** Spectroscopic Graphite -SPG

Uniform levels of fluorescence across the whole surface, noticed in the case of the HRP-HOPG electrode, correspond to uniform level of enzyme distribution (Fig. 4-24a). Additionally, the assumption of the monolayer coverage has been confirmed in the AFM experiment obtained for the same electrode (Fig. 4-24b). The pattern formation observed at the HOPG electrode was strongly pH dependent, showing more expressed branch-like structures at a pH of 7.2 (Fig. 4-25). As can be seen, the average heights of these structures are *approx.* 4 and 5 nm for pH 6.00 and pH 7.2, respectively. These values correspond well to the dimension of the HRP protein (6.2 x 4.2 x 1.2 nm [65, 126]), indicating monolayer formation on the ideally flat surfaces like HOPG. Although the height of these enzymes is only slightly pH dependent, the width of HRP aggregates are pH sensitive, showing more compact structures at higher pH values (*approx.* 100 nm and 300 nm at pH 6.00 and pH 7.2, respectively). Taking into account larger formed HRP aggregates at higher pH and that the mechanism of HRP at the electrode is via DET, this observation can contribute to electrode activity under different pH values.

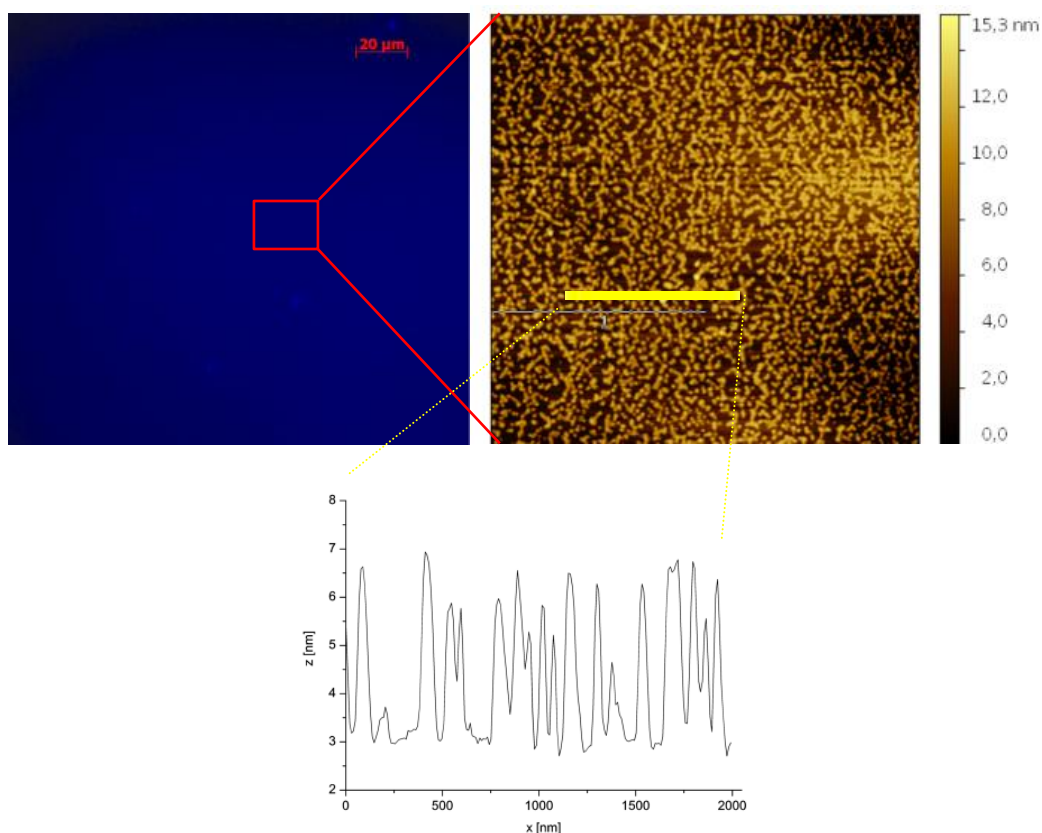


Fig. 4-24 Labeled-HRP on HOPG support visualized by **a)** fluorescence microscopy with exposure time of 200 ms and **b)** AFM image of HRP adsorbed on HOPG in a monolayer at pH 6

On the contrary, FM image of the spectroscopic graphite shows a non-uniform fluorescent distribution with blue spots of different intensities (Fig. 4-26). The dark areas (black) at the image that have low fluorescent levels (ca. 200 A.U.), can be ascribed to the part of the electrode surface without the enzymes. The non-uniform blue spots indicate the non-uniform enzyme distribution at the remaining part of the surface. The spots with higher level of fluorescent intensity e.g. 1500 A.U. points to the enzyme agglomeration in comparison to the spots with lower level of fluorescence e.g. 800 A.U. (which are similar to those obtained at the HOPG surface), indicating monolayer enzyme adsorption. However, the observed non-uniform protein distribution at SPG corresponds well to a higher level of surface roughness compared to HOPG. These results reveal that monolayer of enzymes can be only formed at the ideally flat surfaces like HOPG. Otherwise, the enzyme agglomeration and non-uniform enzyme distribution as a consequence of support roughness can be expected.

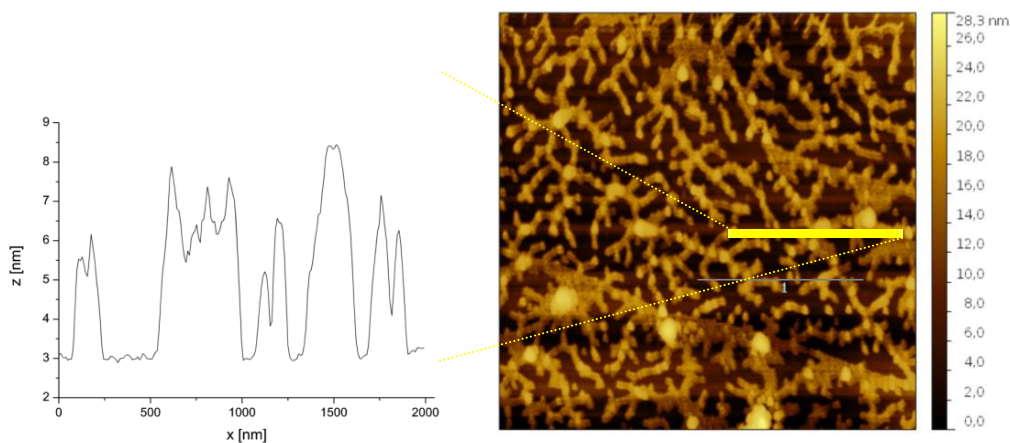


Fig. 4-25 AFM image of HRP adsorbed on HOPG support in a monolayer at pH 7.2

Additionally, it can be assumed that the adsorption strength between protein and surface will vary for different adsorption sites (e.g. flat areas or depressions at the surface). This assumption is confirmed in the representative image taken after constant rotation of the HRP-SPG electrode for 2 h (Fig. 4-26b). One can clearly see that after rotation, the spots with low fluorescent intensity, ascribed to the HRP monolayer, disappear and only enzyme agglomerates at the surface are still present (blue spots observed also in Fig. 4-26a, before rotation). As a consequence of enzyme desorption, the electrode performance is also decreasing with time, as shown in Fig. 4-27. The substrate depletion during the experiment has been calculated to be 0.21% (according to Faraday's law, eq. 2-2) and can be neglected. Thus, the decrease of

electrode activity is indeed due to lower amounts of biocatalysts at the surface with time. This observation confirms the assumption of enzyme leaching and stable electrode behavior after rotation, which was also commented in section 4.1.2.

The enzyme distribution directly influences the overall electrode activity (especially for DET enzymes), where only the enzyme's active sites that are in close proximity to the surface are participating in the catalytic reaction. These results indicate that the enzyme agglomeration at the surfaces decrease the number of active enzymes in direct contact to the conductive surface, which influence the overall activity of the electrode.

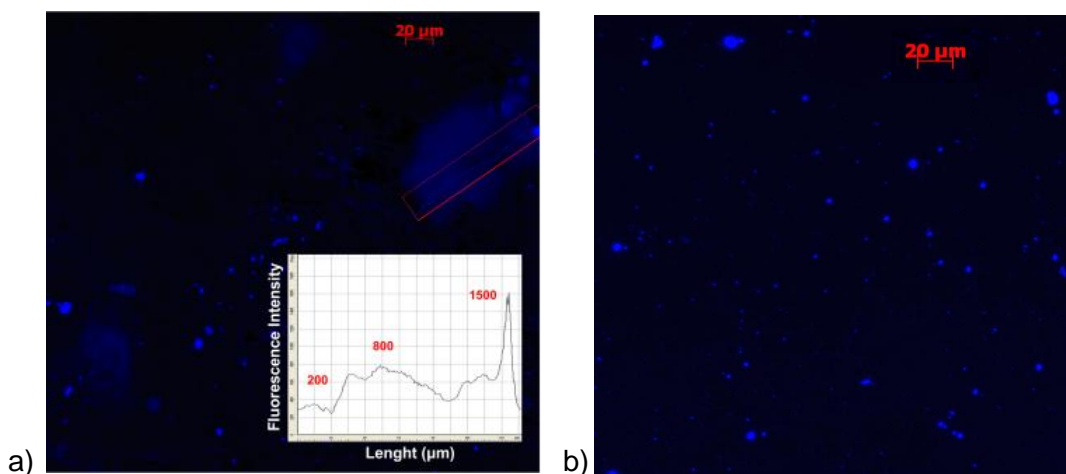


Fig. 4-26 Fluorescence microscopy images of labeled-HRP on the SPG **a)** before rotation, 200 ms exposure time and **b)** after 2 h rotation in RDE, 400 rpm, 100 ms exposure time

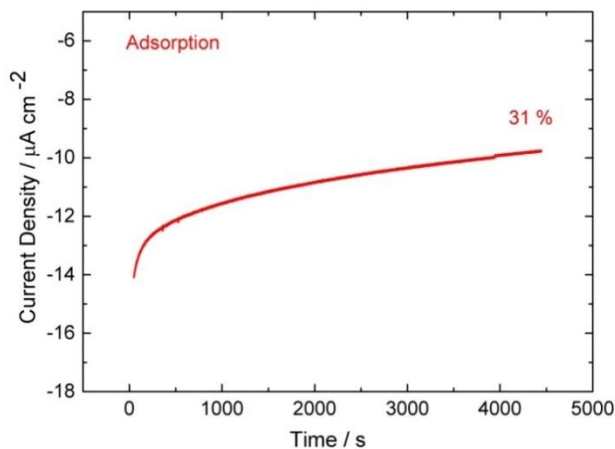


Fig. 4-27 Decrease of electrode activity due to enzyme leaching effect, $E=0.0$ V vs. SCE, $160 \mu\text{M}$, 1000 rpm

4.3.2 Influence of cross-linking

Cross-linking method has been chosen due to the fact that this method stabilizes enzymes at the electrode surface and prevents their leaching from the 3-D structures without influencing their activity (except in the case of extreme ratios between enzymes and cross-linker agents) [133]. Therefore, the enzyme distribution within the porous electrode is not only influenced by the type of material, but the CL agent as well.

First, the effect of cross linking on the enzyme organization was studied at the HOPG and SPG. After the cross-linking method is applied, the enzyme agglomeration at both tested surfaces can be noticed, as demonstrated in Fig. 4-28. At HOPG, one large agglomerate, while on SPG different agglomeration centers that differ in shape and size, can be observed. The average levels of fluorescence for the cross-linked agglomerates at SPG are *ca.* 3200 ± 300 A.U. (Fig. 4-28b, profile shown only for one example). This is a significantly higher level of fluorescence in comparison to the ones observed at the SPG electrode without CL method (*ca.* 1500 A.U, Fig. 4-26).

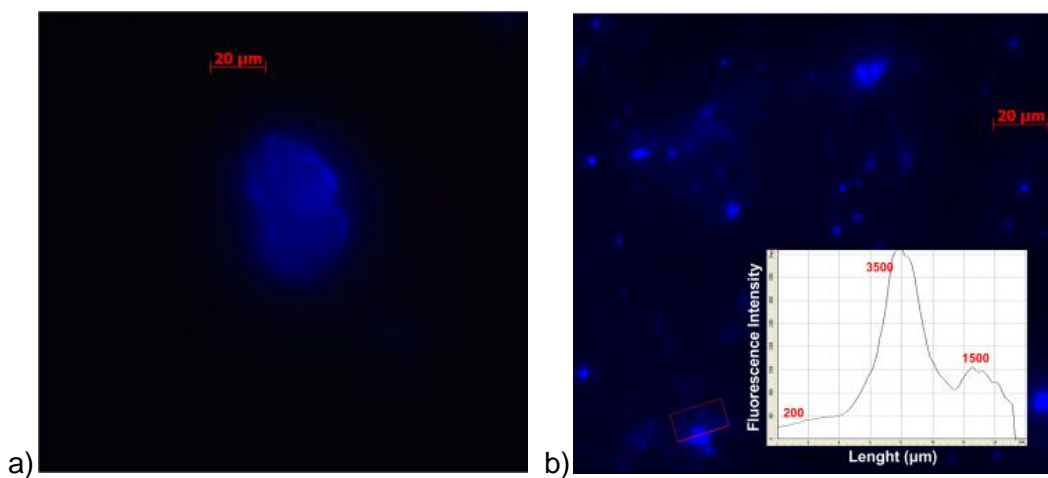


Fig. 4-28 Fluorescence microscopy images of labeled-HRP after CL using 5% glutaraldehyde at **a)** HOPG, imaged with the exposure time of 100 ms and **b)** at spectroscopic graphite surface with 200 ms exposure time

The performance of such a cross-linked electrode, having a high degree of agglomerated enzymes, will be lower due to a decreased number of enzymes that are in touch with the electrode surface. Indeed, this assumption was confirmed in an electrochemical experiment obtained for HRP-SPG electrode with and without CL (Fig. 4-29). It can be noticed that the

percentage of cross-linker also has a significant influence on the electrode activity, most likely influencing level of agglomeration. On the other hand, it has been reported that CL increases the stability of the electrode preventing the enzyme leaching [56].

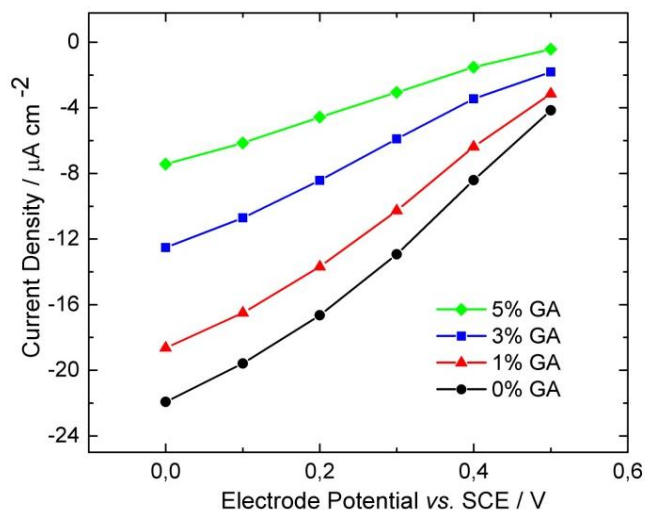


Fig. 4-29 Reduction of hydrogen peroxide at the HRP-modified graphite electrodes prepared without and with cross-linking. Conditions: 160 μM hydrogen peroxide concentration, 400 rpm, pH 6.00, N_2

Next, the mixture of nanomaterials with labeled enzyme in gelatin was cast on the glass support and analyzed for enzyme distribution (Fig. 4-30). Vulcan and Coral Carbon, as representatives of nanoparticle and nanoporous material types were used. For the Vulcan material, small agglomerated particles with sizes between 5 and 10 μm can be observed, while for Coral Carbon, one large agglomerate of 10 x 30 μm can be noticed. The blur area in Fig. 4-30b is due to the focus that was on the particle agglomerate, which was on a higher level than the surroundings. The same spot was further checked with FM in order to visualize enzyme distribution (Fig. 4-30c and d). As can be noticed, Vulcan nanoparticles have been completely covered with the labeled enzymes, while the enzyme distributions at Coral Carbon is more in the pores of the material.

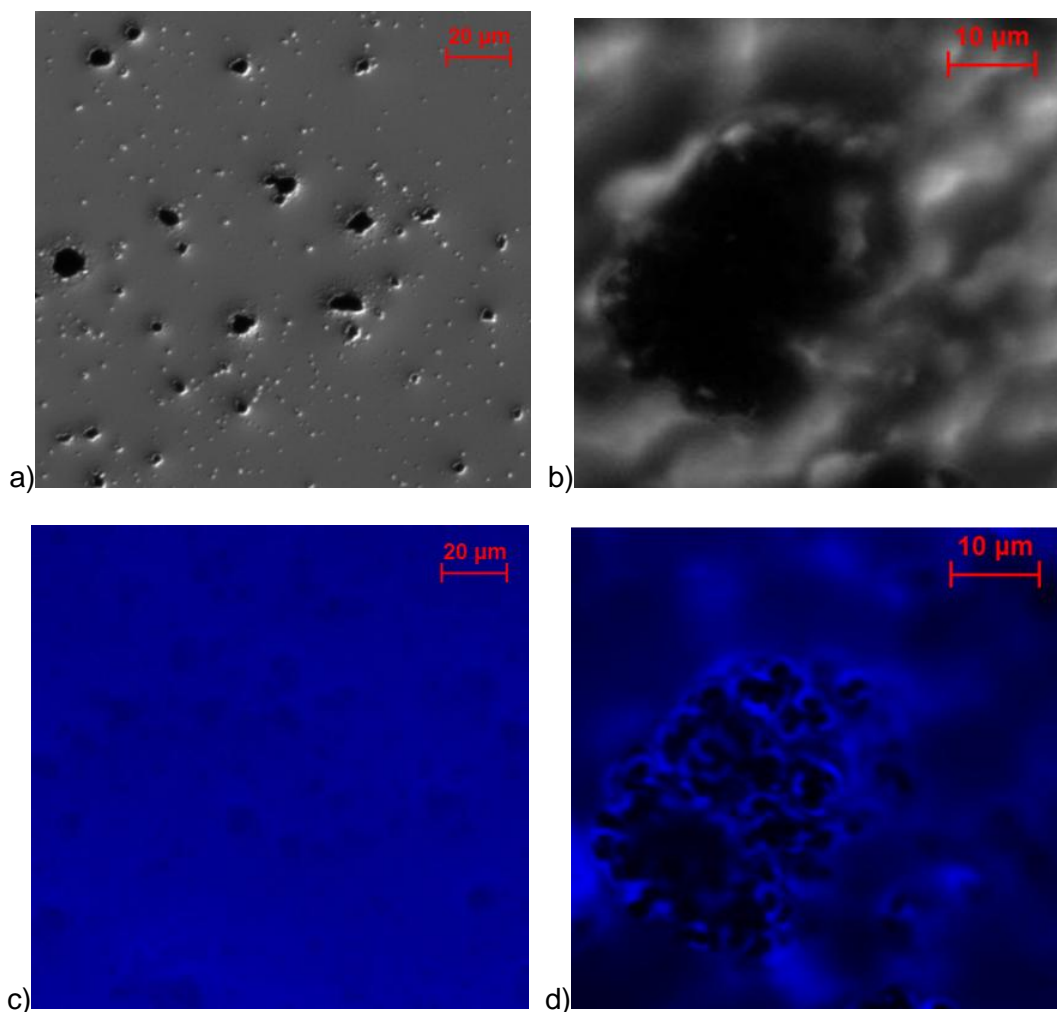


Fig. 4-30 Optical images of **a)** Vulcan and **b)** Coral Carbon at the glass support in gelatin; Fluorescence microscopy images of **c)** Vulcan and **d)** Coral Carbon

Furthermore, the enzyme distribution at nanomaterials after CL has been presented in Fig. 4-31. One can notice intensive enzyme agglomeration around nanoparticle aggregates. This has a large influence on the reduced enzyme contact with support and consequently electrode activity. The result simulates what happens after CL method is applied using the Gelatin procedure for 3-D electrode preparation. Additionally, it confirms the observation that despite a large surface area and high porosity together with a high electrochemical active surface area of Coral Carbon material (section 4.2.1, Fig. 4-9), the enzyme utilization is low, leading to a low overall electrode activity (Fig. 4-11).

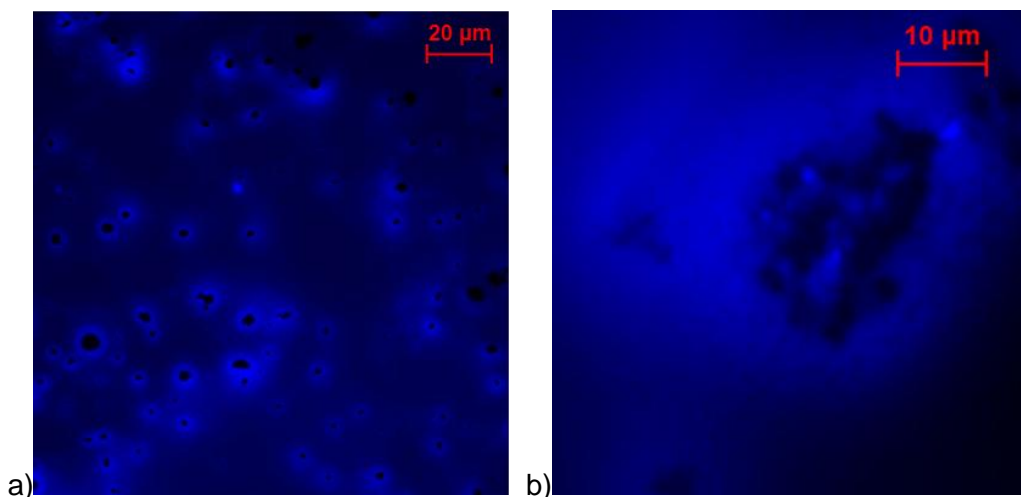


Fig. 4-31 Influence of CL method on the enzyme distribution at the nanomaterial surfaces:
a) Vulcan and **b) Coral Carbon**

4.4 Summary and concluding remarks

Bioelectrocatalytic reduction of hydrogen peroxide on HRP-electrodes, based on a direct electron transfer mechanism between the electrode and heme active site, was successfully demonstrated. The catalytic current can be improved by choosing suitable operating conditions. For example, the electrocatalytic process of peroxide reduction is pH dependent, showing higher performance in more acidic solutions. The optimal substrate concentration should be estimated due to the fact that in excess of H_2O_2 , the inhibition of HRP occurs through the formation of Compound-III, resulting in a decrease of electrode activity.

For the development of the 3-D enzymatic electrode, the first step was towards the evaluation of a suitable nanomaterial support. Two main groups, nanoparticles and nanoporous materials were investigated for peroxide reduction with HRP. It was shown that the highest electrode performance is not correlated to the material with the largest BET and neither to the electrode with largest electrochemical active surface area. SEM characterizations of electrode cross sections reveal pronounced nanomaterial agglomeration, which occurs during the preparation procedure, resulting in the reduction of available surface area for the redox reaction. Therefore, the nanomaterial with the most uniform particle agglomeration in the catalyst layer and the lowest degree of the enzyme agglomeration, which was shown in the case of Vulcan material, determines the electrode overall activity. For instance, enzyme agglomeration that occurs around

approx. 30 μm aggregate presented in Coral Carbon (Fig. 4-32b), lead to decreased surface utilization, since all available pores in nanomaterial that are in nm range are not utilized. Vulcan – based enzymatic electrode results in the highest performance (activity and OCP value for peroxide reduction), and thus, was chosen for further analysis.

The next step was to check the relationship between the immobilization procedure and the enzymatic electrode performance. The goal was, by using two different immobilization methods (Vulcan-PVDF and Vulcan-Gelatin), to understand what causes the difference in activities between two electrodes. It was shown that electrodes prepared without cross linking (Vulcan-PVDF) reach significantly higher catalytic current values for the same nominal enzyme and nanomaterial loading. The reduced number of active catalysts in the Vulcan-Gelatin electrode shifts the loading optimum to higher enzyme loading values (optimum for Vulcan-PVDF: 1 mg cm^{-2} , for Vulcan-Gelatin: 1.75 mg cm^{-2}). SEM cross sections indicate that the thicknesses of both electrodes were similar, but Vulcan-PVDF has higher porosity in comparison to Vulcan-Gelatin. Addition of gelatin leads to stronger Vulcan nanomaterial agglomeration (Vulcan-Gelatin electrode). It was confirmed, that more uniform nanoparticle organization inside the Vulcan-PVDF structure implies a higher surface for enzyme immobilization. Additionally, gelatin film formed on top of the electrode together with reduced electrode porosity produces an additional barrier for mass transport of substrate.

According to the information obtained using fluorescence microscopy, enzyme agglomeration at the electrode surface strongly depends on the surface roughness and it increases when the cross linking procedure is applied. This has a negative effect on the overall enzymatic electrode performance, in both activity and onset potential values. Additionally, it was shown that enzyme utilization on flat electrodes is very small due to enzyme agglomeration as a consequence of electrode morphology. The monolayer enzyme coverage at the electrode surface is only possible if an ideally flat surface like HOPG is used.

It was demonstrated that using a suitable material support (Vulcan nanoparticles) together with a suitable immobilization procedure, electrode activity can be significantly improved: from the starting value of 54 $\mu\text{A cm}^{-2}$ for the flat graphite electrode to the value of 1200 $\mu\text{A cm}^{-2}$ for the optimized 3-D porous electrode. Additionally, by designing the 3-D enzymatic electrode using the same nanomaterial but applying different immobilization strategies, significant improvements in the performance was demonstrated. Providing a more uniform electrode structure, higher electrode porosity and higher biocatalyst utilization *i.e.* number of active enzymes, the electrode

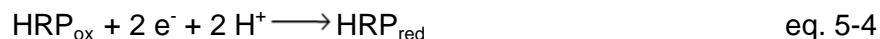
activity was increased from $300 \mu\text{A cm}^{-2}$ (Gelatin procedure) to $1200 \mu\text{A cm}^{-2}$ (PVDF procedure). Optimized electrode (Vulcan-PVDF procedure) shows the highest reported performance in literature so far, for the HRP based electrodes employing DET.

5. GOx-modified enzymatic electrode for glucose oxidation

In the previous chapter, HRP enzymatic electrodes were investigated. It was shown that the choice of immobilization techniques plays an important role for the development of enzymatic electrodes and maximizing their current output. This research was further extended to design enzymatic electrodes using GOx for the selective oxidation of glucose. Bioelectrodes were developed for both sides of the electrochemical reactor (*i.e.* the anode and the cathode). The anode comprises of GOx with TTF (tetrathiafulvalene) as the mediator, while the cathode employs cascade GOx and HRP with direct electron transfer mechanism. In this chapter, the main focus is on analyzing and estimating optimal immobilization and operational conditions for the improvement of GOx-electrode performance before their utilization in the electrochemical reactor.

5.1 Biocathode: GOx–HRP enzymatic electrode

By GOx-HRP cascade, glucose is first enzymatically oxidized with molecular oxygen, producing gluconic acid and hydrogen peroxide as the by-product (eq. 5-1, 5-2). In the next step, peroxide is further reduced to water, while HRP is regenerated electrochemically to its native state (eq. 5-3, 5-4). In this way, hydrogen peroxide is locally removed, which should increase the stability of the enzymes. One of the main challenges in the development of the GOx-HRP enzymatic cathode is optimization of the conditions in order to prevent operation at high peroxide concentrations, which induces HRP inhibition [109, 117] and GOx deactivation [134].



GOx-HRP cascade has been envisioned for application in biosensors and as an oxygen-reducing cathode in enzymatic fuel cells that uses glucose as the fuel. For example, significant

improvement of the device performance and sensitivity, when the GOx-HRP enzymatic electrode was employed for glucose detection in the mediator-less biosensor, has been demonstrated [135, 136]. Additionally, in the biofuel cell research, enzymatic cascade has been proposed as a suitable and efficient alternative for the replacement of conventional biocathodes based on laccase or BOD [107, 115]. The limitation of these multicopper oxidase electrodes is in inefficient and inhibited activity under physiological conditions *i.e.* 5 mM glucose and 0.14 NaCl. On the contrary, the proposed alternative based on the GOx-HRP electrode has shown high activity and resistance in the presence of inhibitors like chloride and urate ions [108]. From the perspective of bioelectrochemical synthesis, the advantage of the enzymatic cascade at the electrode surface is in an efficient removal of the by-product, hydrogen peroxide. Additionally, due to the fact that the electroreduction reaction of H₂O₂ occurs after glucose oxidation, it can be utilized as a cathode in the electroenzymatic reactor for gluconic acid production.

For the previously mentioned applications of bienzymatic electrodes, in biosensors and fuel cells, the research emphasis was on the electrode sensitivity and on the electrode performance in the presence of 5 mM glucose and Cl⁻ ions, simulating conditions for implantable devices [135-137]. For application in a bioelectrochemical reactor, it is necessary to improve electrode performance in terms of catalytic current densities and efficiency for glucose conversion.

5.1.1 Influence of the immobilization procedure

Taking advantage of the successfully developed HRP electrode with efficient DET, the GOx-HRP system was investigated using previously demonstrated preparation procedures. Both electrode modifications, GOx-HRP with Gelatin and PVDF as the binder, were followed in the absence and presence of substrate glucose and oxygen atmosphere.

As can be seen from cyclic voltammograms of bienzymatic electrodes in the presence of PBS, there are no electroenzymatic activity or redox processes that can be ascribed to Fe³⁺/Fe²⁺ of heme iron in HRP or to FAD/FADH₂ cofactor of GOx (Fig. 5-1). The redox processes of these two groups have been observed at -0.08 V and -0.48 V, respectively, for covalently linked enzymes to MWCNT using boronic esters with pyrene [109]. In the present case, the enzymes were physically immobilized (adsorption and entrapment), thus the presence of redox picks is not expected [115]. The resulting CVs of GOx-HRP electrodes appear very similar, showing only features of carbon material [138]. Additionally, the same CVs of two tested electrodes indicate

similar electrochemical surface area, which are comparable to previously investigated electrode based only on the HRP enzyme (Fig. 4-13).

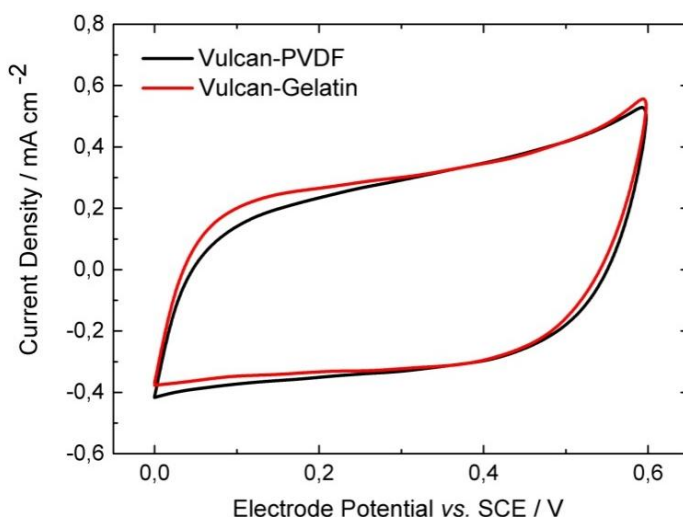


Fig. 5-1 Cyclic voltammograms of Vulcan-Gelatin and Vulcan-PVDF enzymatic biocathode (based on the enzyme cascade GOx-HRP) in 0.1 M phosphate buffer, pH 6.00, 400 rpm, scan rate 5 mV s⁻¹, 22 °C and N₂ atmosphere

As expected, the addition of glucose and oxygen results in an increasing reduction current for both procedures (Fig. 5-2). The activity of the electrode based on Vulcan-PVDF is *ca.* 0.5 mA cm⁻² higher than the electrode activity reached by the Vulcan-Gelatin electrode. The reason for these different behaviors can be explained by the difference in the amount of active catalysts in the electrode structure. As shown in chapter 4, cross-linking that was applied in the case of Vulcan-Gelatin, causes enzyme agglomeration. This effect decreases the number of catalysts that are in contact with the electron conductive surface, which in the case of DET-enzymes leads to a decrease of the electrode performance (Fig. 4-27, 4-31). Therefore, it could have been expected that this effect will have influence on the GOx-HRP/Vulcan-Gelatin activity that rely on DET for HRP regeneration. On the other hand, the GOx-HRP/Vulcan-PVDF electrode shows a current response of *approx.* 0.9 mA cm⁻² at 20 mM glucose. This value confirms a high electrocatalytic activity of bienzyme electrode that is comparable with performances reported for biocathodes based on laccase or BOD enzymatic electrodes used in enzymatic fuel cells (taking into account that 2 instead of 4 electrons are exchanged in the fuel cell case) [54, 103, 139-142]. Additionally, the performance of GOx-HRP/Vulcan-PVDF is significantly higher in comparison to the other tested GOx-HRP electrodes based on DET (Table 5-1). The tested electrodes are

mainly designed for fuel cell application, thus, glucose concentration was 5 mM in all tested systems. The performance of the Vulcan-PVDF electrode is comparable to a current density of *approx.* 1.1 mA cm⁻² obtained for GOx-HRP on a buckypaper employing MET where ABTS served as the mediator [108]. The improved performance of the Vulcan-PVDF procedure motivated the use of that procedure for the enzymatic cathode in the electroenzymatic reactor.

The performance of the enzymatic electrode comprising the GOx-HRP cascade can be compared to the performance of the HRP cathode prepared with the same procedure in the presence of 2 mM hydrogen peroxide (Fig. 4-15).

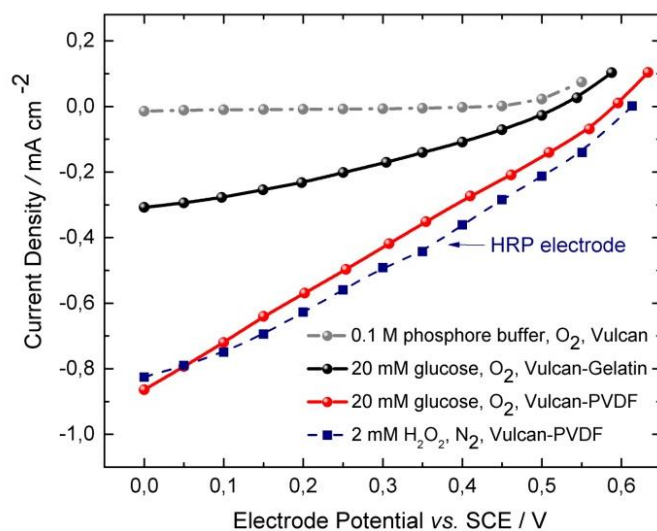


Fig. 5-2 Influence of preparation procedures on steady state polarization behavior of GOx-HRP enzymatic electrode

Table 5-1 Performance comparison of the GOx-HRP electrode for peroxide reduction with DET

Electrode	Conditions	OCP/ V vs. SCE	Concentrations / mM	Current density / $\mu\text{A cm}^{-2}$	Ref.
MWCNT	0.1 M PBS, pH 7.4	0.43	5	10	[109]
GDE	0.05 M PBS, pH 6.0	0.64	5	100	[143]
DWCNT	0.01 M PBS, pH 7.4	0.35	5	125	[107]
CNT / CMF	67 mM PBS, pH 7.0	0.6	5	130	[115]
Vulcan-PVDF	0.1 M PBS, pH 6.0	0.6	20	900	This work

Abbreviations: MWCNT – multiwall carbon nanotubes, GDE – graphite rode electrode, DWCNT – double-walled carbon nanotubes, CNT / CMF – carbon nanotubes / micro-fibers

5.1.2 Optimization of the operating conditions

After the optimal electrode preparation procedure was established, operating conditions (pH, temperature and glucose concentration) were analyzed. Since the enzyme activity depends on the ionization state of the amino acids in the active site, it was necessary to adjust the optimal pH which plays an important role in maintaining the proper enzyme conformation. Additionally, enzymes are highly sensitive to temperature changes where most of them get denatured at temperatures of more than 40°C [134].

The optimal conditions of the enzymatic electrode largely depend on the optimal pH level and temperature of the enzymatic catalysts. According to the literature, optimal conditions for GOx are pH 5.0 to 8.0 at temperature of $T = 37\text{ }^{\circ}\text{C}$ [138, 144-146], while for HRP are pH 5.0 to 7.0 at $T = 22\text{ }^{\circ}\text{C}$ [43, 77, 147]. The influence of these conditions on the electrode performance can be seen in Fig. 5-3. The results indicate pH 6 and $T = 22\text{ }^{\circ}\text{C}$ as optimal values for the biocathode. It can be noticed that the change of pH and temperature influences the onset electrode potential. At the optimal conditions, reduction of H_2O_2 has the highest value for the onset potential (0.6 V vs. SCE), which corresponds well to the onset potential obtained for peroxide reduction on HRP electrodes presented in Fig. 4-13 and as well to the other HRP – modified graphite electrodes [44].

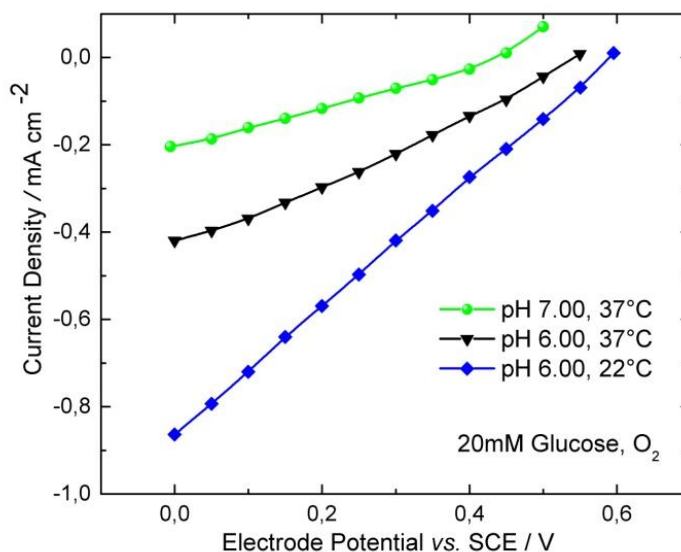


Fig. 5-3 Steady state polarization behavior of the enzymatic cathode (GOx-HRP/Vulcan-PVDF) at two different pH and temperatures, at 400 rpm rotation rate

The optimal glucose concentration needs to be estimated in order to maximize the performance of the bienzymatic electrode and at the same time to prevent enzyme inhibition. Operation at higher glucose concentration leads to excess of by-product, H_2O_2 , that decreases activity and stability of both redox catalysts (inhibition mechanisms presented in [44]). Corresponding polarization curves for concentration dependences are presented in Fig. 5-4. Upon raising the substrate concentration, the catalytic current increases until the maximum current density at 20 mM glucose. As can be seen for lower glucose concentrations, the enzymatic reaction is limited by the substrate concentration, while at higher values the electrochemical step becomes rate-limiting. Further increase of glucose concentration above 20 mM, results in decrease of the catalytic current indicating enzyme inhibition. Therefore, in the case of the GOx-HRP enzymatic electrodes, concentration of 20 mM was chosen as optimal. Fig. 5-4b presents current response as a function of glucose concentration. The shape of the calibration curve suggests typical enzyme dependence with a linear part and plateau under saturated conditions. Additionally, the gradual decrease of catalytic current at higher glucose concentration indicates the progressive formation of the inactive form of HRP (Compound-III).

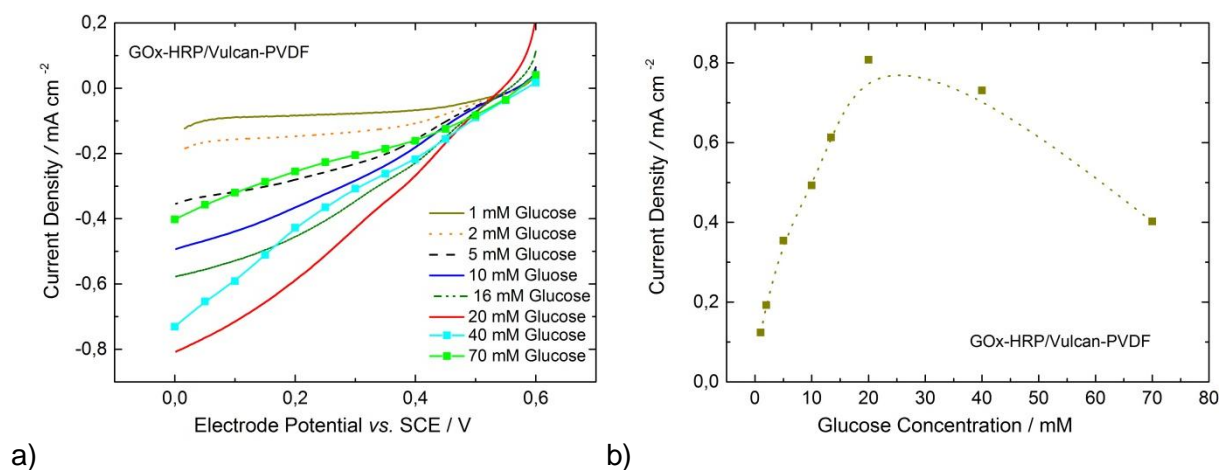


Fig. 5-4 Polarization curves of the enzymatic cathode at different glucose concentrations, pH 6.00, 22 °C, 400 rpm rotation and presence of O_2

The activity of enzyme cascade immobilized at the electrode largely depends on the chosen ratio between GOx and HRP. In the present case, it was demonstrated that higher loadings of HRP are more beneficial for electrode performance (Fig. 5-5). This was also confirmed in Reuillard *et al.* [109], where it was shown that at lower HRP/GOx ratios and high

glucose concentrations, the catalytic activity decreases due to the local overproduction of H_2O_2 . Higher ratios of HRP/GOx enable higher amounts of HRP at the electrode surface preventing rapid saturation and inhibition by peroxide [109]. Thus, the goal is to maximize the amount of HRP and in the same time to keep lower amounts of GOx in order to limit the overproduction of H_2O_2 . Since the loading and amount of active enzymes are largely determined by immobilization techniques used for preparation of particular electrodes, the ratio of 3:1 HRP/GOx was optimal in the case of the Vulcan-PVDF.

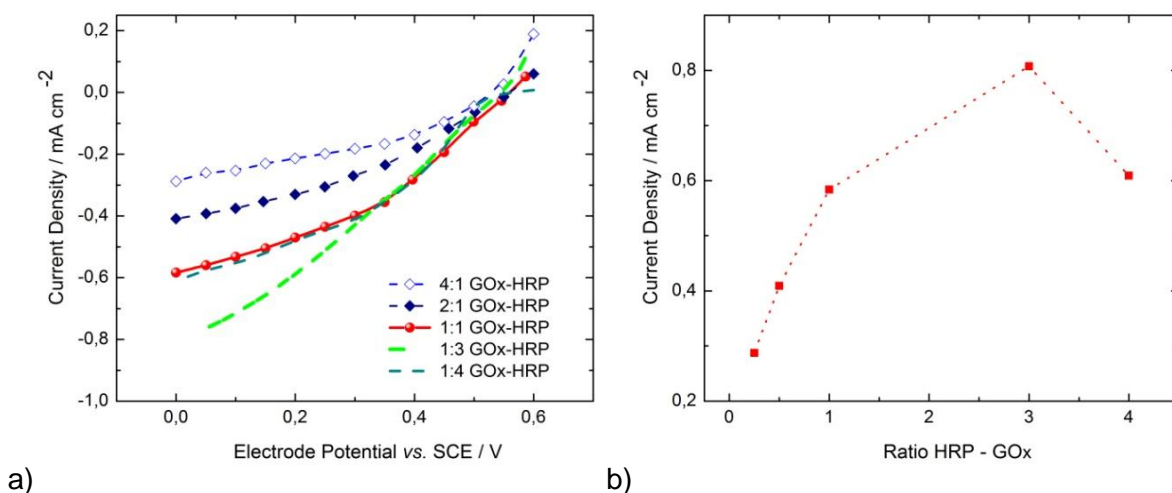


Fig. 5-5 Polarization curves of different HRP-GOx ratios, in presence of 20 mM glucose and oxygen, pH 6.00, 22 °C, at 400 rpm

5.2 Bioanode: GOx–TTF enzymatic electrodes

GOx based electrodes are well characterized and integrated as bioanodes in various enzymatic fuel cells and an additionally in some electroenzymatic reactors [10, 64]. Although GOx is attractive catalyst with high activity, there are difficulties to establish direct electron transfer with conductive support, due to its thick carbohydrate shell. Therefore, in order to be successfully employed as a catalyst at the electrode surface, the presence of an electroactive molecule (mediator) is necessary. Typical mediators that have been used in GOx-electrodes are Os redox polymers, TTF, ferrocene, 8-hydroxyquinoline-5-sulfonic (HQS) etc. [40, 79]. Even though Os hydrogels showed the best performance, due to their complex synthesis procedures and issues with toxicity, TTF was chosen as suitable alternative for the mediator of the GOx electrode. The

reaction kinetic of glucose oxidation on GOx electrode using TTF as the mediator follow the so-called two-substrate ping-pong mechanism [148]. The simplified reaction mechanism can be presented by equations 5-5 to 5-7, where Med_{ox} stands for TTF⁺ and Med_{red} for TTF.



TTF undergoes two redox transformations, to TTF⁺ and TTF²⁺ radical cations. The analysis shows that both of them can be used as mediators for GOx regeneration to its oxidized state [149]. However, in the potential region of interest (from -0.2 V until 0.2 V), one can see the redox process assigned to the TTF/TTF⁺ couple, occurring at the electrode prepared with Vulcan-PVDF-TTF procedure (Fig. 5-6). The oxidation process to TTF⁺ starts at about 0.05 V, while reduction of TTF⁺ back to TTF is visible in a negative scan with a well-defined pick. This behavior corresponds to the tested electrodes prepared with the same commercial Vulcan XC72 nanomaterial as shown by Ivanov *et al.* [104].

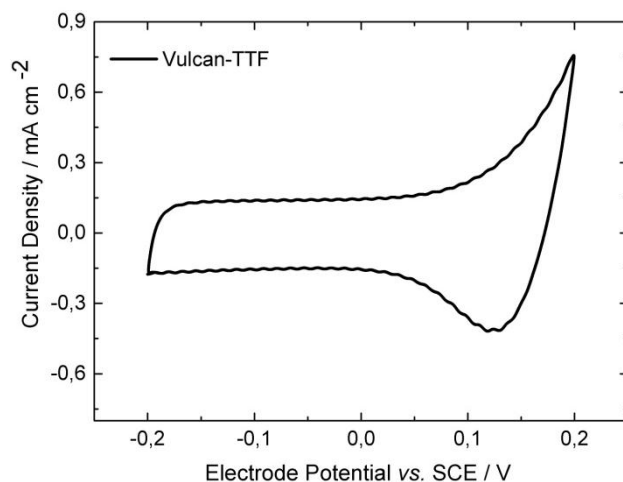


Fig. 5-6 Cyclic voltammogram of Vulcan-TTF-PVDF enzymatic bioanode in 0.1 M phosphate buffer, pH 6.00, scan rate 5 mV s⁻¹, 400 rpm rotation and N₂ atmosphere

5.2.1 Influence of the immobilization procedure

In Fig. 5-7, the performances of the GOx/TTF electrodes, based on the two immobilization strategies (Gelatin and PVDF procedure) in presence of 20 mM glucose, have been presented. As can be seen, the electrode prepared with Vulcan-Gelatin procedure exhibits more negative onset potential (-0.15 V vs. SCE) than the Vulcan-PVDF (-0.05 V vs. SCE). The value of the electrode onset potential can vary depending on the enzyme and mediator concentration used for the immobilization procedure as well as on the substrate concentration [148]. For example, the onset potentials for other electrodes based on TTF as the mediator can reach values between 0 and -0.1 V vs. SCE [53, 150]. From the perspective of fuel cell research, systems with Vulcan-Gelatin as an anode are more beneficial providing higher open circuit voltage.

The evaluation criteria of suitable immobilization procedures for mediated ET enzymatic electrodes are different than for the electrode exhibiting direct ET. For instance, in the case of the GOx-TTF electrode, direct contact between enzyme and electrode surface and effect of enzyme agglomeration are not predominant criteria. Parameters related to mediator contact, its regeneration step, together with possibility of TTF⁺ diffusion out of the catalyst layer under certain conditions [104], all play important roles for the overall electrode response. As can be seen from Fig 5-7, in the potential region up to *approx.* 0.1 V, the procedure with Vulcan-Gelatin shows better performance than electrodes prepared with the PVDF procedure. On the other hand, increasing the potential above 0.1 V, the PVDF procedure exhibits higher current values. It can be anticipated, that due to electrode morphology caused by gelatin as a binder in the case of Vulcan-Gelatin; the diffusion and regeneration of a mediator is limited and it becomes more obvious at higher overpotential. Therefore, optimal procedure will depend on the potential region of interest that is used for the reactor operation. Additionally, it should be taken into account that the bioelectrode prepared in the microenvironment of gelatin will exhibit higher stability [56]. The performance of the GOx-TTF/Vulcan-PVDF electrode (*ca.* 1.4 mA cm⁻² at $E = 0.0$ V vs. SCE) is higher than performances reported for the GOx electrode based on Os polymer as a mediator (0.6 mA cm⁻², at 100 mM glucose) [151] and comparable to other electrodes using Os redox polymer [152-155].

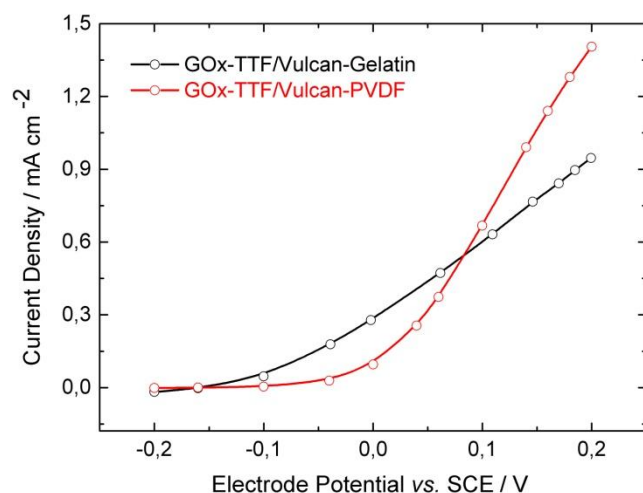


Fig. 5-7 Influence of preparation procedure on the performance of GOx-TTF electrodes for glucose oxidation. Conditions: 20 mM glucose in 0.1 M phosphate buffer, N₂, 400 rpm, pH 6.00, 22 °C.

5.2.2 Optimization of the operating conditions

In the next step, optimal operating conditions for the bioanodes were evaluated. The influences of pH and temperature on the electrode performance have been presented in Fig. 5-8a. The results show that the optimal conditions for the bioanode are pH 7.00 and temperature of 37 °C. However, taking into consideration optimal conditions for the GOx-HRP cathode, it can be concluded that there are different optima for the anode and cathode (pH 7 and T = 37 °C at the anode; pH 6 and T = 22 °C at the cathode). Therefore, in order to combine tested electrodes in the membrane-less reactor configuration, compromise regarding pH, temperature and composition of the electrolyte is required. In the present case, lower pH and temperature were chosen since the whole system is limited electrochemically by the cathode.

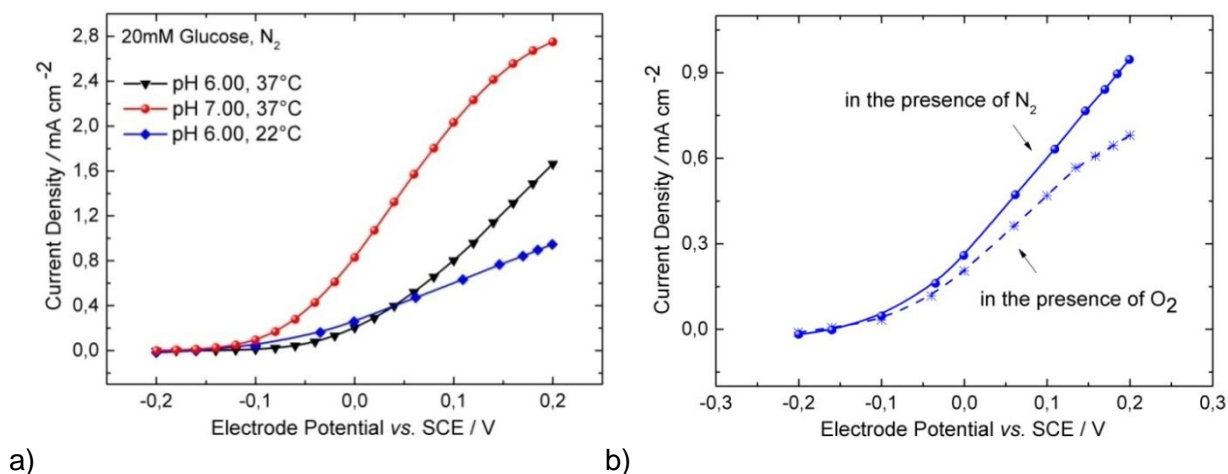


Fig. 5-8 Steady state performance of enzymatic anode (GOx-TTF/Vulcan-Gelatin) **a)** at two different pH and temperatures **b)** under nitrogen and oxygen atmosphere, 400 rpm

Due to the fact that GOx is employed as a catalyst at both sides in the electrochemical reactor, membrane-less design can be used with glucose as a substrate. However, regarding the composition of the electrolyte, the main issue is the presence of oxygen, which as a natural electron acceptor for GOx, competes with TTF at the anode [40]. This can reduce the current density level in the system, since the part of the electronic current is lost as presented in Fig. 5-8b. Additionally, some hydrogen peroxide, which evolves at the anode, can possibly decrease the anode long-term stability. Nevertheless, in order to minimize presence of oxygen at the anode in the present reactor construction, oxygen was supplied only to the cathode from the gas phase. As presented in Fig. 5-8b, the impact of oxygen is more pronounced at more positive overpotentials, which means that careful selection of the operating potential of the anode can reduce this problem.

The performance of the GOx-TTF optimized electrode was tested in the presence of different glucose concentrations (Fig. 5-9). Despite better activity of the GOx-TTF electrode at higher glucose concentration (over 20 mM), the concentration has to be fixed to 20 mM according to the tested biocathode.

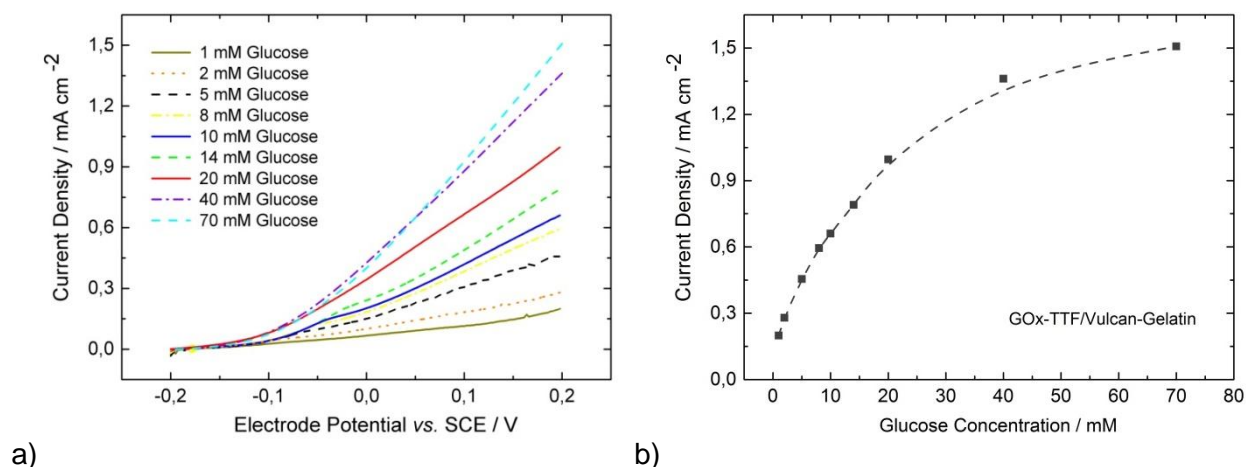


Fig. 5-9 Steady state polarization curves of the enzymatic anode in presence of different glucose concentration, pH 6.00, 400 rpm, N₂

5.3 Summary and concluding remarks

GOx enzymatic electrodes are developed and optimized in order to be integrated in electroenzymatic reactor for glucose oxidation to gluconic acid. The main difference between developed electrodes is in the enzyme regeneration and the final electron acceptor (mediator or oxygen), which determines the final electrochemical reaction. The electrode that is based on the enzymatic cascade (GOx-HRP) exhibits bioelectrochemical reduction of peroxide with enzymatic glucose oxidation, while the GOx-TTF electrode shows bioelectrocatalytic oxidation of glucose through mediated ET. The final goal is to integrate them in the electrochemical reactor, one as anode and the other one as cathode. Before their employment in the electrochemical reactor, the investigations of optimal immobilization procedures and operating parameters such as pH, temperature, substrate concentration were necessary.

For the GOx-HRP electrode, the procedure using enzyme adsorption and PVDF as binder reaches catalytic activity of 0.9 mA cm⁻², which is so far the most efficient performance in comparison to other GOx-HRP electrodes based on DET reported in literature. In the case of the GOx-TTF electrode, due to the different mechanism that is based on MET, both immobilization procedures appear efficient, depending on the choice of operating electrode potential. However, the Gelatin procedure was chosen as the immobilization technique of the anode, due to the

higher stability of Vulcan-Gelatin procedure and the more beneficial OCP value (-0.15 V vs. SCE).

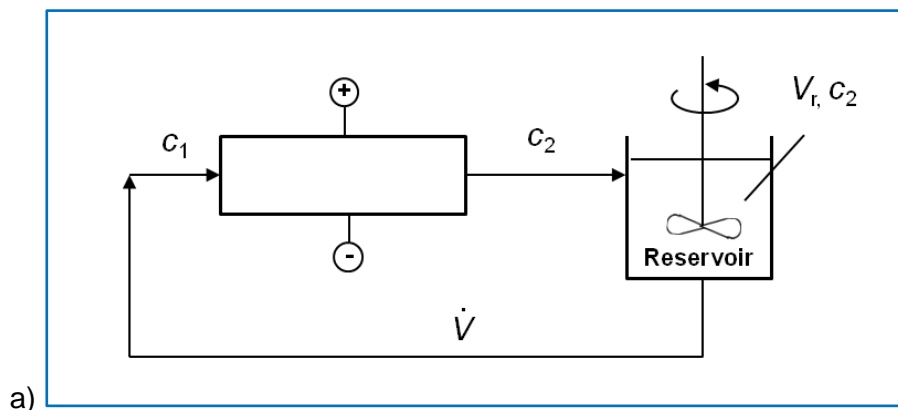
The optimal operating conditions for the reactor, integrating both GOx-electrodes, require a compromise regarding pH and temperature and are chosen according to the conditions of the less active electrode (GOx-HRP). Thus, pH 6.00 and temperature of 22 °C will be employed for the reactor operation. Additionally, the concentration of glucose as the substrate was adjusted to 20 mM, in order to have maximal utilization and in the same time to prevent the enzyme inhibition with by-product (H_2O_2). The optimal ratio between HRP and GOx was set to maximize HRP loading for efficient removal of hydrogen peroxide.

6. Electroenzymatic reactor for partial glucose oxidation to gluconic acid

6.1 Reactor Concept

In the following sections, the feasibility of the electroenzymatic reactor for glucose oxidation to gluconic acid was investigated. The influence of the structural and operational parameters on glucose conversion was studied. Further, the relationship between the electrochemical performance of the reactor and the product selectivity and yield, was presented in detail.

The reactor is comprised of two GOx-enzymatic electrodes described in chapter 5. The GOx-TTF/Vulcan-Gelatin electrode was implemented as the anode and GOx-HRP/Vulcan-PVDF as the cathode. The reactor design has been presented in Fig. 6-1. All the components are immobilized at the electrode surface, where glucose solution was recirculated from a well-mixed reservoir. Oxygen is supplied through a flow field directly to the cathode side. In comparison to other electroenzymatic processes for gluconic acid production, the suggested variant can operate in the co-generation mode, thus the process is running spontaneously as a fuel cell. As previously described, pH of 6.00 and temperature 22 °C were chosen for reactor operating conditions.



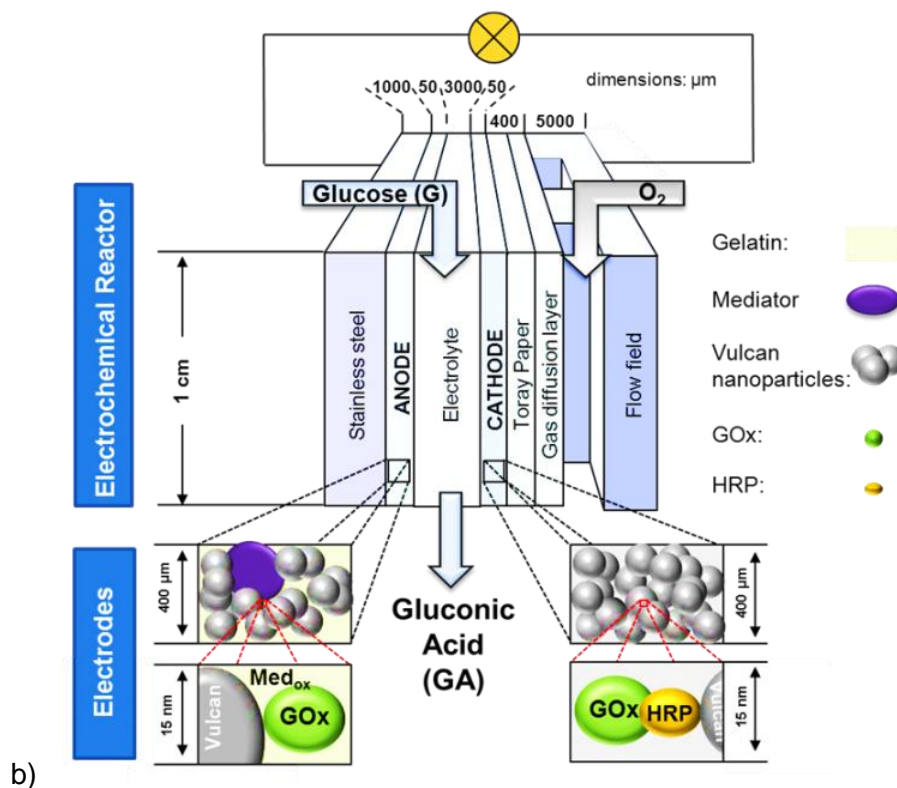


Fig. 6-1 a) Schematic presentation of the reactor setup with recirculation of electrolyte (for more detail see Fig. 3-8) **b)** Schematic representation of electroenzymatic reactor, Anode side: GOx-mediated electron transfer, Cathode side: GOx-HRP enzyme cascade for glucose oxidation

6.2 Development of GOx||GOx-HRP electroenzymatic reactor

6.2.1 Electrochemical performance as an enzymatic fuel cell

Glucose biofuel cells have been studied for nearly 50 years, since the first work was reported in 1964 [63]. Most of them are based on glucose oxidation using GOx or GDH at the anode, and oxygen reduction with laccase or BOD at the cathode. However, they differ significantly in the enzyme immobilization approach and fuel cell design [50, 53, 156]. Due to limited power density from several μW up to 1 mW cm^{-2} , potential specific applications have been found as implantable devices, microchips, drug delivery etc. [157, 158]. Additionally, for such applications, the sustainability and non-toxicity of the materials and system are highly important. The presented electrochemical reactors can be operated in the region of positive voltage values ($E_{\text{cell}} > 0$; $I_{\text{cell}} > 0$),

which corresponds to the fuel cell mode of operation, and reactions at the electrodes are occurring spontaneously without any additional energy input. Therefore, before analyzing the reactor productivity, its electrochemical performance in terms of power output has been shown.

The enzyme and Vulcan nanoparticle loadings at the cathode were changed, while the parameters at the anode were kept constant. Table 6-1 shows variation of these cathode structural parameters. The enzyme loading was adjusted by changing the adsorption time. After 18 h, saturation conditions were reached and the electrode activity was not further changing. The Vulcan loading, which determines the available surface area for catalyst adsorption, electrochemical surface reactions and charge transfer, was increased from 2 to 4 mg cm⁻². Further increase of the Vulcan loading was not possible due to mechanical instability of the electrode.

Table 6-1 Nanomaterial and enzyme loadings at the cathode side

System	Vulcan Loading / mg cm ⁻²	Adsorption time (Enzyme Loading) / h
Reactor 1	2	2
Reactor 2	4	2
Reactor 3	4	18

Polarization and power curves of the electroenzymatic reactors employing three different cathodes are shown in Fig. 6-2. As can be seen, higher enzyme and nanomaterial loadings result in improved performance of investigated electrochemical cells in terms of current density and power output, from *ca.* 300 μA cm⁻² to 600 μA cm⁻² and *ca.* 30 to 100 μW cm⁻², respectively. The performance of Reactor 3 is superior compared to the enzymatic fuel cell with the same combination of enzymes (GOx and HRP), reaching a maximum power density of around 5 μW cm⁻² for 20 mM glucose solution [143]. Additionally, the power performance of Reactor 3 can be compared to other glucose/oxygen fuel cells based on GOx and BOD or laccase as a cathode [159-162]. However, this power level is below the performance of the so far best reported enzymatic fuel cell (*ca.* 1.3 mW cm⁻²) [163].

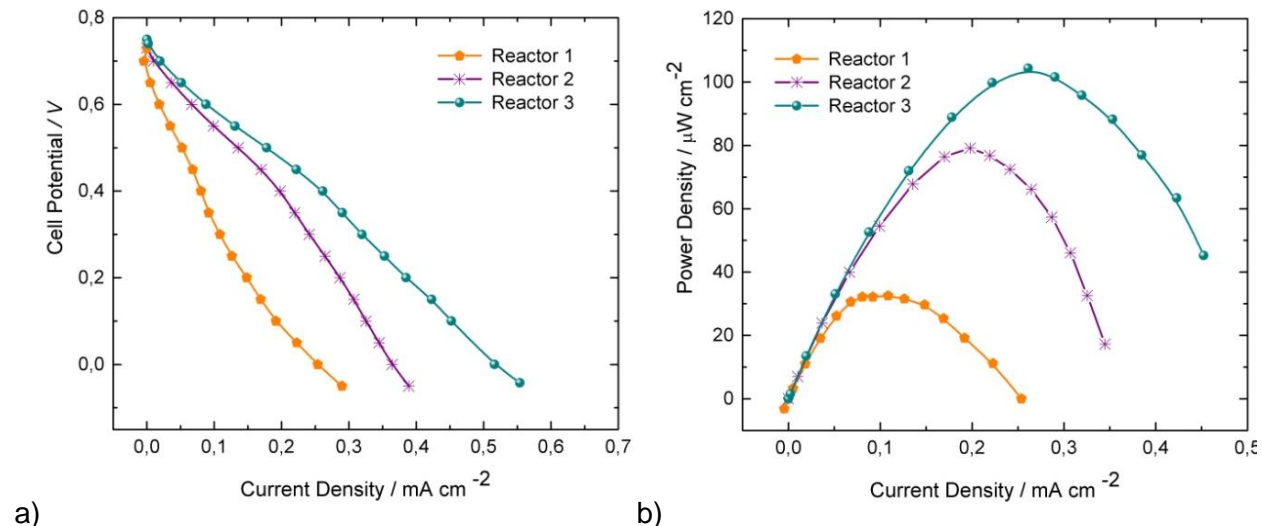


Fig. 6-2 a) Polarization and **b)** power curves of electroenzymatic reactors employing GOx/TTF anode and GOx-HRP cathodes; Conditions: enzyme immobilization: cathode, Vulcan-PVDF; anode, Vulcan-Gelatin, 20 mM glucose in 0.1 M phosphate buffer, 10 ml min⁻¹ flow rate, O₂ supply from the gas phase, pH 6.00, 22°C, volume of the glucose reservoir: 70 ml

The open circuit cell potential (OCV) was found to be independent of Vulcan and enzyme loadings. The value of *approx.* 0.75 V for OCV is in good correlation to the value obtained for open circuit potentials of single electrodes (-0.15 V and 0.6 V vs. SCE, for anode and cathode, respectively). Regarding the open circuit cell potentials for other glucose/oxygen fuel cells, different values were reported in literature. This depends mainly on the choice of enzymes used for the cathode (BOD or laccase), and on the choice of the mediator used for GOx regeneration at the anode. The reported values in literature range from 0.45 V for the fuel cell following similar idea as in the present work, but with phenanthroline as GOx mediator [143]; up to 0.9 V for the fuel cell with the Osmium redox hydrogels as a GOx mediator [164, 165].

6.2.2 Comparison of enzymatic electrode performances

As previously described, the reference electrode is installed in the current reactor set up. This allows differentiation between losses at the anode and cathode separately. In Fig. 6-3, the polarization curves of the anode and cathode performances under the reactor operation are shown for all three reactors. Cathode overpotentials are significantly higher than the anode, indicating the cathode as the limiting electrode for the electrochemical performance of the whole

fuel cell. Due to the higher available surface area for the adsorption provided by increasing the nanomaterial loadings (4 instead of 2 mg cm⁻²), the amount of adsorbed enzymes increases in Reactor 2 compared to Reactor 1. As consequence, significant decrease in cathode overpotentials can be noticed, enabling higher current densities. The difference between Reactor 2 and 3 is also in enzyme loading, achieved by extending adsorption time. However, it can be seen that at the lower overpotentials (*approx.* until $E_c = 0.5$ V), the performance of Cathode 2 (in Reactor 2) is higher than Cathode 3 (Reactor 3), while at higher overpotentials it is the opposite. This can be an indication that there is a HRP inhibition at low overpotentials in Reactor 3 due to discordance between the production and consumption rates of hydrogen peroxide. The production of hydrogen peroxide which occurs enzymatically in the reaction of glucose and oxygen is determined by the enzyme loading, species concentrations and flow conditions, while the electroenzymatic consumption can be accelerated electrochemically through higher current densities in Cathode 3 operated at more negative overpotentials than in Cathode 2 [32].

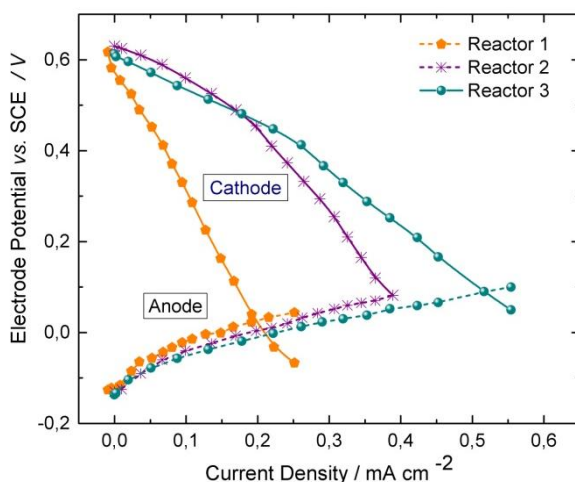


Fig. 6-3 Steady state performances of enzymatic cathode (GOx-HRP) and enzymatic anode (GOx-TTF) under electroenzymatic reactor operation. Conditions as in Fig. 6-2

At the same time, gradual decrease of overpotentials at the anode between Reactors 1, 2 and 3 can be noticed. This observation can be ascribed to deviations between single experiments, but it seems that this change is a clear trend and not a random effect. A possible reason for this increase of the anode overpotential can be the presence of oxygen in the solution. It has been shown in chapter 5 (Fig. 5-8b) that oxygen as natural acceptor for GOx competes with TTF for the electrons causing a decrease in current. That means that at the same current

density at the anodes, the overpotential needs to increase. Since the oxygen was supplied from the gas phase, the amount of O_2 in the liquid phase is determined by the consumption of oxygen by GOx in the enzymatic reaction and diffusion of non-reacted oxygen away from the catalyst layer. Due to concentration gradients between catalyst layer and liquid phase, it can be expected that the non-reacted oxygen will diffuse out to the liquid phase where if convection-diffusion conditions allow, it can reach the anode and react there enzymatically. The results indicate that there is higher oxygen consumption at Cathode 3 compared to Cathode 1, suggesting lower influence of O_2 cross-over in Reactor 3 than in the Reactor 1.

The other advantage of measuring anode and cathode activity under reactor operation is the possibility to compare these performances to the electrode performance obtained in the half-cell. It has been reported that the performance of enzymatic electrodes can differ significantly when tested in the 3- and 2-electrode set-ups. For example, the BOD enzymatic cathode reached 5 mA cm^{-2} in the 3-electrode set-up, but only $200 \text{ } \mu\text{W cm}^{-2}$ when tested in the 2-electrode set-up in the presence of 50 mM glucose and at $37 \text{ }^\circ\text{C}$ and with a pH of 7.2 [159]. However, as can be noticed from the performance of the anode and cathode in the 2-electrode set-up (Reactor 3), plotted against the anode and cathode characterized separately in the 3-electrode set-up (Fig. 6-4), no significant difference was observed.

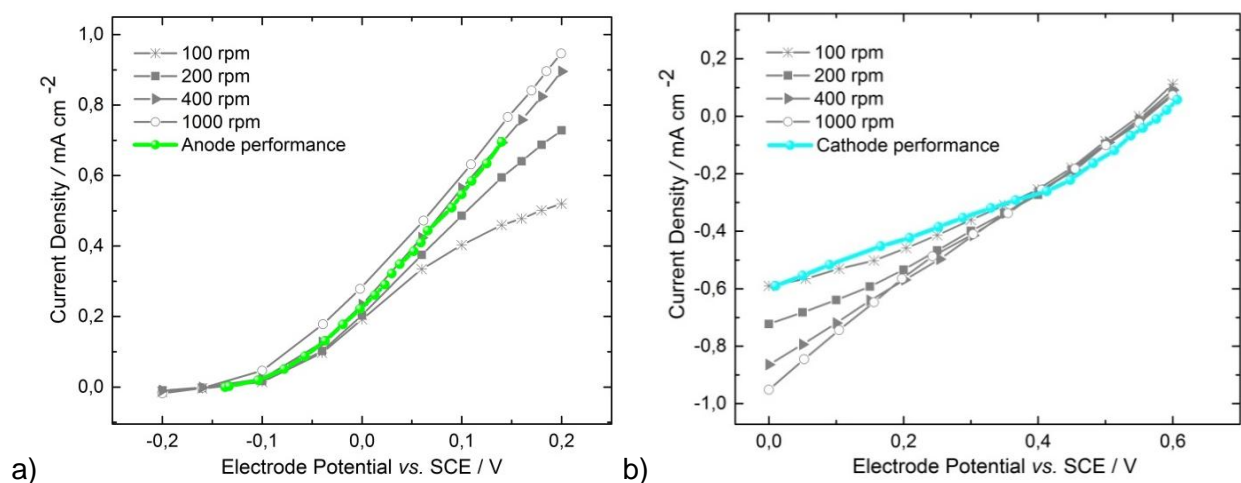


Fig. 6-4 Comparison between steady state performances of **a)** enzymatic anode (GOx-TTF) and **b)** enzymatic cathode (GOx-HRP), tested in half-cell and electroenzymatic reactor. Conditions: 20 mM glucose, pH 6.00, 22°C . Flow rates: 10 ml min^{-1} for glucose solution, O_2 supply from the gas phase in the reactor; rotation rates between 100 and 1000 rpm in the half-cell

Additionally, the experimental data indicate no significant scaling issues (electrode surface used in 3-electrode set-up: 0.28 cm² and in 2-electrode set-up: 1 cm²). On the other hand, some differences in performances can be explained by different flow conditions used in the two different set-ups (rotating disc electrode compared to flow through reactor). To assure direct comparison, the electrodes were always prepared via the same procedure and under the same conditions.

6.2.3 Evaluation of reactor performance toward glucose conversion

For analyzing the glucose conversion in the electrochemical reactor, the time of operation was prolonged and the reactor was operated under constant voltage ($E_{cell} = 0.0$ V). The glucose concentration was followed during 7 h of runtime. The concentration was checked by taking a small sample every hour from the glucose reservoir and was determined with a help of enzymatic assay. The conversion was calculated as in eq. 2-3 (chapter 2), by dividing the converted amount of glucose to the amount of glucose at the beginning.

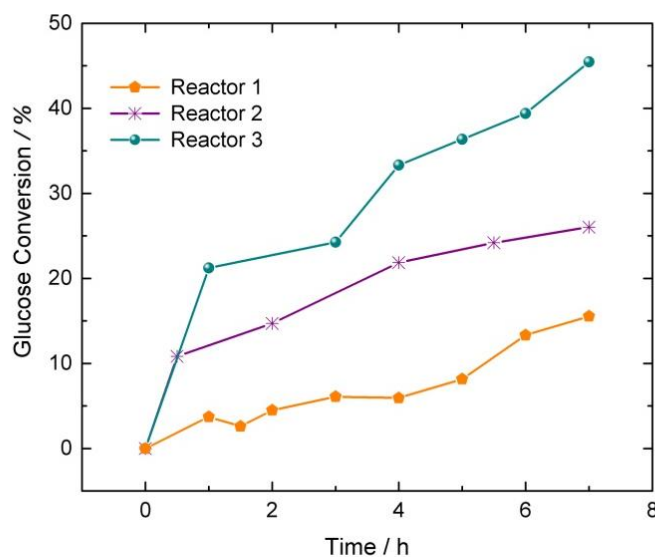


Fig. 6-5 Glucose conversions over 7 h in electroenzymatic reactors (Reactors 1-3 are described in Table 6-1)

After 7 h of reactor operation, glucose conversion increases from 16% (Reactor 1) to 47% (Reactor 3), as can be seen in Fig. 6-5. Due to the higher amount of catalysts and active surface area for glucose oxidation, Reactor 3 shows the highest performance. Additionally, improvement in catalyst loading allows Reactor 3 to operate at higher current densities over time than Reactor 1 and Reactor 2 (Fig. 6-6a).

For the operating cell potential of $E_{cell} = 0.0$ V, the anode and cathode potentials are equal (taking into account that the ohmic drop of electrolyte is negligible). The change in the anode and cathode electrode potentials is given in Fig. 6-6b. It can be noticed that at constant cell potential, both electrode potentials are decreasing over time, which means that the overpotentials were diverging (Fig. 6-7). For example, for a current density of ca. 0.5 mA cm^{-2} , overpotential of the enzymatic anode (ca. 0.2 V) is much lower than of the enzymatic cathode (ca. 0.5 V). This implies that the electroenzymatic reaction at the anode is much faster than at the cathode side. Therefore, in order to provide maximum current output at 0.0 V cell potential, the cathode has to increase the overpotential. The anode follows this requirement by a decrease of overpotential. This indicates that the whole system is controlled by the enzymatic cathode. Additionally, the stability of enzymatic cathode was possibly decreasing during time.

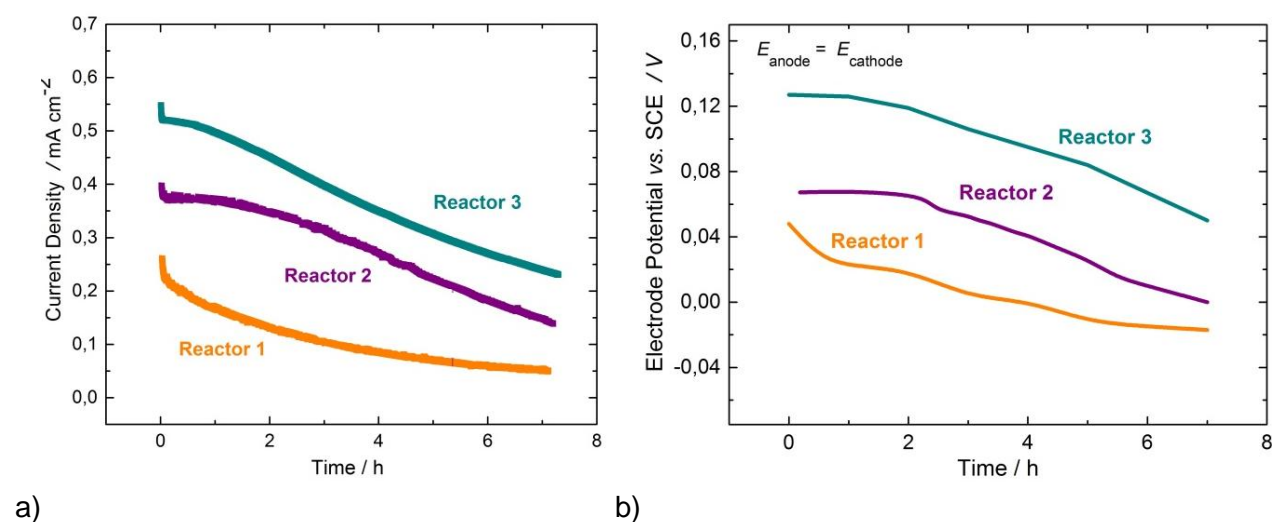


Fig. 6-6 a) Current density change during 7 h of reactor operation under voltastatic conditions ($E_{cell} = 0.0$ V) and **b)** change of anode and cathode electrode potentials during reactors operation

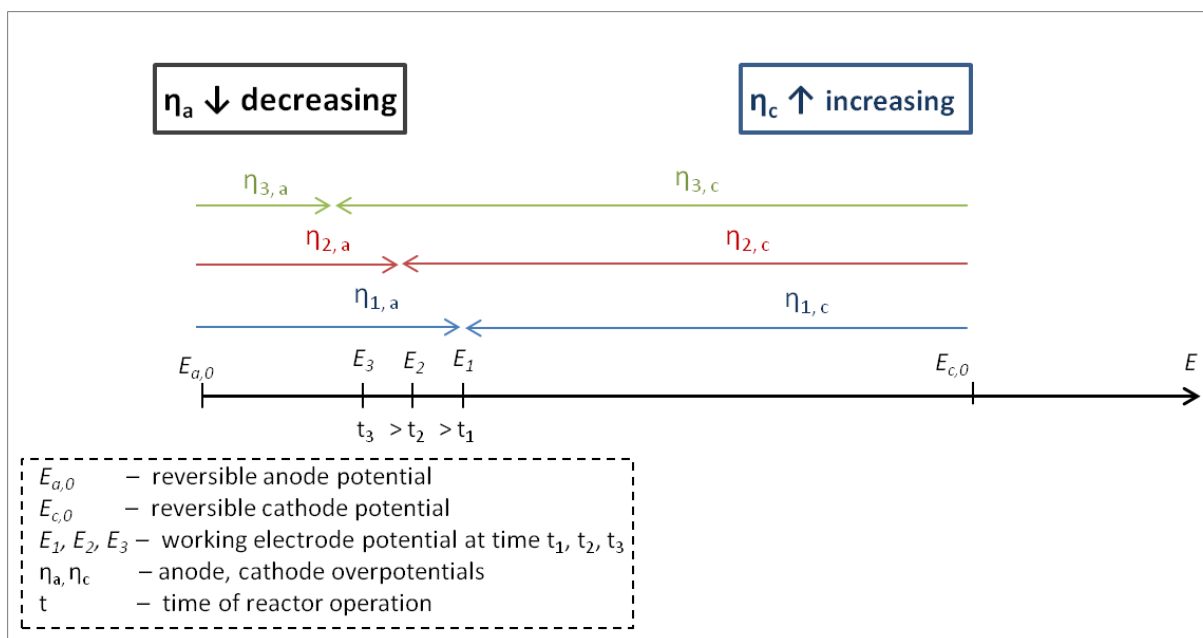


Fig. 6-7 Change of anode and cathode overpotentials with electrode potential change under constant cell potential conditions, $E_{cell} = 0.0 V$

To verify the stability of the electrodes, anode and cathode were tested separately in half cell experiments using chronoamperometry. Under these conditions, glucose conversion spanning over 7 h of operation for the enzymatic anode was 0.58%, which can be considered negligible. For the enzymatic cathode, glucose conversion under these conditions was ca. 2%. Although slightly higher value than at the anode, 2% conversion can be still considered negligible (it corresponds to concentration change from 20 mM to 19.6 mM). The reasons for higher conversion at the cathode will be discussed in the next paragraph. The results in Fig. 6-8 show very stable behavior of the enzymatic anode during time, while the performance of the enzymatic cathode decreases (ca. 25%). This loss can be attributed to the enzyme inhibition effect or to the leaching out of enzymes. However, it seems that the effect of leaching out dominates, since the formation of gelatin film on the top of enzymatic cathode resulted in almost no activity loss during the same time (Fig. 6-8).

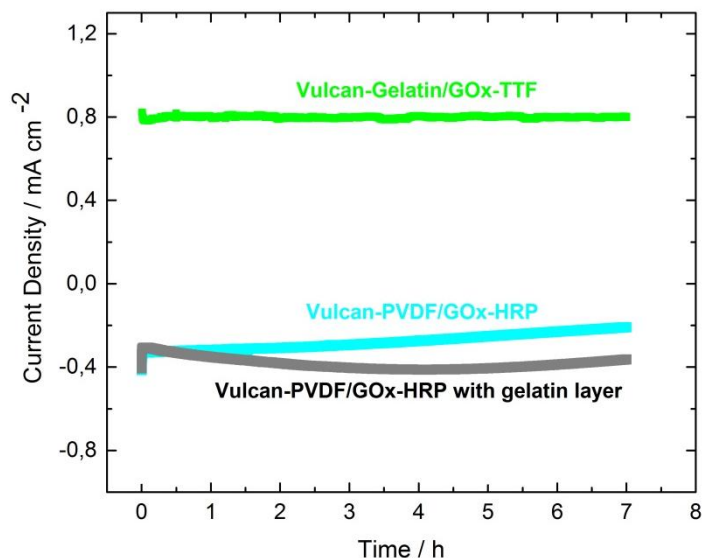


Fig. 6-8 Long-term performance of enzymatic electrodes over 7 h. Conditions: half-cell measurements, 20 mM glucose, pH 6.00, 22 °C, rotation rates 400 rpm, potential of the electrodes: 0.15 V vs. SCE

According to the Faraday's law of electrolysis, in the electrochemical systems the reactant conversion can be calculated from the electric charge passed into the reactor during a certain time (eq. 2-2, chapter 2). In order to implement this equation, current efficiency for a single reaction has to be calculated. Assuming 100% current efficiency for enzymatic reactions of glucose oxidation and taking the number of exchanged electrons (2), based on the Fig. 6-6a, electrochemical glucose conversion was calculated according to Faraday's law. The theoretically obtained conversion value was further multiplied by 2, due to the fact that glucose conversion is performed not only at the anode, but at the cathode as well. The results presented in Table 6-2 show that only small part of conversion is electrochemical, while larger part is purely enzymatic. It can be anticipated that the enzymatic conversion mostly happened at the cathode indicating large amounts of hydrogen peroxide that is not further utilized. However, as presented in Fig. 6-8, there is no significant negative influence of H_2O_2 on the electrode performance during 7 h of GOx/HRP electrode performance. On the other hand, the difference in the conditions of electrode potential for the stability experiment, and during reactor operation, at the cathode should be taken into account.

Table 6-2 Total and partial glucose conversions in electrochemical reactors after 7 h of reactor operation calculated according to Faraday's law of electrolysis

System	Total Conversion / %	Electrochemical part of conversion / %	Enzymatic part of conversion / %
Reactor 1	16	14	86
Reactor 2	30	19	81
Reactor 3	47	17	83

Based on results in Table 6-2, the greatest drive to conversion is enzymatic. Thus, it raises the question that if the reactor is based only on biocatalysts, will it work better and does the electrochemical step make a difference? In general, removal of H₂O₂ has been the main issue of GOx catalyzed glucose oxidation reactions. For gluconic acid production based only on enzymatic catalysts, the removal of peroxide is carried out by the enzyme catalase. This enzyme is a tetramer of four subunits of 54-59 kDa, containing porphyrin heme groups. It catalyzes the decomposition of peroxide to water and oxygen [166]. Therefore, in the present reactor configuration, an electrode comprised of GOx and catalase instead of GOx and HRP was analyzed under the same operating conditions and maintaining the same amount of GOx. The only difference was in the electrochemical step that is necessary for HRP regeneration and was not used in the case when catalase was implemented. As can be seen in Fig. 6-9, the combination of HRP enzyme for peroxide removal and electrochemical enzyme regeneration is a more efficient approach than when only pure enzymatic systems are used. As previously reported, catalase is unstable due to its tetrameric structure [167]. The enzyme is especially sensitive at low concentrations of catalase where the dilution effect leads to dissociation of tetrameric catalase into subunits. Therefore, due to catalase denaturation, glucose conversion was decreased in long term operations [30].

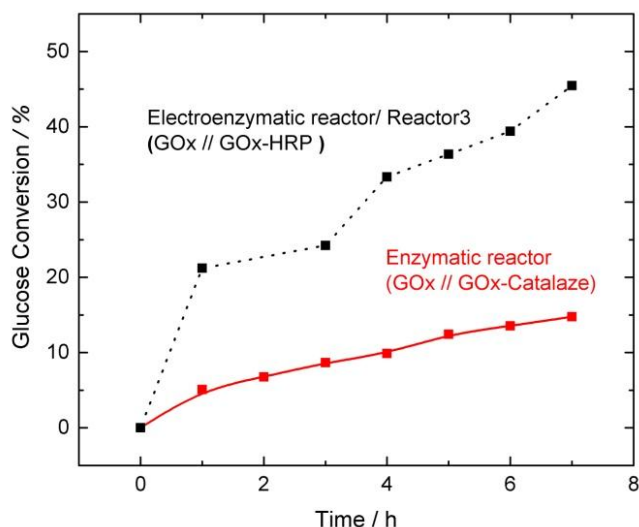


Fig. 6-9 Comparison of electroenzymatic reactor based on GOx-HRP cathode and enzymatic reactor employing catalase for peroxide decomposition

As can be seen, operating conditions in all electroenzymatic reactors for gluconic acid production were very different (Table 6-3), e.g. different total reactor volumes (from 28 to 200 cm³), duration of electrolysis (from 3 to 12 h), electrode surface areas (from 1 to 30 cm²) and glucose concentrations. Therefore, in order to compare the performances of the presented reactors to others, these parameters are combined to calculate the space time yield (STY) of the reactor (the mass of gluconic acid produced per unit time and per unit geometric area of the electrode, mg_{gluconic acid} h⁻¹ dm⁻², eq. 2-7). Due to the fact that all listed processes are in batch mode (or semi-batch) of operation, the mass of gluconic acid produced was calculated based on conversion, total volume in the system and initial concentration of glucose, assuming that the selectivity was 100% for all systems. The comparison and calculated STYs are presented in Table 6-3, where surface area refers to the geometrical surface area of electrodes and the time corresponds to the total time of reactor operation. As can be seen, the best process based on this analysis is not the one related to the highest conversion achieved. Compared to other processes, the performance of Reactor 3 is excellent.

Table 6-3 Comparisons of electroenzymatic reactor performances

System	Enzyme	Enzyme Immobilization	Electron transfer	Electrode surface area / cm ²	Volume / cm ³	Glucose concentration / mM	Time / h	Glucose Conversion / %	STY / mg h ⁻¹ cm ⁻²	Ref.
Membrane (Nafion)	GDH	In solution	direct	24	28	10	12	85	0.16	[33]
Membrane (Nafion)	GDH	Covalent attachment	Mediated (3,4 – DHB)	24	28	100	4	60	3.43	[34]
Membrane (Dialysis)	GOx	Entrapment in dialysis membrane	Mediated (O ₂)	30	44	248	3	30	7.13	[32]
Batch	GOx	In polypyrrole film	Mediated (O ₂)	3.14	10	20	8	62	0.97	[35]
RDE system	G6PDH	Covalent attachment	Mediated (PMS)	19.6	200	9.3	6	43	1.33	[36]
Membrane-less	GOx	3-D electrode	Mediated (TTF, O ₂)	1	70	20	7	47	18.2	This Work

6.3 Optimization of GOx||GOx-HRP reactor performance and selectivity analysis

6.3.1 Influence of flow rate on reactor performance

Glucose conversion largely depends on the available substrate at the electrode surface *i.e.* mass transport of glucose. This parameter can be controlled by flow rate conditions in the reactor. Furthermore, the 3-D approach for preparation of enzymatic electrodes introduces additional mass transport limitations in the catalyst layer, which determines the amount of the catalyst working through the electrode [148]. Therefore, the optimization of the flow rate conditions was the next necessary step.

The electrochemical performance of Reactor 3 was investigated at different glucose flow rates between 0 and 14 ml min⁻¹ under constant oxygen flow (Fig. 6-10). The increase of the flow rate provides more reactant to the electrode surface improving catalytic current density, from 0.2

mA cm^{-2} without electrolyte circulation to ca. 0.6 mA cm^{-2} at 14 ml min^{-1} . The performances of the anode and cathode were plotted in terms of overpotentials, defined with respect to the corresponding OCPs (Fig. 6-10b). Additionally, values of the Ohmic drop in the electrolyte have been presented in the same graph. As can be seen, due to low currents in the electrochemical reactor, the Ohmic drop loss in the electrolyte is very small.

The results in Fig. 6-10b show that the flow rate change has a larger influence on the cathode overpotentials compared to the anode. As shown in Fig. 6-4, due to the different electrode preparation procedures and enzyme immobilization, the anode (Vulcan-Gelatin electrodes) is less influenced by reactant mass transport (rotation rate in investigated 3 set up systems) than the cathode (Vulcan-PVDF electrodes). The reason for this effect has been already discussed in chapter 4.2.2. Nevertheless, despite improved cathode performance with the flow rate increase, its overpotentials are higher in comparison to the anode overpotentials, confirming that the reactor electrochemical performance is limited by the cathode. On the other hand, the GOx-HRP enzymatic electrode is important for gluconic acid production due to the enzymatically catalyzed glucose oxidation.

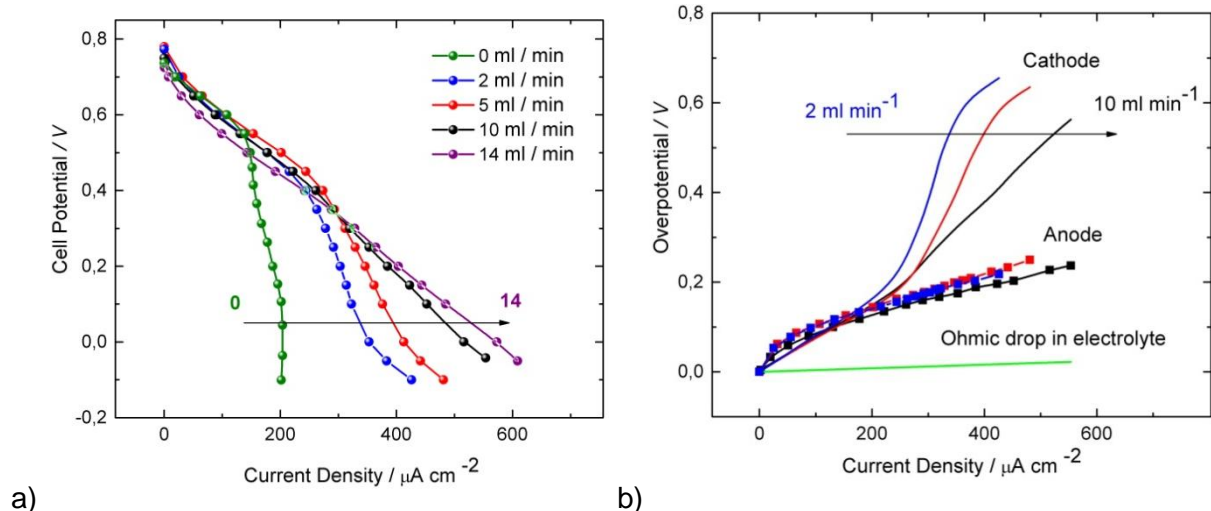


Fig. 6-10 a) Polarization curves of the electroenzymatic reactor at different flow rates; **b)** Potential loss distribution, anode: GOx-TTF/Vulcan-Gelatin, cathode: GOx-HRP/Vulcan-PVDF, Conditions: 20 mM glucose in 0.1 M phosphate buffer, O_2 supply from the gas phase, pH 6.00, 22 °C, volume of the glucose reservoir: 70 ml

Glucose conversion was evaluated during 7 h of voltastatic reactor operation ($E_{cell} = 0.0$ V). As can be seen from Fig. 6-11, the conversion is first increasing with the flow rate reaching a maximum of ca. 60% at 5 ml min^{-1} , while further increase of the flow rate (10 and 14 ml min^{-1}) did not improve glucose conversion (49% and 49.5% respectively; presented only for 10 ml min^{-1}). Flow rate change not only influences glucose mass transport, but also has an indirect impact on the other reaction steps like hydrogen peroxide formation. If the concentration of hydrogen peroxide is high enough, it can cause enzyme inhibition during the reactor operation. Since electrochemical performance was improving with flow rate change, it can be assumed that increased peroxide concentration at the cathode did not have a negative impact on the activity of HRP. On the other hand, enzymatic reaction with GOx is dominant for glucose conversion, thus the performance of GOx was impeded with the flow rate increase. The reason for this can be either inhibition of GOx with high local H_2O_2 concentration close to the electrode surface at higher flow rates or possible leaching out of GOx.

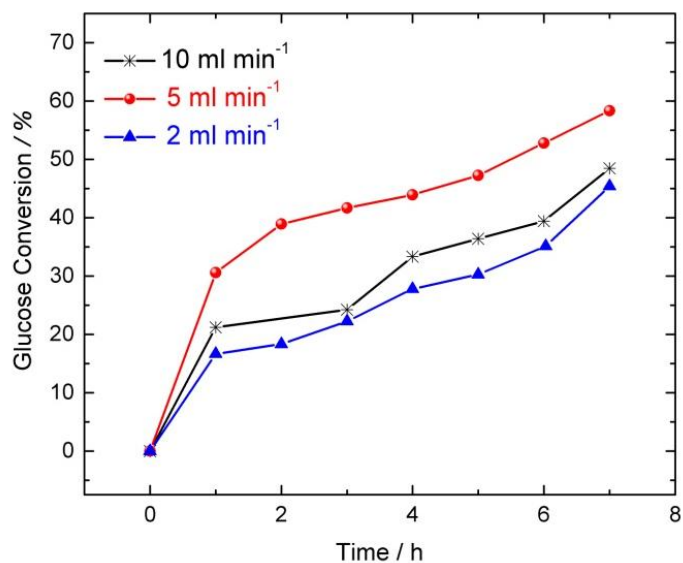


Fig. 6-11 Glucose conversions during 7 h in electroenzymatic reactor at different flow rates of glucose

6.3.2 Analysis of the reactor selectivity and product yield

Product selectivity is normally not an issue for enzymatic processes due to the high selectivity of enzymatic catalysts [168]. The same assumption corresponds to the electroenzymatic processes, and up to date no publication on this topic considers a selectivity issue (references from Table 6-3). Nevertheless, depending on the reactor design (without or with separator), formed by-products, type of biocatalysts and regeneration mechanisms at anode/cathode side, further electrochemical or chemical reactions can take place, decreasing the product selectivity. Due to the high importance of selectivity for technical applications, this issue was studied in detail for the present reactor system. Therefore, the reaction mixtures at different flow rates, the glucose solution before conversion and lyophilized samples were analyzed by NMR spectroscopy. In the Fig. 6-12, representative NMR product spectra with identified peaks has been presented (the other detailed data can be found in Appendix). The ^1H chemical shifts for $\alpha\text{-H1}$ and $\beta\text{-H1}$ at the C1 atom of glucose are 5.2 and 4.6 ppm, confirming the glucose structure previously reported by Holade Y. *et al* [8]. The presence of the gluconic acid in the reaction mixture is verified by the chemical shift of 4.1 ppm that is typical for ^1H at the C2 position of the gluconic acid.

According to the NMR results, the major by-products of the electroenzymatic glucose oxidation under present conditions are formic acid and arabinose. The presence of D-arabinose was confirmed in the ^1H and ^{13}C spectra (obtained from lyophilized sample) with the chemical shifts of 4.5 for H1 and 96.6, 72.3, 71.7, 68.4 and 66.3 ppm for C1 (Fig. A1, Appendix) that are typical for D-arabinose. D-arabinose is a monosaccharide with 5 carbon atoms and it is important for vitamin B2 and DNA syntheses. Although most of the carbohydrates are normally present in their D-form, L-arabinose is more abundant in nature than its D-form [169]. Next, the chemical shift of 8.4 refers to the typical peak position of H1 of formic acid. This has been also confirmed in 1D wet NMR spectra in Zargari N. *et al* [170]. Due to the low amounts of the other by-products, also found in the reaction mixture, they were not taken into consideration for yields and selectivity calculations. Ratios of the obtained peaks for each sample are marked in the spectra (please see Figures in Appendix).

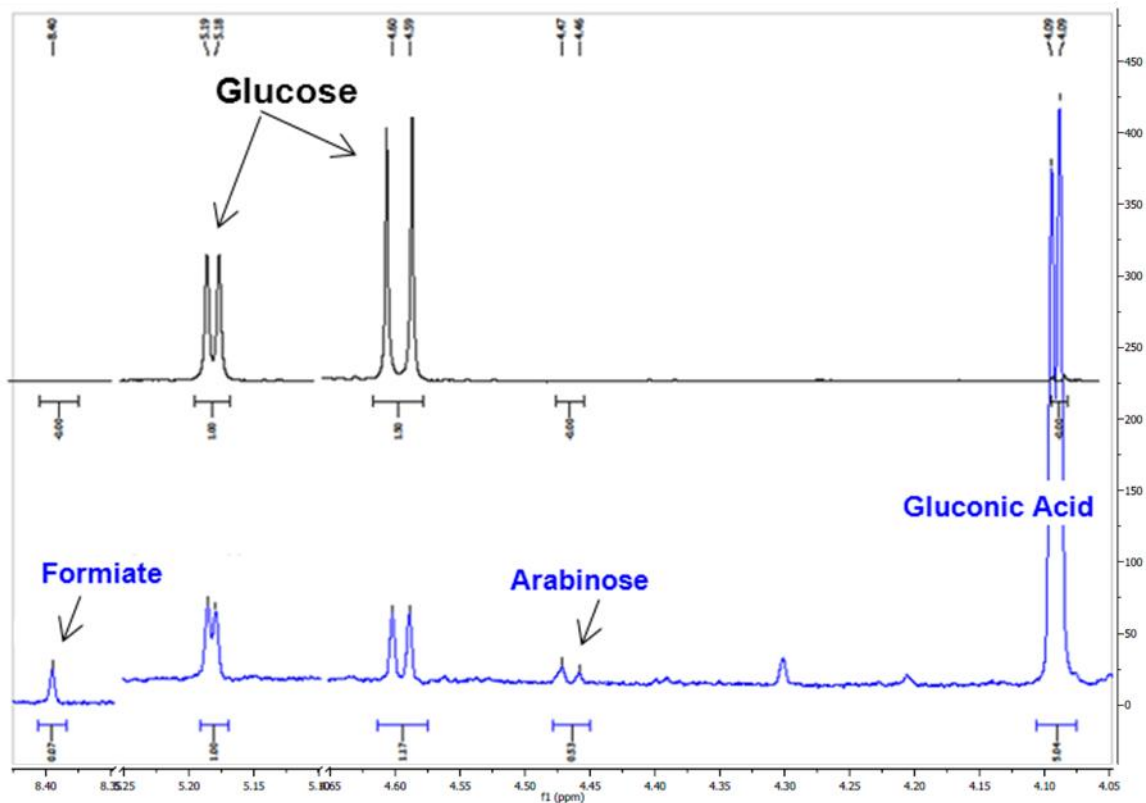


Fig. 6-12 NMR product spectra with identified peaks, black line: initial solution; blue line: final solution after 7 h of reactor operation (Additional NMR spectra for all tested systems in Appendix)

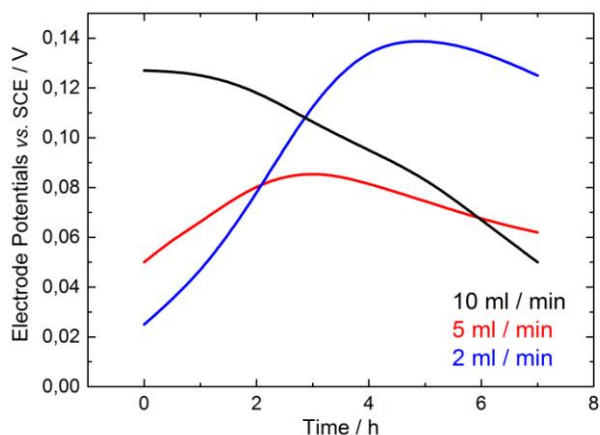
The gluconic acid selectivity and product yields were calculated according to eq. 2-4 and 2-5 (chapter 2), based on the information obtained from ^1H spectra. The data was compared in the Table 6-4 (Fig. A2, Appendix). As can be seen, the total glucose conversion based on NMR correlates well with the values obtained using glucose assay. The selectivity for gluconic acid follows similar dependence on the flow rate as conversion. The highest selectivity value (ca. 97%) with respect to the gluconic acid was observed at the 5 ml min^{-1} flow rate. The largest yield of arabinose (ca. 6.9%) was obtained at the lowest flow rate of 2 ml min^{-1} . At 5 ml min^{-1} only traces of arabinose were detected and ca. 1.6% of the formic acid. At higher flow rates (10 and 14 ml min^{-1}) the selectivity for gluconic acid decreases again and the yield of arabinose increases to ca. 3.2%.

Table 6-4 NMR analysis results after 7 h in electroenzymatic reactors tested at three different flow rates

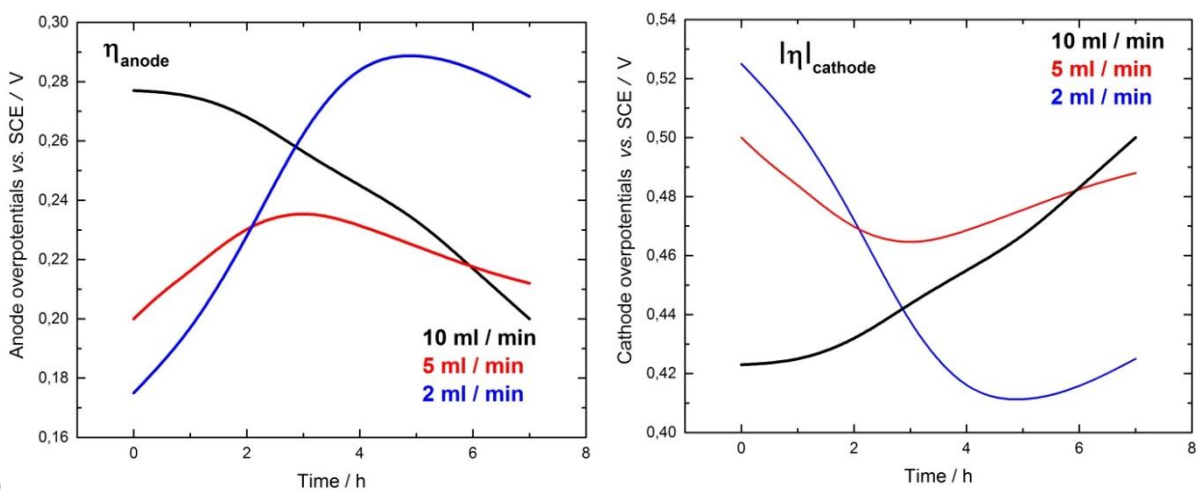
Flow rate / ml min ⁻¹	Conversion / %	Selectivity / %	Y: GA / %	Y: A / %	Y: FA / %
10 and 14	49.3	84.1	41.5	3.2	4.6
5	58.0	97.0	56.0	- Traces	1.6
2	46.1	74.5	34.3	6.9	4.9

The selectivity values obtained in the electroenzymatic reactor (although lower than 100%) are still much higher than normally reported selectivities achieved using chemical catalysts. For instance, it has been shown that when using concentrated FeCl₃ solution at 110 °C to oxidize glucose to gluconic acid, other by-products like formic, acetic acid and humins were formed. The selectivity of this process was reported to be up to 57% [171]. In the electrocatalytic system using a MnO₂/Ti electrode as anode for glucose oxidation, gluconic acid together with glucaric acid were obtained with the yields of 45% and 49%, respectively [29].

Since the by-products are not expected when employing an enzymatic approach, and this was not reported before, the mechanisms of their formation was studied further. The anode and cathode potentials over 7 h of operation were monitored in order to understand the by-product formation in the present electroenzymatic reactor (Fig. 6-13). The lines presented in the Fig. 6-13 describe the changes of both anode and cathode potentials over time at the zero cell potential (the Ohmic drop in the electrolyte was neglected). The changes of overpotentials, expressed with respect to OCP value of anode and cathode, were plotted in the Fig. 6-13b and c, for three different flow rates.



a)



b)

Fig. 6-13 Anode and cathode **a)** electrode potentials recorded during reactor operation, $E_{cell} = 0.0 V$; $E_a = E_c$ (one line is presented) and **b)** calculated overpotential

It can be noticed that at 5 ml min^{-1} , the cathode and anode overpotentials were not changing significantly in comparison to the other flow rates. The initial behavior of the enzymatic reactor at the three different flow rates correspond to the behavior presented in Fig. 6-10. As observed, the enzymatic cathode performs better at higher flow rates, thus the cathode overpotential is lower in comparison to the other flow rates (Fig. 6-13c). Consequently, the anode operates at higher overpotentials (Fig. 6-13b). As the reaction proceeds over time, at 10 ml min^{-1} , the cathode overpotential drastically increases. This is due to the cathode performance deterioration. The possible reasons for this behavior can be due to the enzyme inhibition caused

by high local hydrogen peroxide concentration or leaching out of the catalysts due to the physical adsorption. As shown in Fig. 4-17, for the HRP electrode based on Vulcan-PVDF procedure, which is also used for cathode preparation, HRP inhibition occurs at the concentrations higher than 5 mM H_2O_2 . On the other hand, at the lowest flow rate (2 ml min^{-1}), the cathode overpotential decreases over time, which is also due to the improvement in cathode performance. This can be indication that H_2O_2 removal is the more efficient at this flow rate. However, after *approx.* 4 h of reactor operation at 2 ml min^{-1} , the further increase in cathode overpotential suggests that accumulation of H_2O_2 occurred during the time and enzyme inhibition effect. It can be assumed that the observed overpotential profiles simulate the balance between the hydrogen peroxide consumption rate that is potential dependent, and its production rate, which is dependent on flow rate conditions and the enzyme loading within the catalyst layer, as well as enzyme inhibition kinetics (indirectly potential dependent). Considering this, the presented profiles might indirectly reflect the changes of hydrogen peroxide concentrations in the catalyst layer over time. Therefore, at low cathode overpotentials, H_2O_2 concentration in the catalyst layer is high, which is observed during the 2 ml min^{-1} flow rate after *approx.* 3 h and at 10 ml min^{-1} in the *approx.* first 2 h of reactor operation. At high overpotentials, H_2O_2 concentration is low, noticed at 2 ml min^{-1} in the first 3 h and 10 ml min^{-1} after *approx.* 2 h. The cathode overpotentials at 5 ml min^{-1} are not too low and not too high, which might indicate the best balance between rates of hydrogen peroxide production and consumption, and result in almost 100% selectivity for gluconic acid.

Since peroxide production and consumption occurs at the cathode side, this electrode is considered responsible for the lower process selectivity. To confirm this assumption, both electrodes were studied separately in the half-cell, simulating the change of overpotential over 7 h of operation. Two kinds of experiments were conducted, where anode and cathode potential were predominantly high or predominantly low. The conditions of the half-cell experiments and resulting data have been summarized in Table 6-5 (Fig. A3, Appendix). Again, NMR was employed for the analysis of the reaction mixtures. The results show that the selectivity at the anode is independent of the overpotential and no by-products were detected. At the cathode side, the selectivity was below 100% and it was overpotential dependent (*ca.* 80% at the high overpotentials and *ca.* 70% at the low overpotentials). Additionally, the glucose conversion was dependent on the electrode overpotentials. For instance, at the anode only 6% conversion was achieved at low overpotentials compared to 34% at the high overpotentials. At the cathode side, the overall conversion was higher and they followed the same tendency with overpotential.

Table 6-5 NMR analysis of reaction mixtures after 7 h of enzymatic electrodes operation in half-cell, Conditions: 20 mM glucose in 0.1 M PBS, pH 6.00, 22 °C, 70 ml; cathode: in the presence of O₂, anode: in presence of N₂

Electrode	Ea / Ec / V (time)	Overpotentials / V (time)	Glucose Conversion / %	Selectivity / %	Y: GA / %	Y: A / %	Y: FA / %
ANODE: V-Gel/GOx-TTF	Ea= 0.2 (2 h) Ea= 0.15 (2 h) Ea= 0.1 (3 h)	0.35 (2 h) 0.3 (2 h) 0.25 (3 h)	34	100	34	0	0
ANODE: V-Gel/GOx-TTF	Ea= 0.15 (2 h) Ea= 0.1 (2 h) Ea= 0.05 (3 h)	0.30 (2 h) 0.25 (2 h) 0.20 (3 h)	6	100	6	0	0
CATHODE: V-PVDF/GOx-HRP	Ec= 0.05 (2 h) Ec= 0.0V (2 h) Ec= -0.05 (3 h)	0.50 (2 h) 0.55 (2 h) 0.60 (3 h)	56	80	44	6	6
CATHODE: V-PVDF/GOx-HRP	Ec= 0.15 (2 h) Ec= 0.1 (2 h) Ec= 0.05 (3 h)	0.4 (2 h) 0.45 (2 h) 0.50 (3 h)	43	70	29	7	7

The possible pathways for by-product formation are presented in Fig. 6-14. Hydrogen peroxide can react with D-glucose or with D-gluconic acid, forming D-arabinose in both cases. Depending on the pathway, in addition to D-arabinose, formic acid or CO₂ is produced. Furthermore, D-arabinose can be oxidized stepwise to produce formic acid in the presence of H₂O₂. Although it was reported that D-glucose can be oxidized with H₂O₂ instead of oxygen, the conditions are not comparable to the conditions in the present reactor. For example, the oxidation with hydrogen peroxide at 120 °C and 200 °C temperatures, coupled with hydrothermal electrolysis has been outlined [172]. Still, the selectivity of the described process was very poor and among the many by-products formed, D-arabinose was not reported. The production of D-arabinose and lower carbohydrates is based on chemical oxidation of sodium gluconate with sodium hypochlorite or electrochemical oxidation in the fluidized bed reactor [169, 173, 174]. Additionally, Ruff oxidative degradation of gluconate to arabinose has been reported in the presence of H₂O₂ and iron (III) or copper (II) as catalysts [172]. The formation of D-arabinose based on the pathways suggested in Fig. 6-14 has not been so far reported regarding electroenzymatic systems.

In order to check which of two pathways in Fig. 6-14 is more likely to occur, further experiments with C1 labeled D-glucose were performed. The labeled D-glucose is the glucose molecule that has isotope ¹³C at position C1. The utilization of this glucose type does not change

nor has any influence on reaction mechanism and enzyme catalytic activity. If the route goes through glucose oxidation with H_2O_2 , the products formed are D-formic acid obtained from C1 glucose atom and D-arabinose (Fig. 6-14). If the second route is operative, oxidation of D-gluconic acid results in D-arabinose and CO_2 (formed from C1 glucose atom), that can easily exit the reaction mixture. Therefore, the test with labeled glucose can help to track if the decomposition starts from glucose or gluconic acid, following the position of the chemical shifts of the ^{13}C atom. NMR spectra obtained from this experiment do not show any sharp signal for ^{13}C , at the position typical for formic acid, confirming that D-arabinose is formed by gluconic acid and not by glucose oxidation (Fig. A4, Appendix). This brings to the conclusion that formic acid might be formed by D-arabinose degradation to lower sugars. Unfortunately, their concentrations are too low to be detected by NMR. According to this analysis, it can be assumed that all systems comprised of GOx catalyst, where hydrogen peroxide is generated as by-product, will suffer from lower selectivity.

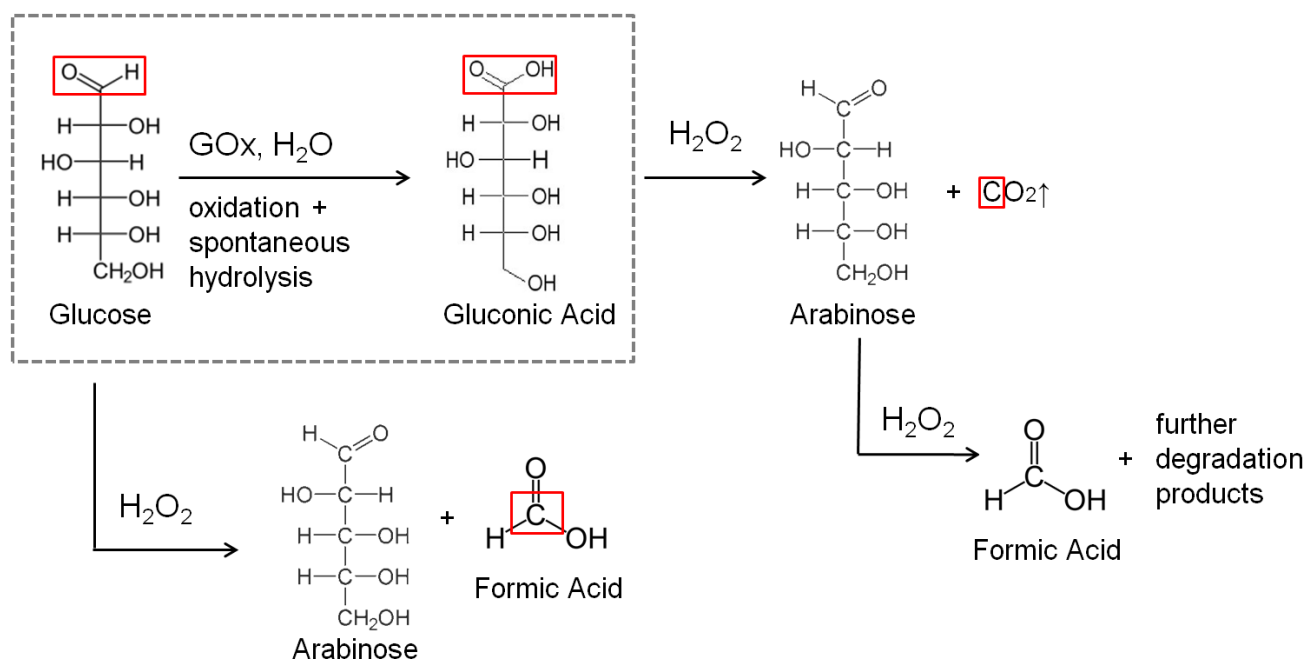


Fig. 6-14 Proposed pathways for glucose oxidation to gluconic acid and other by-products

6.3.3 Influence of cell potential and operating time

The total conversion of glucose is determined by operating time, electrode surface area, total reactor volume and concentration of glucose. Therefore, by changing these parameters, glucose conversion can be further influenced.

The half-cell experiments have shown that the conversion at the anode is stimulated at more positive anode potentials, while at the cathode by more negative. Under the condition of 0.0 V cell potential, anode and cathode potentials are always the same and fuel cell mode of operation results in more positive cathode potential than the anode. Therefore, the logical question was to test the reactor productivity at the ion-pumping mode of operation. The glucose conversion and selectivity were analyzed at a cell potential of -0.1 V during 16 h of operation time. The electrode potentials were monitored and presented in Fig. 6-15. Further, the data on conversion and selectivity were summarized in Table 6-6 (Fig. A5, Appendix). As can be seen, the cathode and anode potentials follow the same trend, observed also in the case of 0.0 V cell potential and at a flow rate 5 ml min^{-1} (Fig. 6-13). During first *ca.* 5 h of operation both anode and cathode potentials become more positive. As already discussed, the changes of potentials into the positive direction might be due to the increased local hydrogen peroxide concentration in the catalyst layer. On the other hand, after 5 h of reactor operation, the potentials become more negative, which is more likely consequence of the decrease in glucose concentration over time. The overall glucose conversion was *approx.* 72% and selectivity remained high (*ca.* 96%).

The main by-product under these conditions is formic acid, and only traces of D-arabinose were detected. During this experiment the cathode potentials were mostly below 0.0 V. In this potential range, oxygen can be electrochemically reduced on Vulcan carbon support (Fig. 6-16). As previously reported, the oxygen reduction on the carbon has a higher tendency to proceed by the two electron pathway where hydrogen peroxide is formed [175, 176]. This causes a decrease in oxygen concentration, which is needed for enzymatic oxidation of glucose. In addition, an excess of hydrogen peroxide is formed. This might explain a small decrease of selectivity in comparison to the experiment at 0.0 V cell potential and presence of D-arabinose only in trace amounts.

In the next experiment, the cell potential change over time was further modified at the prolonged time of operation of 21 h (Fig. 6-15b and c). The cell potential was changing from overall ion-pumping mode (-0.1 V) to overall fuel cell mode of operation (0.05 V). The results of the conversion and selectivity presented in Table 6-6, show a further increase of conversion (to

80%), followed by a small decrease of selectivity. The main side products were D-arabinose and formic acid.

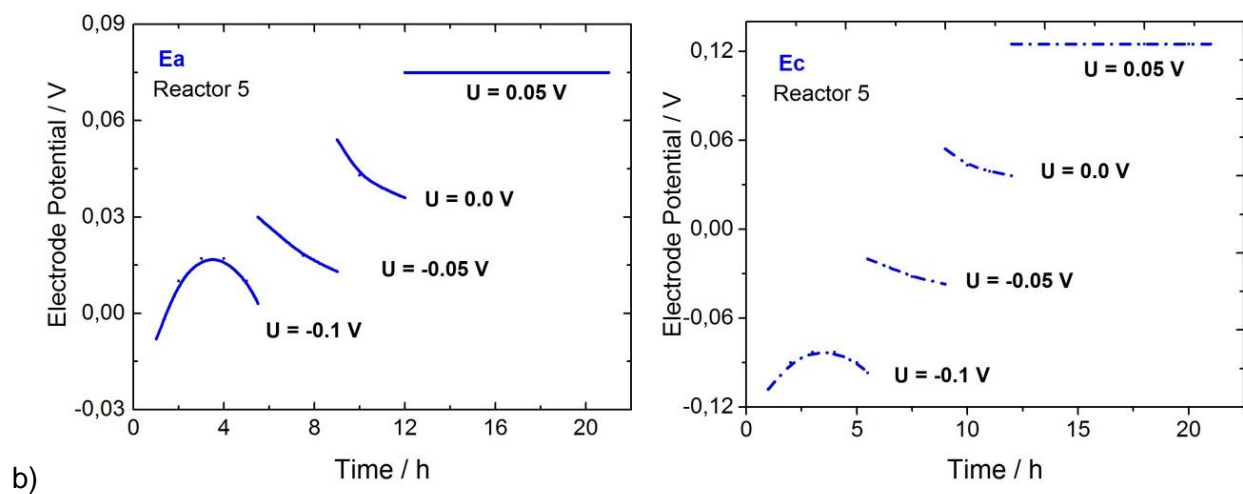
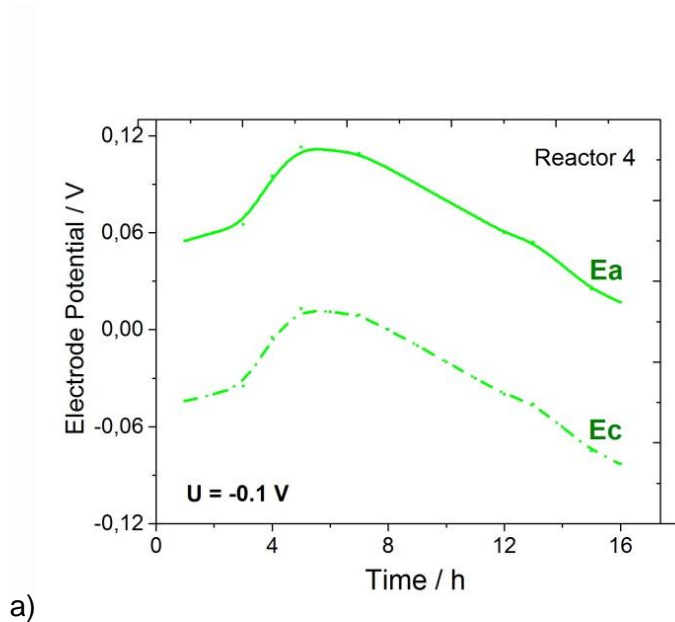


Fig. 6-15 Change of anode and cathode electrode potentials during reactors operation;
Conditions presented in Tab. 6-6

Table 6-6 NMR results for electroenzymatic reactors under different conditions of cell potential and time, 5 ml min⁻¹, 20 mM glucose

Reactor	Time / h	Cell Potential / V	Conversion / %	Selectivity / %	Y: GA / %	Y: A / %	Y: FA / %
4	16	U = -0.1	72	95.8	69	- Traces	3 + other products
5	21	U = -0.1 (5.5 h) U = -0.05 (3.5 h) U = 0.0 (3 h) U = 0.05 (9 h)	80	92	74	4	2

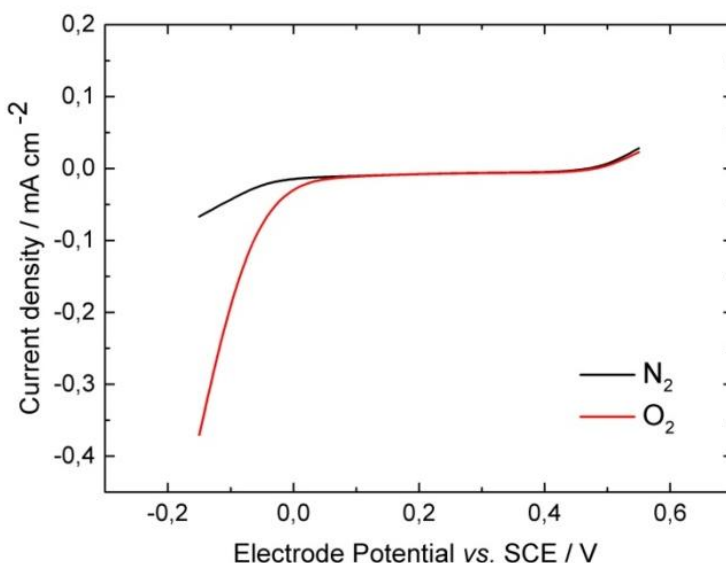


Fig. 6-16 Polarization curves of Vulcan nanomaterial in the presence and absence of oxygen, 0.1 M phosphate buffer, pH 6.00, 22 °C,

6.3.4 Comparison of electroenzymatic to establish fermentation processes

The comparison of productivity (STY) and product titre for the fermentation and electroenzymatic processes has been presented in Table 6-7. As can be seen, the product titre of reported fermentation processes (ca. 100-350 g dm⁻³) is much higher than that of the reported electroenzymatic processes (ca. 1.6 - 14.5 g dm⁻³). The low product titre increases the end price of the product. However, for product titres larger than 10 g dm⁻³, the effect on the production cost becomes negligible [177]. The product titre in the present work (3 g dm⁻³) needs to

quadruple, for the process to be competitive with fermentation. This would require an increase of glucose concentration to at least 80 mM (while maintaining conversion), which appears realistic [40]].

In the previous section 6.2.3, STY is defined with respect to the electrode surface area. This was done in order to account differences in the geometrical electrode surface areas (from 1 cm² to 30 cm²), and total reaction volumes (from 28 to 200 cm³) between the reported electroenzymatic processes (Table 6-3). However, in order to enable more straightforward comparison with fermentation processes, productivity (STY) is expressed with respect to reactor volume. The two values of STY for the present electroenzymatic process are obtained from experiments where the total reaction volume was changing. The conversion time for the smaller volume (30 cm³) was shorter than for the larger one (70 cm³), while the STY was almost the same (ca. 35 ±1 g h⁻¹ dm⁻³). The comparison of STY for fermentation (0.1 – 21 g h⁻¹ dm⁻³) and the present electroenzymatic process (ca. 35 ±1 g h⁻¹ dm⁻³) reveals the high potential of the electroenzymatic process for gluconic acid production.

Table 6-7 Comparison of different processes for the gluconic acid production

Process	STY, g h ⁻¹ dm ⁻³	Product titre, g dm ⁻³	t _{cycle} , h	Reference
Electroenzymatic, others	0.13 – 4.9	1.66 – 14.5	3 – 12	[32-36]
Electroenzymatic, this work	33.7 – 36.1	3.1	8 – 20	This work
Fermentation	0.132 – 21	100 – 350	20 – 100	[17]

6.4 Preliminary results regarding GOx||BOD electroenzymatic reactor

In the previous section, it was demonstrated that selectivity of the glucose oxidation process with GOx in the electroenzymatic reactor was in the range from 74.5 to 97%, depending on the operating conditions. The decrease in selectivity was provoked by the high local hydrogen peroxide concentration close to the electrode surface that has not been further consumed by HRP in the electroenzymatic step. Presence of large amounts of peroxide leads to an inhibitory

effect of the biocatalysts. One of the practical solutions, apart from finding other methods of H_2O_2 removal, is the replacement of the cathode catalyst and utilization of only electroenzymatic systems based on a GOx – modified anode for gluconic acid production.

An electrochemical reactor comprised of only one GOx enzymatic electrode for bioelectrochemical glucose oxidation was developed. The GOx-TTF/Vulcan-Gelatin electrode was employed as an anode, while bilirubin oxidase (BOD) as a biocatalyst for oxygen reduction reaction, was utilized at the cathode. The main advantages of BOD as a catalyst are 1) reaction pathway does not include any intermediate step of hydrogen peroxide formation, 2) compatible operating conditions with GOx optimal conditions, thus pH 7.00 and temperature of 37 °C were chosen for reactor operation and 3) BOD enzymatic electrode has better electrochemical activity in comparison to GOx-HRP electrode (Fig. 6-17).

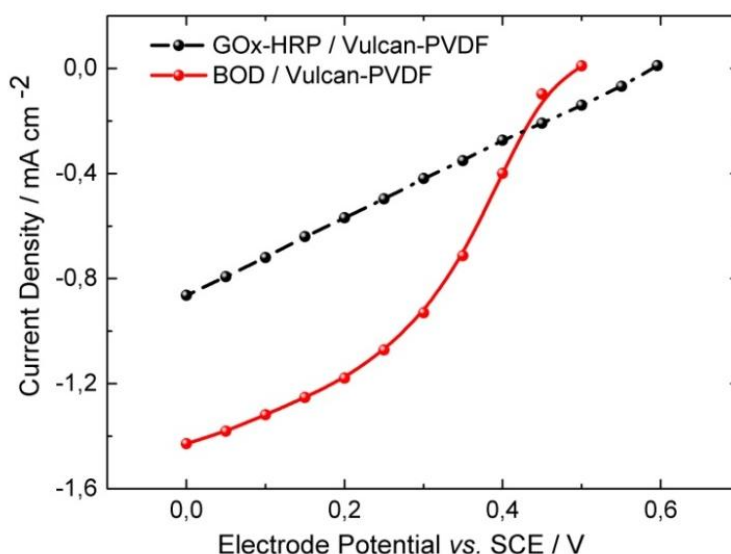


Fig. 6-17 Comparison of the steady state performance of BOD and GOx-HRP enzymatic electrode in 20 mM glucose, Conditions for BOD-electrode: pH 7.00, 37 °C, for GOx-HRP: pH 6.00, 22 °C; 400 rpm, O_2

The comparison of two electrochemical reactors employing different enzymatic cathodes was made in terms of current and power densities. As can be seen from Fig. 6-18, the BOD reactor has a higher performance than the reactor employing GOx-HRP cascade as cathode. The OCV value is around 0.7 V and is slightly lower than for GOx-HRP reactor. This value is

influenced by the open circuit potential of the BOD-cathode, which has lower OCP than peroxide reduction at the GOx-HRP electrode ($E_{\text{ocp_BOD-electrode}} = 0.5 \text{ V vs. SCE}$). The reactor with BOD at the cathode reached a power density of *ca.* 0.2 mW cm^{-2} and current density of *ca.* 0.9 mA cm^{-2} . The reactor performances correspond well to the ones outlined for similar fuel cells in literature [159, 160].

On the other hand, after 7 h of the reactor operation, the conversion in the BOD reactor is about half of the conversion reached in the GOx-HRP reactor (Fig. 6-19). When comparing the conversion for these two systems, different loadings of biocatalysts for glucose oxidation have to be considered, since GOx-HRP reactor is comprised of GOx on both electrodes, while the BOD reactor is comprised of GOx only at the anode. Additionally, NMR results obtained for this reactor demonstrate that the selectivity was 100% (Table 6-8). This proves the assumption that pure electroenzymatic systems can be considered as production systems with high selectivity. However, further improvement is necessary in terms of conversion, electrode design and scale up for utilization of more concentrated glucose solutions.

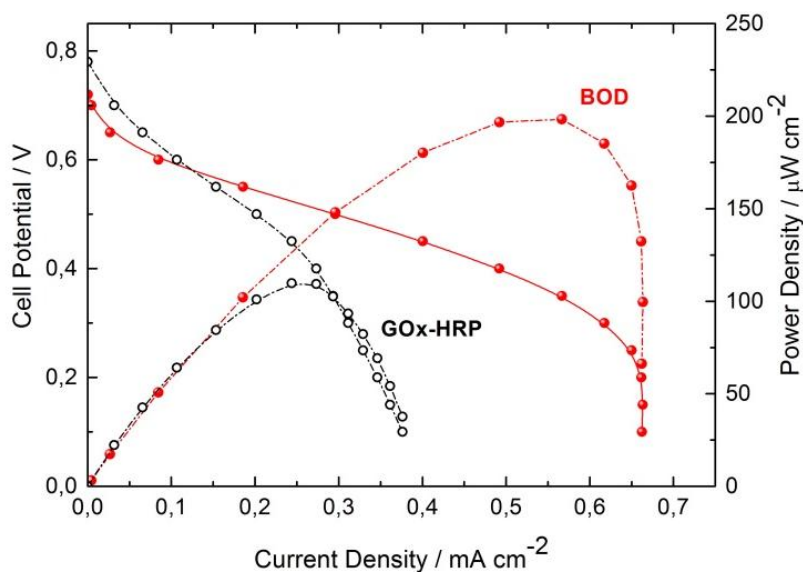


Fig. 6-18 Polarization and power curves of electroenzymatic reactors based on two different cathodes, 5 ml min^{-1} , 20 mM glucose, Conditions for GOx||GOx-HRP: $\text{pH } 6.00$, $22 \text{ }^\circ\text{C}$; GOx||BOD system: $\text{pH } 7.00$, $37 \text{ }^\circ\text{C}$

Table 6-8 NMR results for electroenzymatic reactors employing different cathodes

System	Conditions	Potential / V	Flow rate / ml / min ⁻¹	Selectivity / %
GOx-HRP based cathode	pH 6.00 / 22 °C	$E_{cell} = 0.0$	5	97
BOD based cathode	pH 7.00 / 37 °C	$E_{cell} = 0.0$	5	100

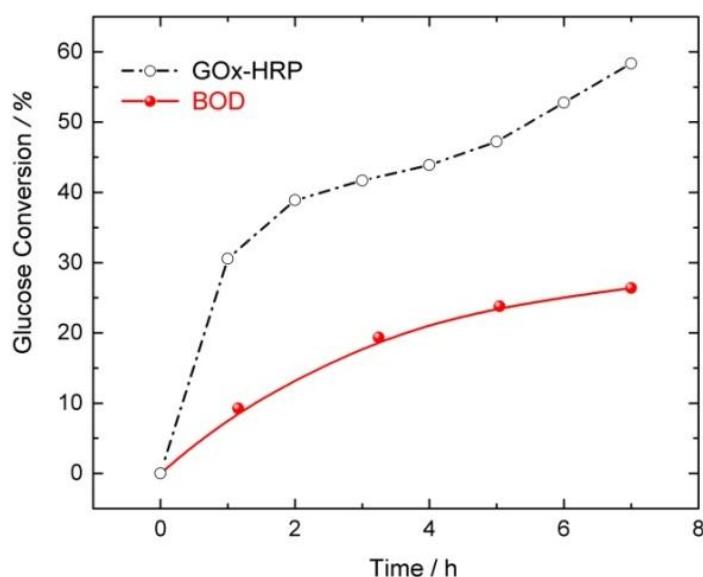


Fig. 6-19 Comparison of glucose conversion in two different reactors

6.5 Summary and concluding remarks

Electroenzymatic reactors with immobilized GOx at the anode and cathode for glucose oxidation were developed and tested with respect to electrochemical performance and productivity (conversion, selectivity, and yield). The influence of electrode structural and operational parameters was evaluated. It was shown that reactor current and power output can be improved by changing catalyst and nanomaterial loadings. Anode and cathode performances recorded under reactor operations reveal: 1) anode performance is slightly influenced by oxygen cross-over 2) even though cathode activity improves significantly with loading increase; it is a limiting

electrode for the reactor overall performance. The power level obtained in the investigated electrochemical reactor is comparable to the other biofuel cells in literature, confirming that this system has potential application as an enzymatic fuel cell as well. Glucose conversion was followed during 7 h of reactor operation ($E_{cell} = 0.0$ V). The improved reactor performance enables operation of reactors at higher current densities increasing conversion from 16% (R1) to 47% (R3). Additionally, it was shown that bioelectrochemical H_2O_2 removal is more efficient in comparison to enzymatic H_2O_2 decomposition with catalase in enzymatic reactor based on GOx and catalase, under the same conditions.

Flow rate, which determines efficient mass transport of glucose to the electrodes, was necessary to adjust. Acceleration of flow rates increases the current densities in the system. During 7 h of reactor runtime, the highest conversion was achieved at the 5 ml min^{-1} flow rate. The decrease in conversion at higher flow rates was ascribed to interplay of the following effects: 1) leaching of catalysts at the cathode, which is enhanced with the increase of the flow rate 2) promotion of H_2O_2 production at higher flow rates that causes biocatalyst inhibition 3) the electrochemical rate of peroxide consumption increases at the more negative cathode overpotentials that are determined by flow rate conditions.

The flow rate also influences the achieved selectivity in the system. Two additional by-products, D-arabinose and formic acid were detected using NMR. The largest selectivity reached was 97% for the flow rate of 5 ml min^{-1} , while the lowest was 74.5% for the lowest tested flow rate (2 ml min^{-1}). Further experiments of bioelectrodes, performed in half-cell system simulating the the operating conditions as in the reactor, demonstrate that at the anode side, where electroenzymatic process occurs, 100% selectivity for all tests were obtained. At the same time, the cathode is the electrode responsible for decreased selectivity due to the mechanism that includes hydrogen peroxide formation. The yield of arabinose was dependent at the cathode electrode potential. Under more positive electrode potentials at the cathode (higher concentration of peroxide close to the electrode surface), the yield of arabinose was higher. In order to investigate mechanism of the by-product formation, additional test with labeled glucose was performed. It was shown that the route for D-arabinose formation goes through oxidative decarboxylation of gluconic acid, where CO_2 is formed from the carboxylic group of gluconic acid. Formic acid is formed in the degradation reaction of arabinose with H_2O_2 to lower sugars. According to these results, it can be assumed that all systems comprised of GOx as a catalyst for glucose oxidation, where a step of peroxide production is present, could have the same

selectivity problem. The operating conditions were optimized so that a glucose conversion of 80% with a selectivity of 92% was reached.

In order to test a purely electroenzymatic system, which does not include intermediate step of an H_2O_2 formation, the enzyme cascade at the cathode was replaced with a BOD catalyst. Selectivity of the GOx || BOD reactor proves to be 100%. However, the conversion has to be improved.

7. Conclusions and outlook

7.1 Conclusions

The new process for the production of gluconic acid has been proposed. The process is based on an electroenzymatic approach, where the partial glucose oxidation was performed by glucose oxidase immobilized at the electrode surface.

In the first step, the importance of the electrode architecture optimization was demonstrated. The main tasks were to understand bottlenecks for the highest biocatalyst utilization within complex 3-D structures, and to improve the electrode activity and stability for potential practical applications. A substantial contact between the enzyme and electrode surface for an efficient electron transfer and enzyme regeneration, and a high electrochemically active surface area for the catalytic reaction are crucial for the development of electrodes with a high performance. Indeed, the results show that an unsuitable immobilization procedure could lead to a significant decrease in available surface area for the redox reaction. In addition, the demonstrated enzyme agglomerations, as consequence of the stabilization procedure (CL), decrease the number of active enzymes, *i.e.* enzymes in direct contact with a conductive surface. Additionally, the formation of a gelatin layer on the top of the electrode surface and a low electrode porosity cause a high mass transport resistance for the substrate in the catalyst layer (*e.g.* case of Vulcan-Gelatin electrode). It was shown that the enzymatic electrode performance can be significantly improved by right choice of parameters that lead to suitable electrode design. For instance, the electrode activity was boosted from 0.05 for a flat graphite electrode to 0.3 mA cm⁻² for a porous gelatin-based electrode. With further optimization, an electrode performance of 1.2 mA cm⁻² was reached. This is to date the highest performance for the HRP electrode exhibiting DET reported in literature.

Further, these findings have been the platform for the development of GOx based electrodes. It was confirmed that the optimal immobilization strategy improves the electrode activity of both cathode (based on cascade GOx-HRP) and anode (based on GOx and mediated ET). However, in order to employ these two electrodes in the membrane-less reactor, a compromise regarding the operating conditions was necessary. They were adjusted according to the conditions of the less active electrode (cathode: GOx-HRP, pH 6.00, 22 °C and 20 mM

glucose). The stability of enzymatic electrodes depended primarily on the immobilization procedure applied. Under present conditions, the enzymatic anode was very stable, while the enzymatic cathode showed a decrease of activity of ca. 25% over time. This loss was attributed to the enzyme leaching out effect.

Single-compartment flow-through reactors comprised of GOx-optimized electrodes were investigated. The design of the electrochemical reactor was similar to the design of a fuel cell, with an additional reference electrode installed; enabling to control the anode and cathode electrode potentials. It was demonstrated that this bioelectrochemical system can work as a glucose enzymatic fuel cell, reaching a power density ($110 \mu\text{W cm}^{-2}$) that is comparable to the literature values reported for similar glucose/ O_2 fuel cells. The glucose conversion was followed every hour during the reactor operation, while the product analysis was investigated using NMR at the end of the reaction time. The reactor performance can be significantly improved by optimizing the structural parameters, e.g. 16% of glucose conversion that was measured for R1 (low catalyst and nanocarbon loading) to ca. 50% for R3 (high catalyst and nanocarbon loadings). Further, by adjusting the operating parameters, the flow rate (5 ml min^{-1}), the cell potential and the operating time (21 h), conversions of up to 80% can be achieved. Unexpectedly, the change of operating parameters not only influences the conversion, but it has an effect on the process selectivity as well. The highest selectivity of 97% was obtained during 7 h of reactor operation under 0.0 V cell potential and 5 ml min^{-1} flow rate. The half-cell measurements were conducted under the same conditions used in the reactor. They reveal that the enzymatic cathode, based on the GOx-HRP cascade, is mainly responsible for the decrease in selectivity. Two main side products were detected, D-arabinose and formic acid. The chemical pathway for their formation is proven to be through the reaction of D-gluconic acid and hydrogen peroxide formed as an intermediate compound at the cathode side. When the reactor was operated under conditions where H_2O_2 was not efficiently removed, the yield of D-arabinose was increasing. This concludes that the same selectivity problem can occur for all systems employing GOx biocatalysts with the enzymatic cycle including an H_2O_2 intermediate step. The comparison of the STY between the fermentation processes ($0.1 - 21 \text{ g dm}^{-3} \text{ h}^{-1}$) and the present electroenzymatic process (ca. $35 \pm 1 \text{ g dm}^{-3} \text{ h}^{-1}$), reveals the potential application of the electroenzymatic process for gluconic acid production.

Additionally, the replacement of the enzymatic cascade at the cathode with a BOD catalyst shows the potential of the electroenzymatic system with a 100% selective process for

gluconic acid production. However, the optimization of the glucose conversion is subject of further investigation.

As a final comment, the results presented here show that bioelectrochemical systems are very promising for the conversion of bio-based platform chemicals in the electroenzymatic reactor.

7.2 Outlook

The investigated electroenzymatic process shows a great potential as a new alternative for gluconic acid production with a productivity higher than the state-of-the-art fermentation processes. Additionally, the reactor concept can be transferred as a benchmark to develop electroenzymatic processes based on the other FAD dependent enzymes to produce various industrially important chemicals [178].

The presented system was investigated at the laboratory scale. This enables the determination of electrochemical thermodynamics and kinetics, optimal operating conditions, as well as the selection of the suitable biocatalysts. Next step would be scale up of the electrochemical reactor, which can be achieved through an increase of the electrode surface area and/or by connecting several electrochemical reactors together in stacks [179]. This concept could be easily applicable for the present reactor system.

Once scale up is carried out, the system can be operated using concentrated glucose solutions and the next logical step would be toward selection of suitable separation unit. For the presented electroenzymatic process, electrodialysis could be the technology of choice. Based on patent data [180], electrodialysis could be used to separate gluconic acid from the reaction mixture, while at the end, the buffer solution and non-reacted glucose could be recycled back to the process. This option has been presented in Fig. 7-1. This choice will simplify the downstream process of the electroenzymatic compared to the fermentation process, which includes many steps, e.g. biomass and residual mother liquid separation, carbon treatment, evaporation and crystallization (presented in Fig. 1-5) [9].

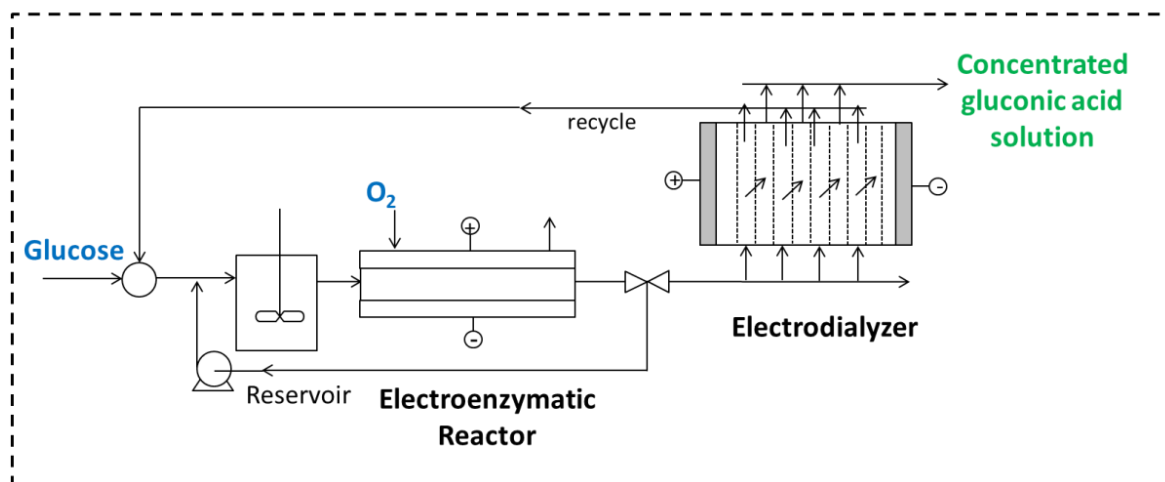
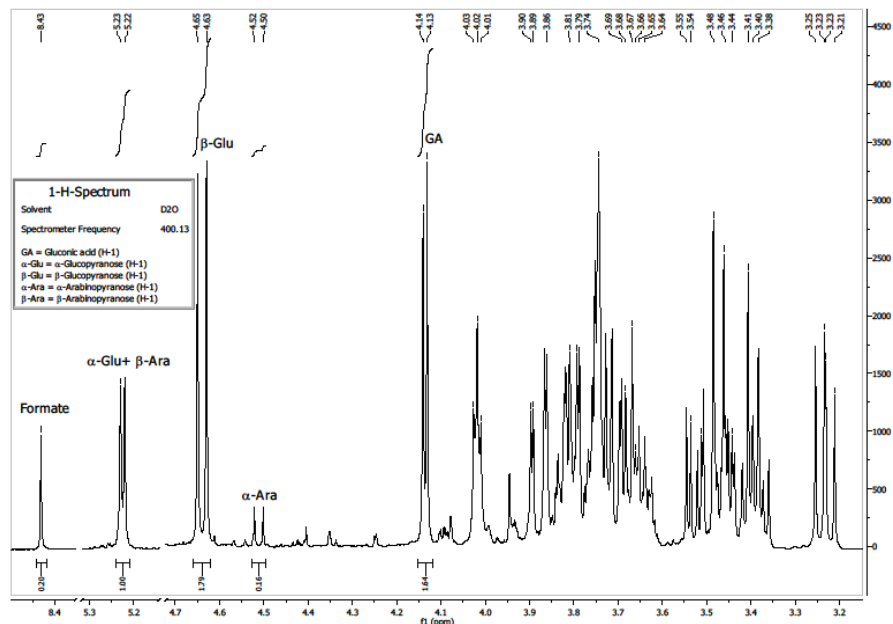


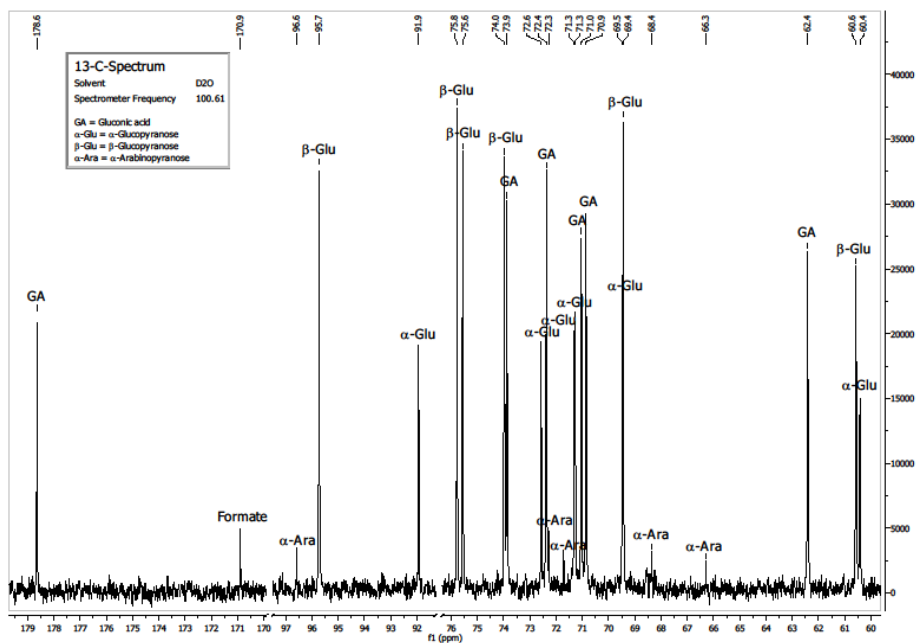
Fig. 7-1 Flow diagram of the electroenzymatic process with a separation unit

The importance of the development of a more sustainable and green synthesis in comparison to already existing processes brings the need for the evaluation of an electroenzymatic route in this direction. The process sustainability can be evaluated by life cycle analysis (LCA) with a cradle-to-grave approach [181]. This requires the inventory and environmental impacts assessment of all input and outputs of the production system. However, due to the multiplicity of processes and chemicals involved, the availability of data, prices, and energy requirements, this approach is hardly applicable for processes in an early stage of development. Thus, this can be subject of future direction.

8. Appendix

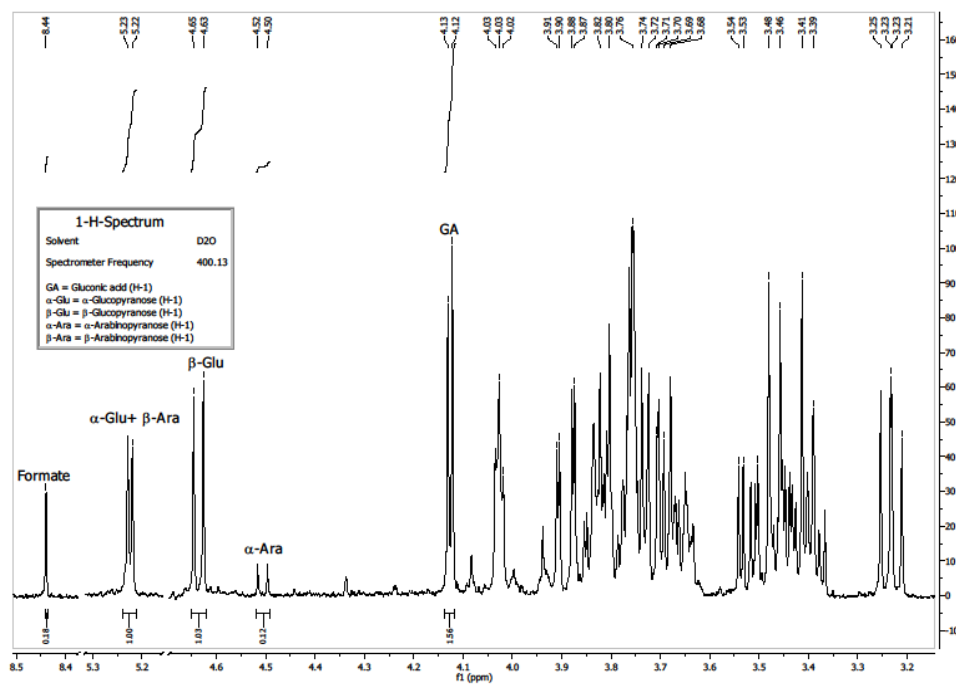


a)

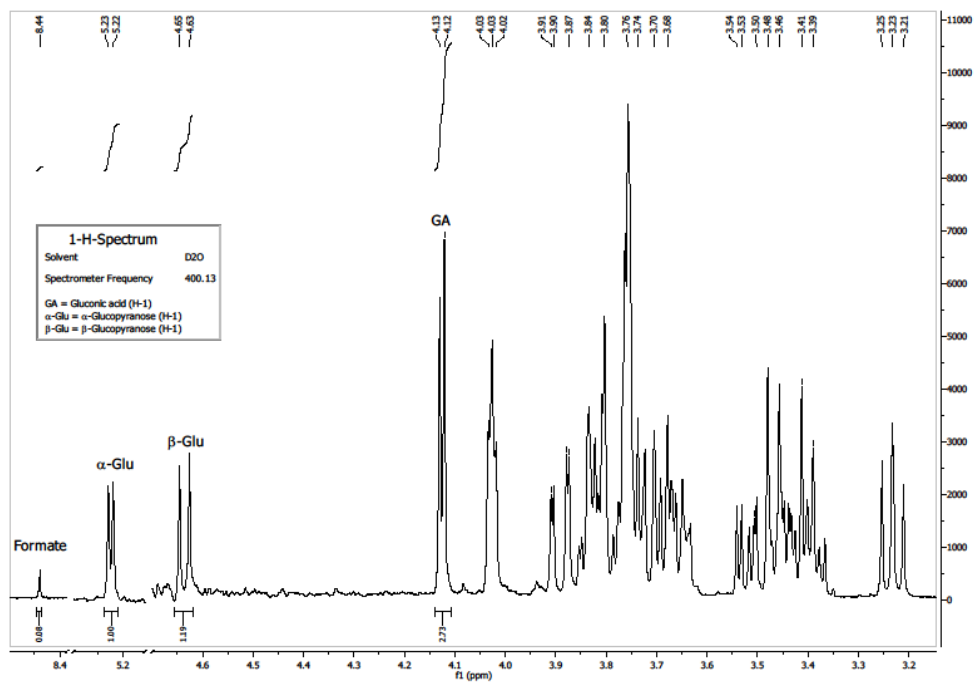


b)

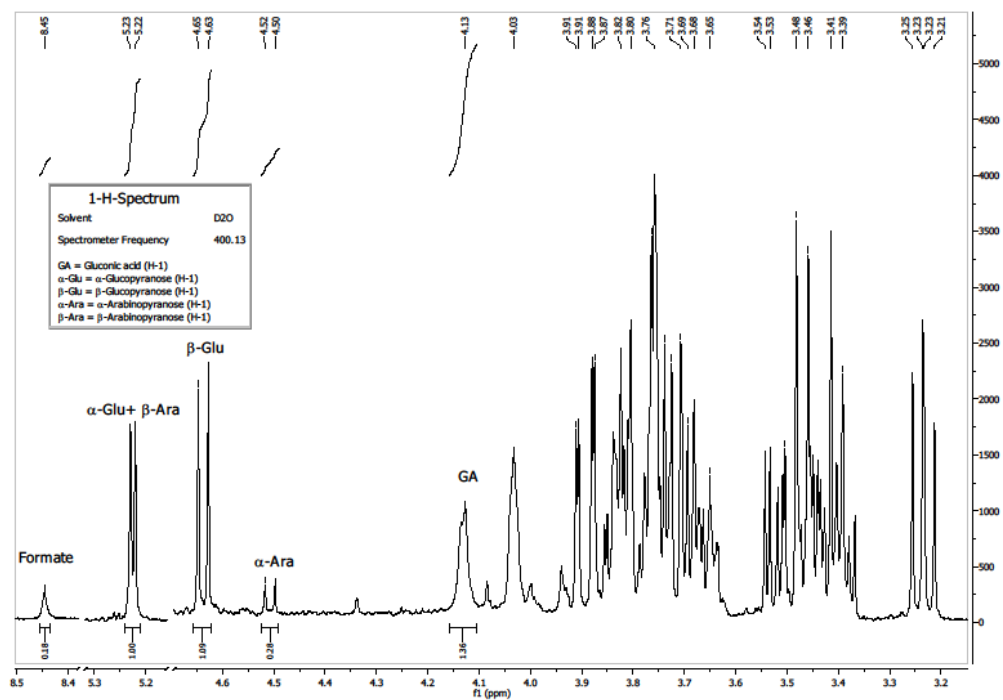
Fig. A1 NMR spectra of lyophilized sample for D-arabinose presentation **a)** ^1H spectra **b)** ^{13}C spectra



a)

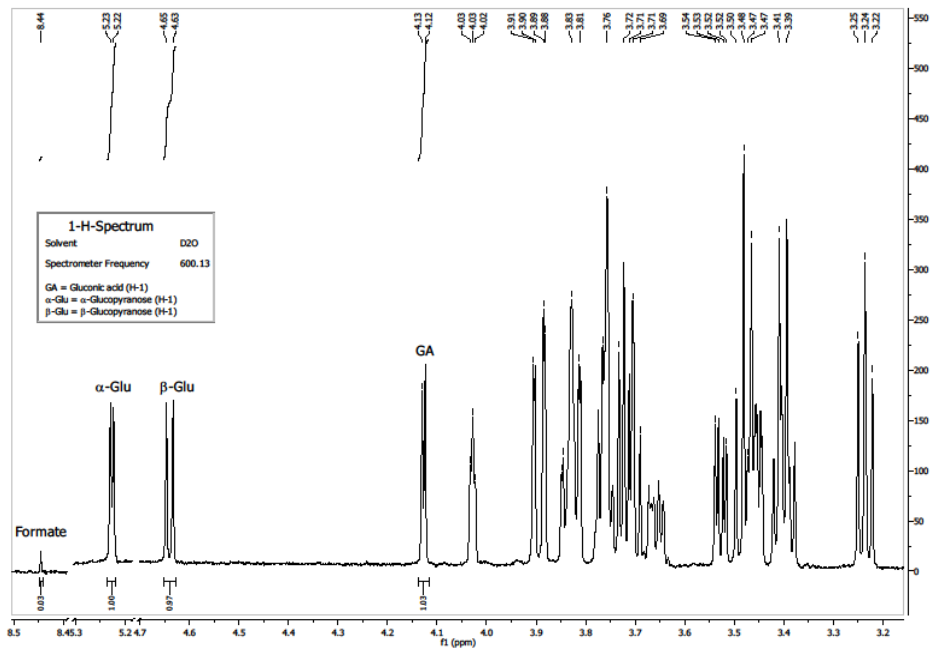


b)

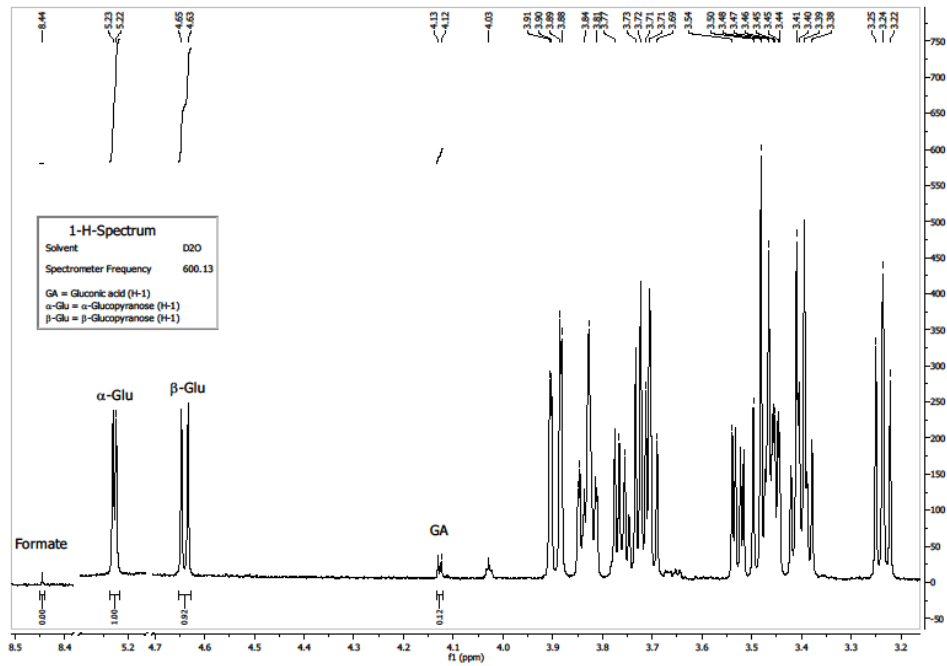


c)

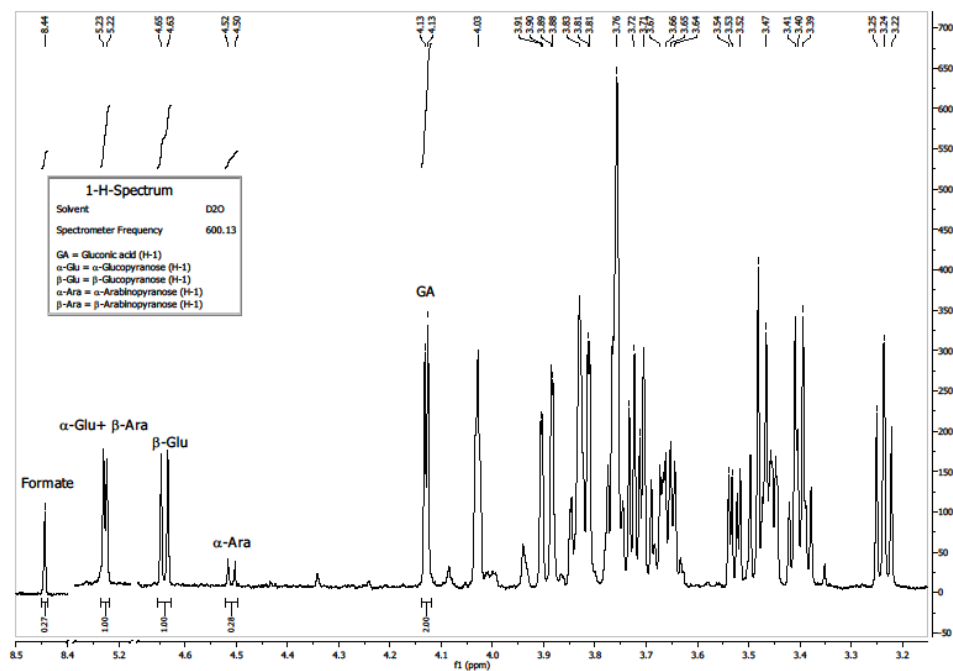
Fig. A2 NMR analysis of reaction solutions after 7 h in electroenzymatic reactors tested at three different flow rates **a)** 10 ml min⁻¹, **b)** 5 ml min⁻¹ and **c)** 2 ml min⁻¹, summarized in Table 6-4



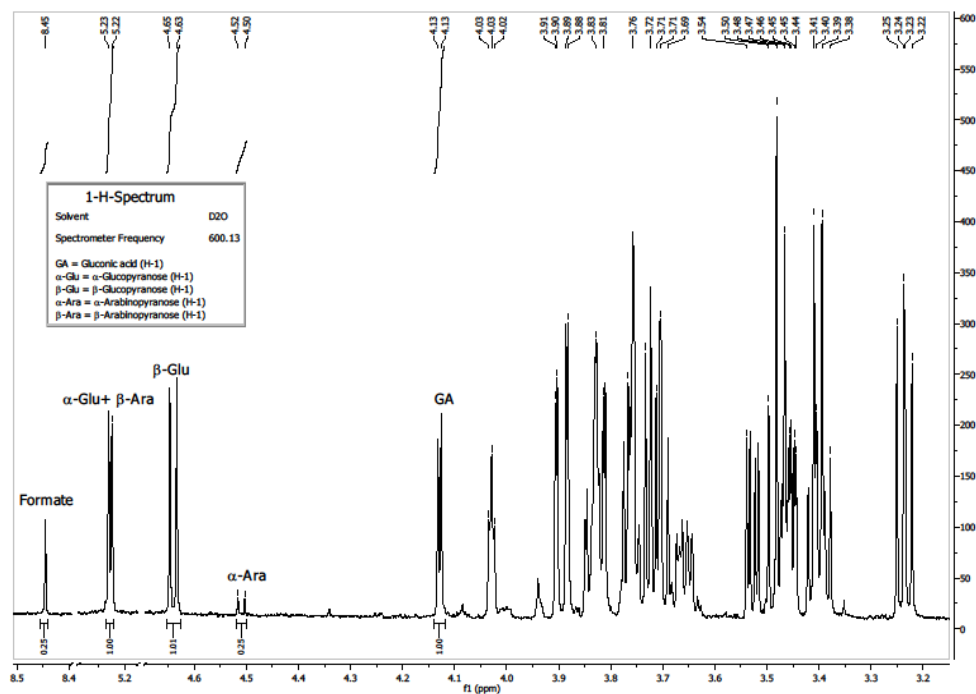
a)



b)

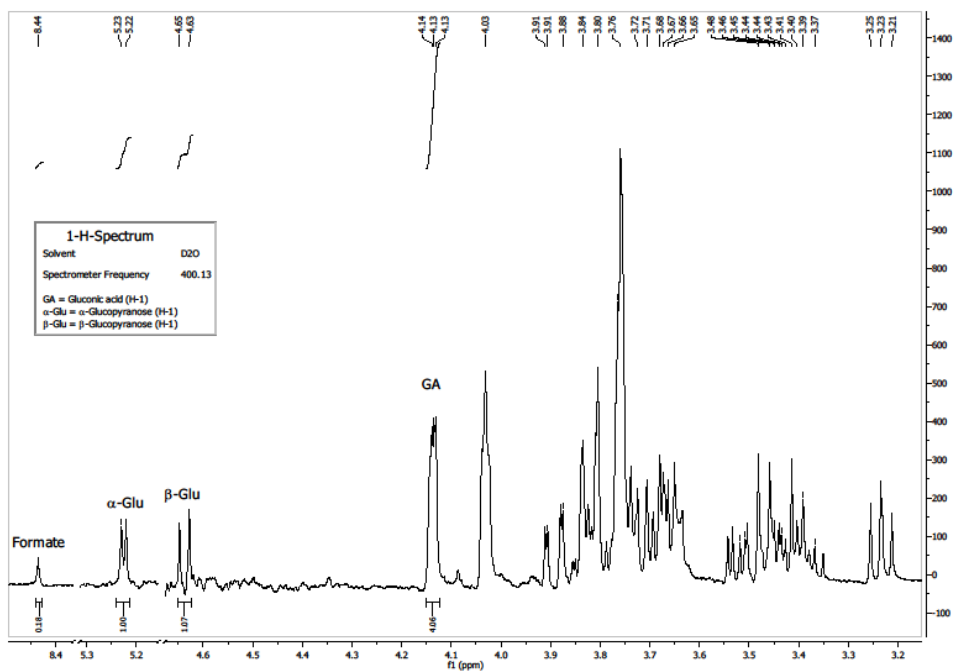


c)

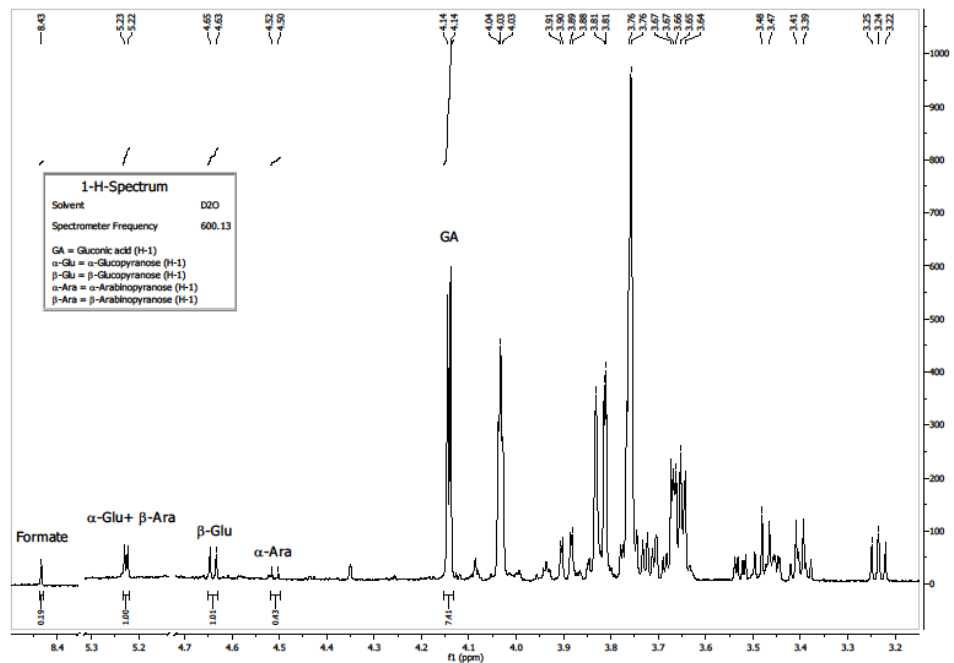


d)

Fig. A3 NMR analysis of reaction mixtures after 7 h of enzymatic electrodes operation in half-cell experiments, **a)** and **b)** anode at different potentials; **c)** and **d)** cathode, at different potentials, Conditions presented in Table 6-5



a)



b)

Fig. A5 NMR results for electroenzymatic reactors operated at two different conditions of cell potential and time, 5 ml min^{-1} **a)** cell potential -0.1 V , time 16 h and **b)** cell potential variation between -0.1 to 0.05 , time 21 h , Conditions presented in Table 6-6

9. List of Tables

Table 1-1 Overview of fermentation processes for the production of gluconic acid	6
Table 1-2 Overview of electroenzymatic processes for the production of gluconic acid	8
Table 4-1 Investigated types of nanomaterials and their characteristics.....	45
Table 4-2 Performance comparison of the HRP porous electrodes for peroxide reduction with DET	57
Table 5-1 Performance comparison of the GOx-HRP electrode for peroxide reduction with DET	74
Table 6-1 Nanomaterial and enzyme loadings at the cathode side	86
Table 6-2 Total and partial glucose conversions in electrochemical reactors after 7 h of reactor operation calculated according to Faraday's law of electrolysis.....	94
Table 6-3 Comparisons of electroenzymatic reactor performances.....	96
Table 6-4 NMR analysis results after 7 h in electroenzymatic reactors tested at three different flow rates	101
Table 6-5 NMR analysis of reaction mixtures after 7 h of enzymatic electrodes operation in half-cell, Conditions: 20 mM glucose in 0.1 M PBS, pH 6.00, 22 °C, 70 ml; cathode: in the presence of O ₂ , anode: in presence of N ₂	104
Table 6-6 NMR results for electroenzymatic reactors under different conditions of cell potential and time, 5 ml min ⁻¹ , 20 mM glucose.....	108
Table 6-7 Comparison of different processes for the gluconic acid production.....	109
Table 6-8 NMR results for electroenzymatic reactors employing different cathodes	112

10. List of Figures

Fig. 1-1 Glucose as platform chemical for synthesis and renewable energy source.....	2
Fig. 1-2 Examples for the use of gluconic acid and its derivatives.....	3
Fig. 1-3 Partial glucose oxidation at the C1 carbon atom	4
Fig. 1-4 Different production routes for glucose oxidation to gluconic acid	4
Fig. 1-5 Flow sheet of a conventional fermentation process for the gluconic acid production.....	5
Fig. 2-1 Simplistic presentation of the enzyme and the “lock-and-key” mechanism for the group of oxidoreductases	11
Fig. 2-2 Enzymatic vs. electroenzymatic catalysis and basic enzyme components (cofactor is further subdivided)	12
Fig. 2-3 Flow scheme of the design pathway and major characteristics for the enzymatic electrodes development	15
Fig. 2-4 Types of bioelectrochemical systems.....	17
Fig. 2-5 Reactor concepts for bioelectrochemical processes [1]	18
Fig. 2-6 Cell potential decomposition to main resistances and depended parameters [70]	19
Fig. 2-7 Possible modes of electrochemical reactor operations [70].....	20
Fig. 3-1 Preparation of HRP modified electrodes at spectroscopically pure carbon (SPG) used in the electrochemical experiments	25
Fig. 3-2 Schematic presentation of the Vulcan-Gelatin preparation procedure.....	27
Fig. 3-3 Schematic presentation of the Vulcan-PVDF preparation procedure	28
Fig. 3-4 Electrodes used for the electrochemical measurements	28
Fig. 3-5 Schematic presentation of the 3-electrode set up (left), working, counter and reference electrode (right).....	30
Fig. 3-6 Qualitative flow field at the rotating disk electrode	31
Fig. 3-7 a) Schematic representation and b) laboratory parts, of a BFC device with components as follows: 1-anode current collector, 2-stainless steel disc with enzymatic catalyst, 3-O-ring, 4-cell body, 5a-toray paper with enzymatic catalyst, 5b-toray paper with PTFE, 6-graphite flow field, 7- cathode current collector, 8-PTFE gasket, 9-end plate 10- Reference electrode	32
Fig. 3-8 Electrochemical reactor: a) schematic presentation b) laboratory setup	33
Fig. 4-1 Schematic representation of optimal electrode designing, including different electrode types and criteria for electrode performance with targeted goal	36
Fig. 4-2 Importance of the immobilization procedure choice	37

Fig. 4-3 Schematic representation of HRP reaction mechanism at the electrode surface	39
Fig. 4-4 Cyclic voltammetry of HRP adsorbed on the graphite electrode, in presence of 0.1 M phosphate buffer and 1 mM hydrogen peroxide, 400 rpm, N ₂ atmosphere, 5 mV s ⁻¹	40
Fig. 4-5 Enzyme leaching effect evaluated in RDE experiment, under constant rotation rate, WE: HRP-graphite electrode, 40 μM hydrogen peroxide, 400 rpm, N ₂ atmosphere.....	41
Fig. 4-6 Steady state experiments of HRP electrode at a) pH 5.00, b) pH 6.00 and c) different hydrogen peroxide concentrations at the E = 0.0 vs. SCE, 400 rpm, N ₂ atmosphere	42
Fig. 4-7 Influence of the H ₂ O ₂ concentration on the performance of the HRP-modified electrode, 400 rpm, pH 6.00, N ₂ atmosphere, E = 0.0 vs. SCE	43
Fig. 4-8 SEM images of a) Vulcan nanomaterial, b) Carbon Hollow Sphere, c) Coral Carbon and d) Carbon Aerogel.....	45
Fig. 4-9 Comparison of CVs obtained for HRP electrodes prepared with different nanomaterials, 0.1 M phosphate buffer, 5 mV s ⁻¹	47
Fig. 4-10 a) Chronoamperometry response and b), c) and d) steady state curves based on current extracted from (a) experiment, in presence of 0.1 M PBS and 3 mM H ₂ O ₂	48
Fig. 4-11 Comparison of HRP electrode activity based on different nanomaterial types, in presence of 3 mM H ₂ O ₂ , N ₂ atmosphere, 400 rpm, pH 5.00.....	49
Fig. 4-12 SEM images of electrode cross sections a) Vulcan nanomaterial b) Carbon Hollow Spheres c) Coral Carbon and d) Carbon Aerogel	50
Fig. 4-13 Cyclic voltammograms of porous enzymatic electrodes in PBS and in 1 mM hydrogen peroxide, without rotation and at 400 rpm a) Vulcan-Gelatin and b) Vulcan-PVDF. Conditions: 5 mV s ⁻¹ , pH 6.00, room temperature, N ₂ atmosphere, enzyme loadings (1 mg cm ⁻² for Vulcan-PVDF and 1.75 mg cm ⁻² for Vulcan-Gelatin electrodes)	51
Fig. 4-14 Comparison of the electrode performance obtained using cyclic voltammetry and steady state methods a) Vulcan-Gelatin and b) Vulcan- PVDF electrodes. Conditions: scan rate 5 mV s ⁻¹ , pH 6.00, N ₂ atmosphere, enzyme loading: Vulcan-PVDF - 1 mg cm ⁻² and Vulcan-Gelatin - 1.75 mg cm ⁻²	52
Fig. 4-15 Comparison of the performances between denatured and native HRP a) cyclic voltammograms b) steady state currents. Conditions: 400 rpm, pH 6.00, 5 mV s ⁻¹ , N ₂	53
Fig. 4-16 a) Influence of enzyme loading on the activity of Vulcan HRP – electrodes b) Comparison of the electrode activities at the same enzyme loading of 1.75 mg cm ⁻² . Conditions: 1 mM hydrogen peroxide, 400 rpm, N ₂ atmosphere, pH 6.00.....	54
Fig. 4-17 Influence of the hydrogen peroxide concentration on the activity of Vulcan HRP – electrodes at optimized enzyme loadings; electrode potential: 0.0 V vs. SCE	55

Fig. 4-18 Influence of pH on the enzymatic electrode performance, conditions as in Fig. 4-15	.56
Fig. 4-19 SEM images of Vulcan HRP electrodes: cross sections of a) Vulcan-Gelatin and b) Vulcan-PVDF; magnified view of the cross-sections of c) Vulcan-Gelatin and d) Vulcan-PVDF and top views of e) Vulcan-Gelatin and f) Vulcan-PVDF58
Fig. 4-20 Modification scheme of labeling procedure: Reaction between amino-reactive dye and protein (P)59
Fig. 4-21 Electrophoresis test: a) gel observed under UV lamp after separation and before standard staining procedure, b) gel with all separated proteins after staining procedure60
Fig. 4-22 Polarization curves obtained for native HRP and labeled HRP adsorbed at the graphite support, 400 rpm, pH 7.2, N ₂ atmosphere61
Fig. 4-23 Microscopy images of electrode surfaces before modification with enzyme a) Highly Ordered Pyrolytic Graphitic - HOPG b) Spectroscopic Graphite -SPG61
Fig. 4-24 Labeled-HRP on HOPG support visualized by a) fluorescence microscopy with exposure time of 200 ms and b) AFM image of HRP adsorbed on HOPG in a monolayer at pH 662
Fig. 4-25 AFM image of HRP adsorbed on HOPG support in a monolayer at pH 7.263
Fig. 4-26 Fluorescence microscopy images of labeled-HRP on the SPG a) before rotation, 200 ms exposure time and b) after 2 h rotation in RDE, 400 rpm, 100 ms exposure time64
Fig. 4-27 Decrease of electrode activity due to enzyme leaching effect, E=0.0 V vs. SCE, 160 μM, 1000 rpm64
Fig. 4-28 Fluorescence microscopy images of labeled-HRP after CL using 5% glutaraldehyde at a) HOPG, imaged with the exposure time of 100 ms and b) at spectroscopic graphite surface with 200 ms exposure time65
Fig. 4-29 Reduction of hydrogen peroxide at the HRP-modified graphite electrodes prepared without and with cross-linking. Conditions: 160 μM hydrogen peroxide concentration, 400 rpm, pH 6.00, N ₂66
Fig. 4-30 Optical images of a) Vulcan and b) Coral Carbon at the glass support in gelatin; Fluorescence microscopy images of c) Vulcan and d) Coral Carbon67
Fig. 4-31 Influence of CL method on the enzyme distribution at the nanomaterial surfaces: a) Vulcan and b) Coral Carbon68
Fig. 5-1 Cyclic voltammograms of Vulcan-Gelatin and Vulcan-PVDF enzymatic biocathode (based on the enzyme cascade GOx-HRP) in 0.1 M phosphate buffer, pH 6.00, 400 rpm, scan rate 5 mV s ⁻¹ , 22 °C and N ₂ atmosphere73

Fig. 5-2 Influence of preparation procedures on steady state polarization behavior of GOx-HRP enzymatic electrode	74
Fig. 5-3 Steady state polarization behavior of the enzymatic cathode (GOx-HRP/Vulcan-PVDF) at two different pH and temperatures, at 400 rpm rotation rate.....	75
Fig. 5-4 Polarization curves of the enzymatic cathode at different glucose concentrations, pH 6.00, 22 °C, 400 rpm rotation and presence of O ₂	76
Fig. 5-5 Polarization curves of different HRP-GOx ratios, in presence of 20 mM glucose and oxygen, pH 6.00, 22 °C, at 400 rpm	77
Fig. 5-6 Cyclic voltammogram of Vulcan-TTF-PVDF enzymatic bioanode in 0.1 M phosphate buffer, pH 6.00, scan rate 5 mV s ⁻¹ , 400 rpm rotation and N ₂ atmosphere.....	78
Fig. 5-7 Influence of preparation procedure on the performance of GOx-TTF electrodes for glucose oxidation. Conditions: 20 mM glucose in 0.1 M phosphate buffer, N ₂ , 400 rpm, pH 6.00, 22 °C.....	80
Fig. 5-8 Steady state performance of enzymatic anode (GOx-TTF/Vulcan-Gelatin) a) at two different pH and temperatures b) under nitrogen and oxygen atmosphere, 400 rpm.....	81
Fig. 5-9 Steady state polarization curves of the enzymatic anode in presence of different glucose concentration, pH 6.00, 400 rpm, N ₂	82
Fig. 6-1 a) Schematic presentation of the reactor setup with recirculation of electrolyte (for more detail see Fig. 3-8) b) Schematic representation of electroenzymatic reactor, Anode side: GOx-mediated electron transfer, Cathode side: GOx-HRP enzyme cascade for glucose oxidation ...	85
Fig. 6-2 a) Polarization and b) power curves of electroenzymatic reactors employing GOx/TTF anode and GOx-HRP cathodes; Conditions: enzyme immobilization: cathode, Vulcan-PVDF; anode, Vulcan-Gelatin, 20 mM glucose in 0.1 M phosphate buffer, 10 ml min ⁻¹ flow rate, O ₂ supply from the gas phase, pH 6.00, 22°C, volume of the glucose reservoir: 70 ml	87
Fig. 6-3 Steady state performances of enzymatic cathode (GOx-HRP) and enzymatic anode (GOx-TTF) under electroenzymatic reactor operation. Conditions as in Fig. 6-2	88
Fig. 6-4 Comparison between steady state performances of a) enzymatic anode (GOx-TTF) and b) enzymatic cathode (GOx-HRP), tested in half-cell and electroenzymatic reactor. Conditions: 20 mM glucose, pH 6.00, 22°C. Flow rates: 10 ml min ⁻¹ for glucose solution, O ₂ supply from the gas phase in the reactor; rotation rates between 100 and 1000 rpm in the half-cell	89
Fig. 6-5 Glucose conversions over 7 h in electroenzymatic reactors (Reactors 1-3 are described in Table 6-1).....	90

Fig. 6-6 a) Current density change during 7 h of reactor operation under voltastatic conditions ($E_{\text{cell}} = 0.0 \text{ V}$) and b) change of anode and cathode electrode potentials during reactors operation	91
Fig. 6-7 Change of anode and cathode overpotentials with electrode potential change under constant cell potential conditions, $E_{\text{cell}} = 0.0 \text{ V}$	92
Fig. 6-8 Long-term performance of enzymatic electrodes over 7 h. Conditions: half-cell measurements, 20 mM glucose, pH 6.00, 22 °C, rotation rates 400 rpm, potential of the electrodes: 0.15 V vs. SCE	93
Fig. 6-9 Comparison of electroenzymatic reactor based on GOx-HRP cathode and enzymatic reactor employing catalase for peroxide decomposition	95
Fig. 6-10 a) Polarization curves of the electroenzymatic reactor at different flow rates; b) Potential loss distribution, anode: GOx-TTF/Vulcan-Gelatin, cathode: GOx-HRP/Vulcan-PVDF, Conditions: 20 mM glucose in 0.1 M phosphate buffer, O_2 supply from the gas phase, pH 6.00, 22 °C, volume of the glucose reservoir: 70 ml	97
Fig. 6-11 Glucose conversions during 7 h in electroenzymatic reactor at different flow rates of glucose	98
Fig. 6-12 NMR product spectra with identified peaks, black line: initial solution; blue line: final solution after 7 h of reactor operation (Additional NMR spectra for all tested systems in Appendix).....	100
Fig. 6-13 Anode and cathode electrode potentials recorded during reactor operation over 7 h; $E_{\text{cell}} = 0.0 \text{ V}$; $E_a = E_c$ (one line is presented).....	102
Fig. 6-14 Proposed pathways for glucose oxidation to gluconic acid and other by-products ...	105
Fig. 6-15 Change of anode and cathode electrode potentials during reactors operation; Conditions presented in Tab. 6-6	107
Fig. 6-16 Polarization curves of Vulcan nanomaterial in the presence and absence of oxygen, 0.1 M phosphate buffer, pH 6.00, 22 °C,	108
Fig. 6-17 Comparison of the steady state performance of BOD and GOx-HRP enzymatic electrode in 20 mM glucose, Conditions for BOD-electrode: pH 7.00, 37 °C, for GOx-HRP: pH 6.00, 22 °C; 400 rpm, O_2	110
Fig. 6-18 Polarization and power curves of electroenzymatic reactors based on two different cathodes, 5 ml min^{-1} , 20 mM glucose, Conditions for GOx GOx-HRP: pH 6.00, 22 °C; GOx BOD system: pH 7.00, 37 °C	111
Fig. 6-19 Comparison of glucose conversion in two different reactors	112
Fig. 7-1 Flow diagram of the electroenzymatic process with a separation unit	118

11. Literature (References)

1. Krieg, T., et al., *Reactor concepts for bioelectrochemical syntheses and energy conversion*. Trends in Biotechnology, 2014. **32**(12): p. 645-655.
2. Horst, A.E.W., K.-M. Mangold, and D. Holtmann, *Application of Gas Diffusion Electrodes in Bioelectrochemical Syntheses and Energy Conversion*. Biotechnology and Bioengineering, 2016. **113**(2): p. 260-267.
3. Steckhan, E., *Electroenzymatic synthesis*. Electrochemistry V, 1994. **170**: p. 83-111.
4. DevauxBasseguy, R., P. Gros, and A. Bergel, *Electroenzymatic processes: A clean technology alternative for highly selective synthesis*. Journal of Chemical Technology and Biotechnology, 1997. **68**(4): p. 389-396.
5. Hollmann, F. and A. Schmid, *Electrochemical regeneration of oxidoreductases for cell-free biocatalytic redox reactions*. Biocatalysis and Biotransformation, 2004. **22**(2): p. 63-88.
6. Dencic, I., et al., *From a Review of Noble Metal versus Enzyme Catalysts for Glucose Oxidation Under Conventional Conditions Towards a Process Design Analysis for Continuous-flow Operation*. Journal of Flow Chemistry, 2011. **1**(1): p. 13-23.
7. Murzin, D.Y. and R. Leino, *Sustainable chemical technology through catalytic multistep reactions*. Chemical Engineering Research & Design, 2008. **86**(9A): p. 1002-1010.
8. Holade, Y., et al., *Highly Selective Oxidation of Carbohydrates in an Efficient Electrochemical Energy Converter: Cogenerating Organic Electrosynthesis*. Chemsuschem, 2016. **9**(3): p. 252-263.
9. Anastassiadis, S.a.M., I.G., *Gluconic Acid Production*. Recent Patents on Biotechnology, 2007. **1**: p. 167-180.
10. Ramachandran, S., et al., *Gluconic acid: Properties, applications and microbial production*. Food Technology and Biotechnology, 2006. **44**(2): p. 185-195.
11. Dewilt, H.G.J., *Oxidation of Glucose to Gluconic Acid. Survey of Techniques*. Industrial & Engineering Chemistry Product Research and Development, 1972. **11**(4): p. 370.
12. Velizarov, S. and V. Beschkov, *Biotransformation of glucose to free gluconic acid by *Gluconobacter oxydans*: substrate and product inhibition situations*. Process Biochemistry, 1998. **33**(5): p. 527-534.
13. Blom, R.H., et al., *Sodium gluconate production. fermentation with *aspergillus niger**. Industrial and Engineering Chemistry, 1952. **44**(2): p. 435-440.

14. Sankpal, N.V. and B.D. Kulkarni, *Optimization of fermentation conditions for gluconic acid production using Aspergillus niger immobilized on cellulose microfibrils*. Process Biochemistry, 2002. **37**(12): p. 1343-1350.
15. Anastassiadis, S., A. Aivasidis, and C. Wandrey, *Continuous gluconic acid production by isolated yeast-like mould strains of Aureobasidium pullulans*. Applied Microbiology and Biotechnology, 2003. **61**(2): p. 110-117.
16. Curie JN, K.J.a.F.A., *Process for producing gluconic acid by fungi*. United States patent 1,893,819, Chem Abstr 1931. **27**: p. 2249.
17. Pal, P., R. Kumar, and S. Banerjee, *Manufacture of gluconic acid: A review towards process intensification for green production*. Chemical Engineering and Processing, 2016. **104**: p. 160-171.
18. Doneva, T., C. Vassilieff, and R. Donev, *Catalytic and biocatalytic oxidation of glucose to gluconic acid in a modified three-phase reactor*. Biotechnology Letters, 1999. **21**(12): p. 1107-1111.
19. Lu, F., et al., *Enhancing gluconic acid production by controlling the morphology of Aspergillus niger in submerged fermentation*. Process Biochemistry, 2015. **50**(9): p. 1342-1348.
20. Sun, W.-J., et al., *Continuous 2-keto-gluconic acid (2KGA) production from corn starch hydrolysate by Pseudomonas fluorescens AR4*. Biochemical Engineering Journal, 2013. **77**: p. 97-102.
21. Znad, H., J. Markos, and V. Bales, *Production of gluconic acid from glucose by Aspergillus niger: growth and non-growth conditions*. Process Biochemistry, 2004. **39**(11): p. 1341-1345.
22. Klein, J., et al., *Biotransformation of glucose to gluconic acid by Aspergillus niger - study of mass transfer in an airlift bioreactor*. Biochemical Engineering Journal, 2002. **10**(3): p. 197-205.
23. Sun, W., et al., *Non-sterile and buffer-free bioconversion of glucose to 2-keto-gluconic acid by using Pseudomonas fluorescens AR4 free resting cells*. Process Biochemistry, 2015. **50**(4): p. 493-499.
24. Crognale, S., et al., *Fed-batch gluconic acid production from Penicillium variabile P16 under different feeding strategies*. Enzyme and Microbial Technology, 2008. **42**(5): p. 445-449.

25. Ikeda, Y., E.Y. Park, and N. Okuda, *Bioconversion of waste office paper to gluconic acid in a turbine blade reactor by the filamentous fungus Aspergillus niger*. Bioresource Technology, 2006. **97**(8): p. 1030-1035.
26. Singh, O.V., N. Kapur, and R.P. Singh, *Evaluation of agro-food byproducts for gluconic acid production by Aspergillus niger ORS-4.410*. World Journal of Microbiology & Biotechnology, 2005. **21**(4): p. 519-524.
27. Biella, S., L. Prati, and M. Rossi, *Selective oxidation of D-glucose on gold catalyst*. Journal of Catalysis, 2002. **206**(2): p. 242-247.
28. Zhang, H.J., et al., *Catalytically highly active top gold atom on palladium nanocluster*. Nature Materials, 2012. **11**(1): p. 49-52.
29. Bin, D.S., et al., *Controllable oxidation of glucose to gluconic acid and glucaric acid using an electrocatalytic reactor*. Electrochimica Acta, 2014. **130**: p. 170-178.
30. Liu, H.U. and Z.F. Cui, *Optimization of operating conditions for glucose oxidation in an enzymatic membrane bioreactor*. Journal of Membrane Science, 2007. **302**(1-2): p. 180-187.
31. Bourdillon, C., R. Lortie, and J.M. Laval, *Gluconic acid production by an immobilized glucose oxidase reactor with electrochemical regeneration of an artificial electron acceptor*. Biotechnology and Bioengineering, 1988. **31**(6): p. 553-558.
32. Basseguy, R., K. Delecoulis-Servat, and A. Bergel, *Glucose oxidase catalysed oxidation of glucose in a dialysis membrane electrochemical reactor (D-MER)*. Bioprocess and Biosystems Engineering, 2004. **26**(3): p. 165-168.
33. Obón, J.M., et al., *Stabilization of Glucose Dehydrogenase with Polyethyleneimine in an Electrochemical Reactor with NAD(P) + Regeneration*. Biotechnology Progress, 1997. **13**(5): p. 557-561.
34. Manjón, A., et al., *Increased activity of glucose dehydrogenase co-immobilized with a redox mediator in a bioreactor with electrochemical NAD⁺ regeneration*. Biotechnology Letters, 2002. **24**(15): p. 1227-1232.
35. Gros, P. and A. Bergel, *Electrochemically enhanced biosynthesis of gluconic acid*. Aiche Journal, 2005. **51**(3): p. 989-997.
36. Miyawaki, O. and T. Yano, *Electrochemical bioreactor with immobilized glucose-6-phosphate dehydrogenase on the rotating graphite disc electrode modified with phenazine methosulfate*. Enzyme and Microbial Technology, 1993. **15**(6): p. 525-529.
37. Wichmann, R. and D. Vasic-Racki, *Cofactor regeneration at the lab scale*, in *Technology Transfer in Biotechnology: From Lab to Industry to Production*. 2005. p. 225-260.

38. Mirkin, M.V., *Encyclopedia of Electrochemistry. Volume 9. Bioelectrochemistry Edited by George S. Wilson (University of Kansas). ISBN 3-527-30401-0.* Journal of the American Chemical Society, 2003. **125**(22): p. 6834-6835.
39. Wilson, R. and A.P.F. Turner, *Glucose oxidase: an ideal enzyme.* Biosensors & Bioelectronics, 1992. **7**(3): p. 165-185.
40. Ivanov, I., T. Vidakovic-Koch, and K. Sundmacher, *Recent Advances in Enzymatic Fuel Cells: Experiments and Modeling.* Energies, 2010. **3**(4): p. 803-846.
41. Cooney, M.J., et al., *Enzyme catalysed biofuel cells.* Energy & Environmental Science, 2008. **1**(3): p. 320-337.
42. Dunford, H.B., *Heme Peroxidase.* Wiley-VCH, New York, 1999.
43. Ruzgas, T., et al., *Peroxidase-modified electrodes: Fundamentals and application.* Analytica Chimica Acta, 1996. **330**(2-3): p. 123-138.
44. Ferapontova, E.E., *Direct Peroxidase Bioelectrocatalysis on a Variety of Electrode Materials.* Electroanalysis, 2004. **16**(13-14): p. 1101-1112.
45. Woodley, J.M., *Protein engineering of enzymes for process applications.* Current Opinion in Chemical Biology, 2013. **17**(2): p. 310-316.
46. Li, Y. and P.C. Cirino, *Recent advances in engineering proteins for biocatalysis.* Biotechnology and Bioengineering, 2014. **111**(7): p. 1273-1287.
47. Fried, D.I., F.J. Brieler, and M. Froba, *Designing Inorganic Porous Materials for Enzyme Adsorption and Applications in Biocatalysis.* Chemcatchem, 2013. **5**(4): p. 862-884.
48. Yu, E.H. and K. Scott, *Enzymatic Biofuel Cells-Fabrication of Enzyme Electrodes.* Energies, 2010. **3**(1): p. 23-42.
49. Barton, S.C., J. Gallaway, and P. Atanassov, *Enzymatic biofuel cells for Implantable and microscale devices.* Chemical Reviews, 2004. **104**(10): p. 4867-4886.
50. Kim, J., H.F. Jia, and P. Wang, *Challenges in biocatalysis for enzyme-based biofuel cells.* Biotechnology Advances, 2006. **24**(3): p. 296-308.
51. Kim, J., J.W. Grate, and P. Wang, *Nanostructures for enzyme stabilization.* Chemical Engineering Science, 2006. **61**(3): p. 1017-1026.
52. Kim, J.B., *Nanobiocatalysis and its potential applications.* Journal of Biotechnology, 2010. **150**: p. S71-S71.
53. Nazaruk, E., et al., *Enzymatic electrodes nanostructured with functionalized carbon nanotubes for biofuel cell applications.* Analytical and Bioanalytical Chemistry, 2010. **398**(4): p. 1651-1660.

54. Tsujimura, S., Y. Kamitaka, and K. Kano, *Diffusion-controlled oxygen reduction on multi-copper oxoclase-adsorbed carbon aerogel electrodes without mediator*. *Fuel Cells*, 2007. **7**(6): p. 463-469.
55. Luz, R.A.S., et al., *Enzyme Biofuel Cells: Thermodynamics, Kinetics and Challenges in Applicability*. *Chemelectrochem*, 2014. **1**(11): p. 1751-1777.
56. Varnicic, M., et al., *Combined electrochemical and microscopic study of porous enzymatic electrodes with direct electron transfer mechanism*. *Rsc Advances*, 2014. **4**(69): p. 36471-36479.
57. Wang, X.J., et al., *Mediatorless sugar/oxygen enzymatic fuel cells based on gold nanoparticle-modified electrodes*. *Biosensors & Bioelectronics*, 2012. **31**(1): p. 219-225.
58. Kihara, T., et al., *Direct electron transfer to hydrogenase for catalytic hydrogen production using a single-walled carbon nanotube forest*. *International Journal of Hydrogen Energy*, 2011. **36**(13): p. 7523-7529.
59. Svedruzic, D., et al., *High-Performance Hydrogen Production and Oxidation Electrodes with Hydrogenase Supported on Metallic Single-Wall Carbon Nanotube Networks*. *Journal of the American Chemical Society*, 2011. **133**(12): p. 4299-4306.
60. Hwang, E.T. and M.B. Gu, *Enzyme stabilization by nano/microsized hybrid materials*. *Engineering in Life Sciences*, 2013. **13**(1): p. 49-61.
61. Meunier, C.F., et al., *Biofuel cells Based on the Immobilization of Photosynthetically Active Bioentities*. *Chemcatchem*, 2011. **3**(3): p. 476-488.
62. Davis, J.B. and H.F. Yarbrough, *P Preliminary Experiments on a Microbial Fuel Cell*. *Science*, 1962. **137**(3530): p. 615.
63. Yahiro, A.T., S.M. Lee, and D.O. Kimble, *Bioelectrochemistry: I. Enzyme utilizing bio-fuel cell studies*. *Biochimica Et Biophysica Acta*, 1964. **88**(2): p. 375.
64. Leech, D., P. Kavanagh, and W. Schuhmann, *Enzymatic fuel cells: Recent progress*. *Electrochimica Acta*, 2012. **84**: p. 223-234.
65. Osman, M.H., A.A. Shah, and F.C. Walsh, *Recent progress and continuing challenges in bio-fuel cells. Part I: Enzymatic cells*. *Biosensors & Bioelectronics*, 2011. **26**(7): p. 3087-3102.
66. Bullen, R.A., et al., *Biofuel cells and their development*. *Biosensors & Bioelectronics*, 2006. **21**(11): p. 2015-2045.
67. Liu, H. and B.E. Logan, *Electricity generation using an air-cathode single chamber microbial fuel cell in the presence and absence of a proton exchange membrane*. *Environmental Science & Technology*, 2004. **38**(14): p. 4040-4046.

68. Krieg, T., et al., *Gas diffusion electrode as novel reaction system for an electro-enzymatic process with chloroperoxidase*. *Green Chemistry*, 2011. **13**(10): p. 2686-2689.
69. Holtmann, D., et al., *Electroenzymatic process to overcome enzyme instabilities*. *Catalysis Communications*, 2014. **51**: p. 82-85.
70. Sundmacher, K., L.K. Rihko-Struckmann, and V. Galvita, *Solid electrolyte membrane reactors: Status and trends*. *Catalysis Today*, 2005. **104**(2-4): p. 185-199.
71. Rismani-Yazdi, H., et al., *Cathodic limitations in microbial fuel cells: An overview*. *Journal of Power Sources*, 2008. **180**(2): p. 683-694.
72. Selembo, P.A., M.D. Merrill, and B.E. Logan, *The use of stainless steel and nickel alloys as low-cost cathodes in microbial electrolysis cells*. *Journal of Power Sources*, 2009. **190**(2): p. 271-278.
73. Soussan, L., et al., *Electrochemical reduction of CO₂ catalysed by Geobacter sulfurreducens grown on polarized stainless steel cathodes*. *Electrochemistry Communications*, 2013. **28**: p. 27-30.
74. Zhang, X.Y., et al., *Scalable air cathode microbial fuel cells using glass fiber separators, plastic mesh supporters, and graphite fiber brush anodes*. *Bioresource Technology*, 2011. **102**(1): p. 372-375.
75. Dumas, C., R. Basseguy, and A. Bergel, *Microbial electrocatalysis with Geobacter sulfurreducens biofilm on stainless steel cathodes*. *Electrochimica Acta*, 2008. **53**(5): p. 2494-2500.
76. Larminie, J., et al., *Efficiency and Open Circuit Voltage*, in *Fuel Cell Systems Explained*. John Wiley & Sons, Ltd, 2013 p. 25-43.
77. Andreu, R., et al., *Direct electron transfer kinetics in horseradish peroxidase electrocatalysis*. *Journal of Physical Chemistry B*, 2007. **111**(2): p. 469-477.
78. Vidakovic-Koch, T., et al., *Application of electrochemical impedance spectroscopy for studying of enzyme kinetics*. *Electrochimica Acta*, 2013. **110**: p. 94-104.
79. Ivanov, I., T. Vidakovic-Koch, and K. Sundmacher, *Direct hybrid glucose-oxygen enzymatic fuel cell based on tetrathiafulvalene-tetracyanoquinodimethane charge transfer complex as anodic mediator*. *Journal of Power Sources*, 2011. **196**(22): p. 9260-9269.
80. Tamaki, T., *Enzymatic Biofuel Cells Based on Three-Dimensional Conducting Electrode Matrices*. *Topics in Catalysis*, 2012. **55**(16-18): p. 1162-1180.

81. Cracknell, J.A., K.A. Vincent, and F.A. Armstrong, *Enzymes as working or inspirational electrocatalysts for fuel cells and electrolysis*. Chemical Reviews, 2008. **108**(7): p. 2439-2461.
82. Yaropolov, A.I., M.R. Tarasevich, and S.D. Varfolomeev, *Electrochemical Properties of Peroxidase*. Bioelectrochemistry and Bioenergetics, 1978. **5**(1): p. 18-24.
83. Razumas, V.J., J.J. Jasaitis, and J.J. Kulys, *Electrocatalysis on enzyme-modified carbon materials*. Bioelectrochemistry and Bioenergetics, 1984. **12**(3-4): p. 297-322.
84. Bogdanovskaya, V.A., et al., *Electrochemical transformations of proteins adsorbed at carbon electrodes*. Bioelectrochemistry and Bioenergetics, 1988. **19**(3): p. 581-584.
85. Csoregi, E., G. Jonssonpettersson, and L. Gorton, *Mediatorless electrocatalytic reduction of hydrogen peroxide at graphite electrodes chemically modified with peroxidases*. Journal of Biotechnology, 1993. **30**(3): p. 315-337.
86. Ho, W.O., et al., *Mediatorless horseradish peroxidase enzyme electrodes based on activated carbon: potential application to specific binding assay*. Journal of Electroanalytical Chemistry, 1993. **351**(1-2): p. 185-197.
87. Lindgren, A., et al., *Direct electron transfer catalysed by recombinant forms of horseradish peroxidase: insight into the mechanism*. Electrochemistry Communications, 1999. **1**(5): p. 171-175.
88. Zhao, J.G., et al., *Direct electron transfer at horseradish peroxidase—colloidal gold modified electrodes*. Journal of Electroanalytical Chemistry, 1992. **327**(1-2): p. 109-119.
89. Razumas, V.J., A.V. Gudavicius, and J.J. Kulys, *Kinetics of peroxidase redox conversion on viologen-modified gold electrodes*. Journal of Electroanalytical Chemistry, 1986. **198**(1): p. 81-87.
90. Razumas, V.J., A.V. Gudavicius, and J.J. Kulys, *Redox conversion of peroxidase on surface-modified gold electrode*. Journal of Electroanalytical Chemistry, 1983. **151**(1-2): p. 311-315.
91. Durliat, H., A. Courteix, and M. Comtat, *Reactions of horseradish peroxidase on a platinum cathode*. Bioelectrochemistry and Bioenergetics, 1989. **22**(3): p. 197-209.
92. Comtat, M. and H. Durliat, *Some examples of the use of thin layer spectroelectrochemistry in the study of electron transfer between metals and enzymes*. Biosensors & Bioelectronics, 1994. **9**(9-10): p. 663-668.
93. Sassolas, A., L.J. Blum, and B.D. Leca-Bouvier, *Immobilization strategies to develop enzymatic biosensors*. Biotechnology Advances, 2012. **30**(3): p. 489-511.

94. Jonsson, G. and L. Gorton, *An electrochemical sensor for hydrogen peroxide based on peroxidase adsorbed on a spectrographic graphite electrode*. *Electroanalysis*, 1989. **1**(5): p. 465-468.
95. Sun, D.M., et al., *Direct electrochemical reaction of horseradish peroxidase immobilized on the surface of active carbon powders*. *Chinese Chemical Letters*, 2004. **15**(4): p. 453-454.
96. Yamazaki, I., M. Tamura, and R. Nakajima, *Horseradish peroxidase-C*. *Molecular and Cellular Biochemistry*, 1981. **40**(3): p. 143-153.
97. Farhangrazi, Z.S., et al., *Variable-temperature spectroelectrochemical study of horseradish peroxidase*. *Biochemistry*, 1995. **34**(9): p. 2866-2871.
98. Ruzgas, T., et al., *Kinetic models of horseradish peroxidase action on a graphite electrode*. *Journal of Electroanalytical Chemistry*, 1995. **391**(1-2): p. 41-49.
99. Tatsuma, T., K. Ariyama, and N. Oyama, *Kinetic analysis of electron transfer from a graphite coating to horseradish peroxidase*. *Journal of Electroanalytical Chemistry*, 1998. **446**(1-2): p. 205-209.
100. Ferapontova, E.E. and L. Gorton, *Effect of proton donors on direct electron transfer in the system gold electrode-horseradish peroxidase*. *Electrochemistry Communications*, 2001. **3**(12): p. 767-774.
101. Nakajima, R. and I. Yamazaki, *The Mechanism of Oxypoxidase Formation from Ferryl Peroxidase and Hydrogen Peroxide*. *Journal of Biological Chemistry*, 1987. **262**(6): p. 2576-2581.
102. Minter, S.D., *Nanobioelectrocatalysis and Its Applications in Biosensors, Biofuel Cells and Bioprocessing*. *Topics in Catalysis*, 2012. **55**(16-18): p. 1157-1161.
103. Habrioux, A., et al., *Electrochemical characterization of adsorbed bilirubin oxidase on Vulcan XC 72R for the biocathode preparation in a glucose/O₂ biofuel cell*. *Electrochimica Acta*, 2010. **55**(26): p. 7701-7705.
104. Ivanov, I., T. Vidakovic-Koch, and K. Sundmacher, *Alternating electron transfer mechanism in the case of high-performance tetrathiafulvalene-tetracyanoquinodimethane enzymatic electrodes*. *Journal of Electroanalytical Chemistry*, 2013. **690**: p. 68-73.
105. Gao, F., et al., *Electrocatalytic activity of carbon spheres towards NADH oxidation at low overpotential and its applications in biosensors and biofuel cells*. *Rsc Advances*, 2011. **1**(7): p. 1301-1309.

106. Chekin, F., L. Gorton, and I. Tapsoba, *Direct and mediated electrochemistry of peroxidase and its electrocatalysis on a variety of screen-printed carbon electrodes: amperometric hydrogen peroxide and phenols biosensor*. Analytical and Bioanalytical Chemistry, 2015. **407**(2): p. 439-446.
107. Agnes, C., et al., *A double-walled carbon nanotube-based glucose/H₂O₂ biofuel cell operating under physiological conditions*. Electrochemistry Communications, 2013. **34**: p. 105-108.
108. Reuillard, B., et al., *Biomimetic versus enzymatic high-potential electrocatalytic reduction of hydrogen peroxide on a functionalized carbon nanotube electrode*. Chemical Science, 2015. **6**(9): p. 5139-5143.
109. Reuillard, B., et al., *Non-covalent functionalization of carbon nanotubes with boronic acids for the wiring of glycosylated redox enzymes in oxygen-reducing biocathodes*. Journal of Materials Chemistry B, 2014. **2**(16): p. 2228-2232.
110. Katanyoota, P., et al., *Novel polybenzoxazine-based carbon aerogel electrode for supercapacitors*. Materials Science and Engineering B-Advanced Functional Solid-State Materials, 2010. **167**(1): p. 36-42.
111. Li, J., et al., *Studies on preparation and performances of carbon aerogel electrodes for the application of supercapacitor*. Journal of Power Sources, 2006. **158**(1): p. 784-788.
112. Li, M.G., et al., *Direct electrochemistry of horseradish peroxidase on graphene-modified electrode for electrocatalytic reduction towards H₂O₂*. Electrochimica Acta, 2011. **56**(3): p. 1144-1149.
113. Jia, W.Z., et al., *Towards a high potential biocathode based on direct bioelectrochemistry between horseradish peroxidase and hierarchically structured carbon nanotubes*. Physical Chemistry Chemical Physics, 2010. **12**(34): p. 10088-10092.
114. Gomez, C., S. Shipovskov, and E.E. Ferapontova, *Peroxidase biocathodes for a biofuel cell development*. Journal of Renewable and Sustainable Energy, 2010. **2**(1).
115. Jia, W., et al., *Glucose Oxidase/Horseradish Peroxidase Co-immobilized at a CNT-Modified Graphite Electrode: Towards Potentially Implantable Biocathodes*. Chemistry-a European Journal, 2012. **18**(10): p. 2783-2786.
116. Walgama, C. and S. Krishnan, *Tuning the Electrocatalytic Efficiency of Heme-Protein Films by Controlled Immobilization on Pyrene-Functionalized Nanostructure Electrodes*. Journal of the Electrochemical Society, 2014. **161**(1): p. H47-H52.

117. Limoges, B., J.M. Saveant, and D. Yazidi, *Quantitative analysis of catalysis and inhibition at horseradish peroxidase monolayers immobilized on an electrode surface*. Journal of the American Chemical Society, 2003. **125**(30): p. 9192-9203.
118. Bang, J.H., et al., *Porous carbon supports prepared by ultrasonic spray pyrolysis for direct methanol fuel cell electrodes*. Journal of Physical Chemistry C, 2007. **111**(29): p. 10959-10964.
119. Gode, P., et al., *Influence of the composition on the structure and electrochemical characteristics of the PEFC cathode*. Electrochimica Acta, 2003. **48**(28): p. 4175-4187.
120. ElKaoutit, M., et al., *Electrochemical AFM investigation of horseradish peroxidase enzyme electro-immobilization with polypyrrole conducting polymer*. Synthetic Metals, 2009. **159**(5-6): p. 541-545.
121. Song, Y.H., et al., *A novel hydrogen peroxide sensor based on horseradish peroxidase immobilized in DNA films on a gold electrode*. Sensors and Actuators B-Chemical, 2006. **114**(2): p. 1001-1006.
122. Zhang, J.L., et al., *Graphene Oxide as a Matrix for Enzyme Immobilization*. Langmuir, 2010. **26**(9): p. 6083-6085.
123. Besteman, K., et al., *Enzyme-coated carbon nanotubes as single-molecule biosensors*. Nano Letters, 2003. **3**(6): p. 727-730.
124. De Wael, K., et al., *Surface characterization of a cross-linked cytochrome c film on cysteamine-modified gold electrodes*. Surface and Interface Analysis, 2009. **41**(5): p. 389-393.
125. Wang, J.H., L.W. Ruddock, and A.E.G. Cass, *Microscopic investigations of the interaction of proteins with surfaces*. Biosensors & Bioelectronics, 1994. **9**(9-10): p. 647-655.
126. Zhang, J.D., et al., *In situ electrochemical scanning tunnelling microscopy investigation of structure for horseradish peroxidase and its electrocatalytic property*. Bioelectrochemistry and Bioenergetics, 1996. **39**(2): p. 267-274.
127. Hsiao, A.P. and M.J. Heller, *Electric-Field-Directed Self-Assembly of Active Enzyme-Nanoparticle Structures*. Journal of Biomedicine and Biotechnology, 2012. p. 1-9.
128. Rosenwald, S.E., et al., *Laser interference pattern ablation of a carbon fiber microelectrode: Biosensor signal enhancement after enzyme attachment*. Analytical Chemistry, 2000. **72**(20): p. 4914-4920.

129. Xiong, M., et al., *Glucose microfluidic biosensors based on reversible enzyme immobilization on photopatterned stimuli-responsive polymer*. *Biosensors and Bioelectronics*, 2013. **50**(0): p. 229-234.
130. Olea, D., P. Moreau, and C. Faure, *Polypyrrole-glucose oxidase biosensor. Effect of enzyme encapsulation in multilamellar vesicles on film growth and morphology*. *Journal of Electroanalytical Chemistry*, 2007. **605**(2): p. 125-135.
131. Uygun, A., et al., *Fluorescence study of protein immobilization on poly(4-hydroxyphenyl thiophene-3-carboxylate)-coated electrodes*. *Materials Science & Engineering C-Materials for Biological Applications*, 2010. **30**(6): p. 868-872.
132. Wetzl, B., et al., *Set of fluorochromophores in the wavelength range from 450 to 700 nm and suitable for labeling proteins and amino-modified DNA*. *Journal of Chromatography B-Analytical Technologies in the Biomedical and Life Sciences*, 2003. **793**(1): p. 83-92.
133. Sheldon, R.A., *Cross-Linked Enzyme Aggregates as Industrial Biocatalysts*. *Organic Process Research & Development*, 2011. **15**(1): p. 213-223.
134. Bankar, S.B., et al., *Glucose oxidase - An overview*. *Biotechnology Advances*, 2009. **27**(4): p. 489-501.
135. Zhu, L.D., et al., *Bienzymatic glucose biosensor based on co-immobilization of peroxidase and glucose oxidase on a carbon nanotubes electrode*. *Biosensors & Bioelectronics*, 2007. **23**(4): p. 528-535.
136. Yao, Y.L. and K.K. Shiu, *A Mediator-Free Bienzyme Amperometric Biosensor Based on Horseradish Peroxidase and Glucose Oxidase Immobilized on Carbon Nanotube Modified Electrode*. *Electroanalysis*, 2008. **20**(19): p. 2090-2095.
137. Csoregi, E., L. Gorton, and G. Markovarga, *Amperometric microbiosensors for detection of hydrogen peroxide and glucose based on peroxidase-modified carbon fibers*. *Electroanalysis*, 1994. **6**(11-12): p. 925-933.
138. Snejdarkova, M., M. Rehak, and M. Otto, *Design of a glucose minisensor based on streptavidin-glucose oxidase complex coupling with self-assembled biotinylated phospholipid membrane on solid support*. *Analytical Chemistry*, 1993. **65**(6): p. 665-668.
139. Filip, J., et al., *Electrochemistry of bilirubin oxidase and its use in preparation of a low cost enzymatic biofuel cell based on a renewable composite binder chitosan*. *Electrochimica Acta*, 2013. **87**: p. 366-374.
140. Blanford, C.F., R.S. Heath, and F.A. Armstrong, *A stable electrode for high-potential, electrocatalytic O₂ reduction based on rational attachment of a blue copper oxidase to a graphite surface*. *Chemical Communications*, 2007 (17): p. 1710-1712.

141. Hussein, L., G. Urban, and M. Kruger, *Fabrication and characterization of buckypaper-based nanostructured electrodes as a novel material for biofuel cell applications*. Physical Chemistry Chemical Physics, 2011. **13**(13): p. 5831-5839.
142. Hussein, L., et al., *A highly efficient buckypaper-based electrode material for mediatorless laccase-catalyzed dioxygen reduction*. Biosensors & Bioelectronics, 2011. **26**(10): p. 4133-4138.
143. Krikstolaityte, V., et al., *Biofuel Cell Based on Anode and Cathode Modified by Glucose Oxidase*. Electroanalysis, 2013. **25**(12): p. 2677-2683.
144. Sung, W.J. and Y.H. Bae, *A glucose oxidase electrode based on electropolymerized conducting polymer with polyanion-enzyme conjugated dopant*. Analytical Chemistry, 2000. **72**(9): p. 2177-2181.
145. Zhao, W., et al., *Multilayer membranes via layer-by-layer deposition of organic polymer protected Prussian blue nanoparticles and glucose oxidase for glucose biosensing*. Langmuir, 2005. **21**(21): p. 9630-9634.
146. Yonhin, B.F.Y., et al., *Covalent electropolymerization of glucose oxidase in polypyrrole. Evaluation of methods of pyrrole attachment to glucose oxidase on the performance of electropolymerized glucose sensors*. Analytical Chemistry, 1993. **65**(15): p. 2067-2071.
147. Yang, S., et al., *Simple Approach for Efficient Encapsulation of Enzyme in Silica Matrix with Retained Bioactivity*. Analytical Chemistry, 2009. **81**(9): p. 3478-3484.
148. Do, T.Q.N., et al., *Dynamic and steady state 1-D model of mediated electron transfer in a porous enzymatic electrode*. Bioelectrochemistry, 2015. **106**: p. 3-13.
149. Liu, H.Y. and J.Q. Deng, *An amperometric glucose sensor based on Eastman-AQ-tetrathiafulvalene modified electrode*. Biosensors & Bioelectronics, 1996. **11**(1-2): p. 103-110.
150. Kowalewska, B. and P.J. Kulesza, *Application of Tetrathiafulvalene-Modified Carbon Nanotubes to Preparation of Integrated Mediating System for Bioelectrocatalytic Oxidation of Glucose*. Electroanalysis, 2009. **21**(3-5): p. 351-359.
151. Rengaraj, S., P. Kavanagh, and D. Leech, *A comparison of redox polymer and enzyme co-immobilization on carbon electrodes to provide membrane-less glucose/O₂ enzymatic fuel cells with improved power output and stability*. Biosensors & Bioelectronics, 2011. **30**(1): p. 294-299.
152. MacAodha, D., et al., *Crosslinked redox polymer enzyme electrodes containing carbon nanotubes for high and stable glucose oxidation current*. Physical Chemistry Chemical Physics, 2012. **14**(42): p. 14667-14672.

153. Mano, N., F. Mao, and A. Heller, *Electro-oxidation of glucose at an increased current density at a reducing potential*. Chemical Communications, 2004(18): p. 2116-2117.
154. Grampp, G., A. Kapturkiewicz, and W. Jaenicke, *Homogeneous and Heterogeneous Electron Transfer Rates of the Tetrathiafulvalene-System*. Berichte Der Bunsen-Gesellschaft-Physical Chemistry Chemical Physics, 1990. **94**(4): p. 439-447.
155. Limoges, B., J. Moiroux, and J.M. Saveant, *Kinetic control by the substrate and the cosubstrate in electrochemically monitored redox enzymatic immobilized systems. Catalytic responses in cyclic voltammetry and steady state techniques*. Journal of Electroanalytical Chemistry, 2002. **521**(1-2): p. 8-15.
156. de Poulpiquet, A., A. Ciaccafava, and E. Lojou, *New trends in enzyme immobilization at nanostructured interfaces for efficient electrocatalysis in biofuel cells*. Electrochimica Acta, 2014. **126**: p. 104-114.
157. Falk, M., et al., *Miniature Direct Electron Transfer Based Enzymatic Fuel Cell Operating in Human Sweat and Saliva*. Fuel Cells, 2014. **14**(6): p. 1050-1056.
158. Falk, M., et al., *Biofuel cell as a power source for electronic contact lenses*. Biosensors & Bioelectronics, 2012. **37**(1): p. 38-45.
159. Flexer, V., et al., *A novel three-dimensional macrocellular carbonaceous biofuel cell*. Physical Chemistry Chemical Physics, 2013. **15**(17): p. 6437-6445.
160. Reid, R.C., et al., *Enzymatic Biofuel Cell with a Flow-through Toray Paper Bioanode for Improved Fuel Utilization*. Journal of the Electrochemical Society, 2013. **160**(9): p. H612-H619.
161. Zebda, A., et al., *Electrochemical performance of a glucose/oxygen microfluidic biofuel cell*. Journal of Power Sources, 2009. **193**(2): p. 602-606.
162. Zebda, A., et al., *A microfluidic glucose biofuel cell to generate micropower from enzymes at ambient temperature*. Electrochemistry Communications, 2009. **11**(3): p. 592-595.
163. Zebda, A., et al., *Mediatorless high-power glucose biofuel cells based on compressed carbon nanotube-enzyme electrodes*. Nature Communications, 2011. **2**.
164. Soukharev, V., N. Mano, and A. Heller, *A four-electron O₂-electroreduction biocatalyst superior to platinum and a biofuel cell operating at 0.88 V*. Journal of the American Chemical Society, 2004. **126**(27): p. 8368-8369.
165. Mano, N., et al., *A miniature biofuel cell operating at 0.78 V*. Chemical Communications, 2003(4): p. 518-519.

166. Anjum, N.A., et al., *Catalase and ascorbate peroxidase-representative H₂O₂-detoxifying heme enzymes in plants*. Environmental Science and Pollution Research, 2016. **23**(19): p. 19002-19029.
167. Yoshimoto, M., et al., *Glucose oxidation catalyzed by liposomal glucose oxidase in the presence of catalase-containing liposomes*. Biotechnology Progress, 2006. **22**(3): p. 704-709.
168. Wohlgemuth, R., *Biocatalysis - key to sustainable industrial chemistry*. Current Opinion in Biotechnology, 2010. **21**(6): p. 713-724.
169. Chou, C.F. and T.C. Chou, *Paired electrooxidation IV. Decarboxylation of sodium gluconate to D-arabinose*. Journal of Applied Electrochemistry, 2003. **33**(8): p. 741-745.
170. Zargari, N., Y. Kim, and K.W. Jung, *Conversion of saccharides into formic acid using hydrogen peroxide and a recyclable palladium(II) catalyst in aqueous alkaline media at ambient temperatures*. Green Chemistry, 2015. **17**(5): p. 2736-2740.
171. Zhang, H. and N. Li, *Oxidative conversion of glucose to gluconic acid by iron(III) chloride in water under mild conditions*. Green chemistry, 2016. **16**: p. 2558.
172. Moreno, T., et al., *Uncatalysed wet oxidation of D-glucose with hydrogen peroxide and its combination with hydrothermal electrolysis*. Carbohydrate Research, 2012. **349**: p. 33-38.
173. Vallieres, C. and M. Matlosz, *A multisectioned porous electrode for synthesis of D-arabinose*. Journal of the Electrochemical Society, 1999. **146**(8): p. 2933-2939.
174. Jiricny, V. and V. Stanek, *Production of d-arabinose in a pilot plant fluidized bed electrochemical reactor*. Journal of Applied Electrochemistry, 1994. **24**(9): p. 930-935.
175. Gara, M. and R.G. Compton, *Activity of carbon electrodes towards oxygen reduction in acid: A comparative study*. New Journal of Chemistry, 2011. **35**(11): p. 2647-2652.
176. Watson, V.J., C.N. Delgado, and B.E. Logan, *Improvement of activated carbons as oxygen reduction catalysts in neutral solutions by ammonia gas treatment and their performance in microbial fuel cells*. Journal of Power Sources, 2013. **242**: p. 756-761.
177. Parish, J.H., *A Revolution in Biotechnology: Edited by Jean L Marx. pp 227. ISBN 0-521-32749-0*. Biochemical Education, 1990. **18**(2): p. 104-104.
178. Fry, A.J., *Organic Electrochemistry, Fourth Edition. ISBN 0-8247-0430-4*. Journal of the American Chemical Society, 2001. **123**(36): p. 8880-8880.
179. Jüttner, K., *Technical Scale of Electrochemistry, Encyclopedia of Electrochemistry, in Electrochemical Engineering*, A.J.B.a.M. Stratmann, Editor. 2007. p. 1-21.

180. Genders, J.D., et al., *Electrodialysis methods for purification and recovery of gluconic acid derivatives*. 2003, Patent US6187570
181. Gallezot, P., *Conversion of biomass to selected chemical products*. *Chemical Society Reviews*, 2012. **41**(4): p. 1538-1558.